Investigation on focusing of Bessel beams

by:

Pamela Bravo Cassab
B.S., BUAP

A Dissertation
submitted to the Program in Optics,
Department of Optics
in partial fulfillment of the requirements for the degree of

MASTER IN OPTICS

at the

Instituto Nacional de Astrofísica, Óptica y Electrónica

Tonantzintla, Puebla
July, 2024

Advisor:

Dr. Sabino Chávez Cerda
Principal Research Scientist
Department of Optics
INAOE

Summary

This work is a detailed analysis of the focusing characteristics of the Bessel beam, that gathers and expands on all the concepts required to fully understand the formalism based on the traveling conical waves that form these beam-like light structures.

In Chapters 2 and 3, we review in three coordinate systems the general solution to the wave equation, the one is represented by the sum of two traveling waves in opposite directions. Furthermore, we demonstrate the relation between the phase of a light wave and its wavefront, which helps us have a prediction of the shape the wavefront takes as the wave travels in space.

In Chapter 4 we present a revisitation of the diffraction subject. We discuss conditions such as Sommerfeld's radiation condition that have to be satisfied to consider valid the results obtained with the diffraction integrals, otherwise, it can lead to inaccurate descriptions of these. The most striking part of this section is the emphasis made on the definition of diffraction, which ultimately states that any element that modifies the amplitude and/or phase of the propagating wave will result in diffraction. Here, we are only concerned with apertures (and obstacles), therefore we provide numerous examples that prove we cannot talk about diffraction if there are no transverse limitations applied to the diffraction integrals.

Finally, Chapter 5 starts with a brief section dedicated to the focal shift effect and the Gaussian beam focusing case, which helps to explain the former is a diffraction effect related to the geometry of the aperture. Later, an analytical expression for the apertured Bessel beam at the focal plane is presented, this solution is described as the product of Bessel functions that represent an annular ring function. Additionally, we explain the nature of the Bessel beams in terms of its constituent conical waves, as well as the axial and transversal behavior of these beams when focused, the axial intensity is characterized by a Lorentzian curve and a "pseudo-focal" point. The transverse case section provides a method to calculate the transversal wavevector of the Bessel beam for each point along the axis. Lastly, we analyze two apodization functions to reduce the oscillations on the focused Bessel beam caused by diffraction: the Super Gaussian and the Flattened Gaussian beams. We employ theorems of energy conservation to obtain the relations between the parameters that modulate the functions and the radius of their waist. Both functions reduce the oscillations however with the Super Gaussian profile the peak intensities reached were bigger than for the Flattened Gaussian beam, but the latter demonstrated that for some cases the smaller the focal length considered, the smaller the oscillations obtained. Finally, we derive two geometrical approximations of the evolution of the Bessel beam passing through a lens and analyze its focusing characteristics.

Resumen

Este trabajo es un análisis detallado acerca de las características de enfocamiento de un haz Bessel, que reúne y expande todos los conceptos necesarios para tener un entendimiento completo del formalismo basado en las ondas cónicas viajeras que forman estos haces estructurados.

En los capítulos 2 y 3, hacemos un repaso de la solución general de la ecuación de onda , representada por la suma de dos ondas viajando en direcciones opuestas. Además, demostramos la relación entre la fase de la onda de luz y su frente de onda, la cual nos ayuda a tener una predicción de la forma que el frente de onda toma mientras la onda se propaga.

En el capítulo 4 revisitamos el tema de difracción, y discutimos las condiciones, tal como la Condición de Radiación de Sommerfeld, que tienen que ser satisfechas para obtener resultados validos con el uso de las integrales de difracción, porque de no ser así esto puede llevar a interpretaciones erróneas de estos resultados. Pero, el punto más importante de esta sección es el énfasis hecho en la definición de difracción, la cual nos dice que cualquier elemento que modifique y/o la fase de la onda propagándose causará difracción. Además, se dan ejemplos que prueban que no se puede hablar de difracción si no existen límites transversales en las integrales de difracción.

Por último, el capítulo 5 comienza con una breve sección dedicada al efecto de desplazamiento focal y al caso de enfocamiento del haz Gaussiano, que ayuda a explicar que el primero es un efecto de difracción relacionado con la geometría de la apertura. Posteriormente, se presenta una expresión analítica para el haz de Bessel limitado por una apertura en el plano focal, esta solución se describe como el producto de funciones de Bessel que representan un patrón de anillo. Además, explicamos la naturaleza de los haces de Bessel en términos de sus ondas cónicas fundamentales, así como el comportamiento axial y transversal de estos haces cuando se enfocan. La intensidad axial se caracteriza por una curva Lorentziana y un punto "pseudo-focal", mientras que la sección del caso transversal proporciona un método para calcular el vector de onda transversal del haz de Bessel para cada punto a lo largo del eje. Finalmente, analizamos dos funciones apodizadoras para reducir las oscilaciones en el haz de Bessel enfocado causadas por la difracción: la Super Gaussiana y la Gaussiana Aplanada. Empleamos los teoremas de conservación de la energía para obtener las relaciones entre los parámetros que modulan las funciones y el radio de su cintura. Ambas funciones reducen las oscilaciones sin embargo con el perfil Super Gaussiano las intensidades máximas alcanzadas son mayores que para el haz Gaussiano Aplanado, pero este último demuestra que para algunos casos cuanto menor es la distancia focal considerada, menores son las oscilaciones obtenidas. Al final, derivamos dos aproximaciones geométricas de la evolución del haz de Bessel que atraviesa una lente y estudiamos sus propiedades de enfocamiento.

A mi familia...

Acknowledgements

I could not have undertaken this journey without the guidance of my advisor Dr. Sabino Chávez Cerda, whose support and feedback were fundamental in the development not only of this dissertation but in my development and growth as a scientist.

I would also like to express my deepest appreciation to my defense committee formed by Dr. Gabriel Martínez Niconoff, Dr. Jesús Emmanuel Gómez Correa, and Dr. Ulises Ruiz Corona, who not only generously provided expertise but were very patient with me through all the process.

I am also very grateful to the CONAHCYTC national scholarships program and the INAOE, for the resources and the opportunity of being one of the many students who can study a postgraduate masters in our country.

I would like to extend my sincere thanks to the professors, who provided knowledge, and to all the Department of Optics, and the INAOE technical and administrative staff for all the considerate guidance and assistance. Special thanks to the security staff, the librarians, and the custodians for their kindness and hard work.

Lastly, thanks should also go to my family and friends, for their constant support. Your presence and belief in me have been instrumental in my success. And to my two dogs, for providing me with enough distractions.

Contents

Chapter 1

Introduction

In general terms, structured light refers to tailored intensity distribution, polarization and phase, and the numerous combinations of the three [1]. This subject and its application is vast and it is continuously evolving due to technological advancements. Many of these

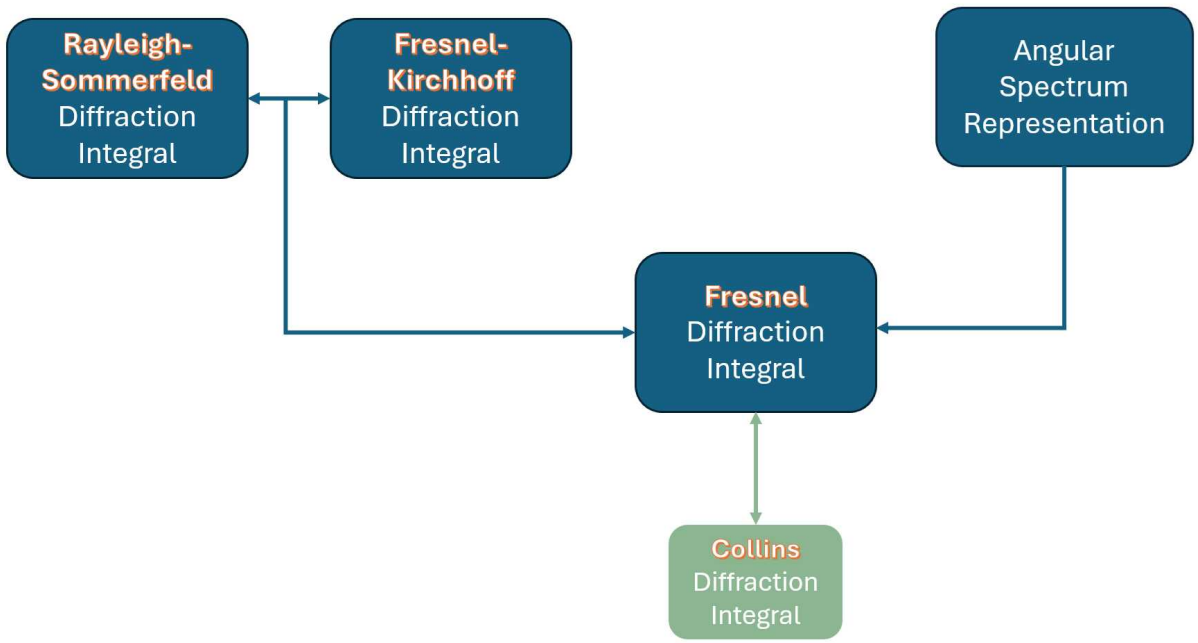

FIGURE 1.1: Categories of the scalar diffraction theories.

applications involve the propagation of these structured waves through a medium and/or optical system, consequently giving rise to the diffraction effect. For this reason, the study of the evolution of a structured beam is intertwined with the scalar diffraction theory. We

divide the scalar diffraction theories into three categories as shown in Figure 1.1 by the blue rectangles.

The angular spectrum representation also called the Plane-Wave Propagation Method consists of the decomposition of the light field into plane wave components traveling at different angles with respect to the propagating axis and the solution is reached through Fourier transformations [2]. For its part, the Fresnel-Kirchhoff (FK) and Rayleigh-Sommerfeld (RS) diffraction theories main difference lies in the boundary conditions imposed to reach the analytical equations. The KF theory presents a mathematical inconsistency that in most practical cases can be ignored and provide accurate results, however, this inconsistency is absent in the RS theory. These three theories under paraxial approximation give rise to the widely used Fresnel diffraction integral, which is usually the most common integral applied to calculate the paraxial propagation of light in homogeneous mediums. We do not include the Collins integral theory as one of the categories because Collins is a generalization of the Fresnel integral, nevertheless is included in the diagram because it is highly useful to study propagation through paraxial ABDC optical systems [3]. Albeit the RS diffraction theory gives exact solutions to the Helmholtz equation because no paraxial approximation is applied to it, the formulas are rarely used due to the mathematical difficulties when tried to be solved analytically.

But before delving into that a short review of the development of the diffraction theory which led to the formulation of the Rayleigh-Sommerfeld theory is made.

Grimaldi was the first to properly describe the diffraction phenomenon in 1665 when he observed the light passing through an obstacle and deviating from the rectilinear path. This was reported in what we could consider the first textbook on optics *Physicomathesis de lumine coloribus et iride* [4, 5].

Years later in 1690 C. Huygens, who was a contemporary to Newton, wrote a theorem that went against Newton's corpuscles theory, in it, he declared "each element of a wave-front may be regarded as the center of a secondary disturbance which gives rise to spherical wavelets; and that the position of the wave-front at any later time is the envelope of all such wavelets" [4]. However, it would take more than 100 years until Huygens's ideas were retaken because the prestige and authority Newton had around that time would cause his

theory of light to prevail for a whole century.

Through the years 1802-1804 Young and his experiments with light led him to propose a boundary diffraction wave theory, that opposed the corpuscular theory. His *Lectures on Natural Philosophy* (1897) discussed the double-slit experiment, where the concept of interference of light was discussed [6, 5].

Unfortunately, his ideas were not valued enough and were mostly ignored by the scientific community. It would have to pass a decade for Fresnel to appear and challenge once again the corpuscular theory. Fresnel discovered independently the principle of interference when studying the diffraction pattern by a thin rod. A few years later, in 1818, he presented his complete diffraction theory. The basic principles were [5]:

- The diffracting object is merely an obstruction.
- Light is composed of long trains of waves.
- The Huygens' principle must be applied at each point of the wavefront.
- The interference principle must be applied to account for the light distribution as a superposition of the disturbances originated at the wavefront.

The conjunction of Huygens and Fresnel ideas evolved into the Huygens-Fresnel principle, a fundamental part of the diffraction theory [4].

The next year, Fresnel submitted his work for a contest at the Academy of Science of France. However, the mathematician Poisson, who was part of the panel of judges and a strong defender of Newton's corpuscular theory, commented that Fresnel's theory predicted that a bright spot should be formed in the middle of the dark circular shadow after parallel light has encountered a circular obstacle, which made no sense to Poisson. F. Arago, who was also one of the judges and a good friend of Fresnel, performed the experiment and found the bright spot, this diffraction pattern is now called either Poissons' spot or Arago's spot [7].

Continuing with one of the most popular names that pop up when talking about diffraction. Joseph Fraunhofer was a manufacturing optician, who conducted experiments on diffraction with the novelty of the usage of optical instruments. His investigations on this

matter were reported in the years 1821 and 1822, and this class of diffraction phenomena is nowadays named after him [5]. Also in 1821, he accidentally formed a diffraction grating when studying a series of parallel slits. This optical structure had already been discovered and described by Rittenhouse [8] in 1785, but it drew no attention [4].

In 1882, Kirchhoff gave mathematical formalism to the Huygens-Fresnel principle when he derived an integral theorem that Helmholtz had previously obtained in acoustics, the theory found the solution of the homogeneous wave equations at a point P by applying Green's theorem to a closed surface that surrounds this point P [4]. This solution takes the name of Helmholtz-Kirchhoff theorem integral.

Additionally, Kirchhoff proposed boundary conditions to the aperture in a screen, he established that the field and its normal derivative on the aperture are unaltered by it and that the field on the opaque screen and elsewhere are equal to zero. These boundary conditions and the Helmholtz-Kirchhoff theorem are the basis of Kirchhoff's diffraction theory [3].

As we mentioned at the beginning diffraction problems tend to be difficult and require rigorous mathematical approaches, which is why Sommerfeld's work studying the diffraction of a plane wave over a semi-infinite thin plane screen and obtaining the exact result is noteworthy. After his results, other mathematicians performed variations of this problem over the years 1899-1916 [9].

A few years later, Lord Rayleigh published *"On the Passage of Waves through Apertures in Plane Screens and Allied Problems"*, where he discussed boundary value problems by considering a circular aperture of radius $a \leq \lambda$ or an extremely narrow slit so the effects of the edge could not be ignored [10]. In that same paper, he derived the diffraction formula that takes his name.

To obtain his diffraction integral Sommerfeld went on and proposed boundary conditions different from Kirchhoff's, he considered that either the field or its normal derivative is zero on the screen and elsewhere, but not both. The combination of his boundary conditions with the condition of radiation (in optics called Sommerfeld's radiation condition) led to the Rayleigh-Sommerfeld diffraction theory, which consists of two diffraction integrals where the main difference between them lies on the inclination factor [11].

So far, it is clear it took centuries to arrive at the scalar diffraction theories we use

nowadays, but ultimately each contribution was concerned with the study of the amplitude distribution of the light after "breaking" around the border of an object, this simple fact is often overlooked which leads to misinterpretations of results because the diffraction theories are used without consideration of the conditions these theories were constructed on. Consequently, we repeat ourselves, the analysis of the propagation of wave beams requires a strong understanding of diffraction theories, and similarly, the study of wave beams has taken many years to establish its basis. However up to date the theory that surrounds Bessel beams is yet not fully understood as we will show next.

During the sixties, numerous studies about laser resonators were conducted. In 1961, Fox and Li [12] simultaneously with Boyd and Gordon [13] showed the existence of modes in a Fabry-Perot interferometer that acted as a resonator. The latter represented these modes in terms of Hermite-Gaussian functions. Around the same time, the description of the modes of optical resonators was expanded [14, 15].

While the concept of mode referred to field distributions that reproduced their phase and transversal profile as they traveled inside a cavity [15], the concept of wave beams was introduced by Goubau and Schwering [14], nowadays we know them as light beams, and in general they refer to a field whose intensity distributions are concentrated near the axis of propagation [16], in other words, these light beams are solutions to the paraxial Helmholtz wave equation. One of the most well-known solutions is the Gaussian beam.

Thus, in the following years multiple studies about the Gaussian beam were conducted, these works were concerned with its propagation through free space, lenslike media, and its interaction with different optical structures [17, 18, 16].

Fast forwarding to 1987, a key year for this work, when Durin used the term “non-diffracting” beam [19] when he proposed a solution to the Helmholtz equation in free-space, his solution was composed of a plane wave propagating on the z-axis and a zeroth-order Bessel function, the nowadays called Bessel beam. It is interesting to point out that in 1941 [20], this solution had already been discovered but it did not attract any attention.

Durin et.al. [19] showed that the intensity distribution of his solution did not depend on the z variable, which translated to a light beam that was not subjected to the diffraction effects. However, he commented that it would require an infinite amount of energy to be able

to create a Bessel beam, so he restricted to analyzing apertured Bessel beams and showed that the Bessel beam intensity is invariant to propagation over a distance range Z_{max} that depends on the aperture radius.

The same year that Durin introduced his "diffraction-free" beams, these were experimentally demonstrated [21]. Attention was brought to the fact the Bessel beam was an exact and nonsingular analytical solution to the Helmholtz equation for the free space case because for the Bessel beam to be realizable in a real-life experiment an aperture of infinite dimensions would have to be used, so their work aimed to investigate the behavior of a truncated Bessel beam. They found that the Bessel beam after passing through an aperture retained its intensity transverse distribution over a propagation distance much larger than the non-spreading range of a Gaussian beam. These truncated Bessel beams are often referred to as realistic or realizable in the laboratory this is due again to the idea that "ideal" Bessel beams are endowed with infinite energy [19, 21].

In their early stage, Bessel beams were a mystery, so in the later years, many works tried to explain their formation and their characteristics. Here we supply a few demonstrative examples.

One of the first attempts to explain how a Bessel beam is formed can be found in ref. [22], where the authors describe the Bessel beams of zeroth-order as the simplest solution to the scalar wave equation in cylindrical coordinates by only considering the nonsingular solution to the Bessel differential equation. Additionally, they provide two interpretations of the zeroth-order Bessel beam formation, one based on the imaging of the interference of the spherical waves emitted by a ring source, and the other is related to the interference field produced by the spherical waves originating from the source at the image space aka a secondary ring source (which is the Fourier spectrum of a Bessel function). However, this interpretation lacks an extensive formalism to be considered a definite description of the Bessel beams. Albeit it is noteworthy to point out they solved the Fresnel diffraction integral and found an analytical expression for the amplitude of the truncated Bessel beam at the focal plane with the clever use of the Lommer integral. Moreover, they wrote the Fresnel integral into a power series to analyze what happens with the Bessel beam axial intensity and concluded that the maximum is shifted with respect to the focal plane when

the focal lens used has a pupil radius larger than the central spot of the input Bessel beam, this last result lacks significance when we consider that for a pupil lens smaller than the central spot we would have a plane wave passing through a circular aperture which results in the well-known Airy pattern, whose peak intensity is found at the focal plane, consequently, we can conclude the authors were unable to clarify why the shift in the axial intensity.

Another work regarding the focusing of a Bessel beam during those years was carried out by Baida Lü et.al. [23], they also calculated the axial intensity of the focused beam by solving analytically the Huygens-Fresnel diffraction integral and performed numerical calculations of their results which showed a Bessel beam focused by a lens forms a ring structure at the focal plane, this was expected and in accordance with the observed experimentally. The noteworthy result of this work is the expression they provided for the shifted position of the peak axial intensity with respect to the focal plane, that they derived with geometrical optics, and agrees well with their numerical simulations. However, they failed to give a proper explanation of this result, this shift of the position of maximum intensity with respect to the focal plane is attributed to the diffraction effect known as focal shift. Further, they mentioned that the focal shift would be zero for an unapertured Bessel beam propagating, but this is obvious, the absence of a converging lens is equivalent to a $f \to \infty$ which is exactly the same case presented in [19]. The other limiting case they presented, is for a Bessel beam whose central spot is much larger than the lens diameter which leads to the same result in ref. [22]. Once again, we notice that the lack of understanding not only of the nature of the Bessel beams but of diffraction effects such as the focal shift leads to incomplete descriptions of the properties of these beams. Another example of these efforts to explain the properties of the Bessel beams can be found in ref. [24] where the self-healing feature of the Bessel beams is explained through Babinet's principle.

However, at the beginning of the ninety's decade, a new analysis of the formation of the Bessel beams was presented, one based on the superposition of conical traveling waves [25]. This work showed that the second singular solution to the Bessel differential equation (Neumann function) should not be ignored and gave a specific complex linear combination of the two solutions to build the first and second Hankel functions. Furthermore, they provided a clear explanation for the formation of Bessel beams, they stated these beams are formed by

a longitudinal series of transverse standing waves created by the interference of the Hankel waves. Additionally, a physical description indicated that the Hankel waves represented an outgoing and incoming conical wave, both with respect to the propagation axis.

This interpretation of the Bessel beams demonstrated that these exist within a cone shaped region and can be created with finite energy because these traveling-wave approach is in agreement with the Sommerfeld's radiation condition. Further, the dynamics of the incoming and outgoing conical waves helped to understand some of the features of these beams like the self-healing [26].

Despite the completeness of the conical-wave formalism and the posterior works analyzing the focusing characteristics of Bessel beams [27, 28, 29, 30] based on it, to this day it is common to find that in the literature Durin's interpretation is still widely accepted and therefore the "mythes" surrounding the Bessel beams such as the idea they require infinite power to be created or that Bessel beam can not be focused prevail. Not only that, mistakes are made when studying the propagation of these beams, mistakes not related to their nature but to the lack of understanding of the diffraction theory, as is the case of a work published last year where the authors tried to find analytical solutions to the paraxial (Fresnel) and non-paraxial (Rayleigh-Sommerfeld) diffraction integrals for the Bessel beam case in a homogenous and GRIN media [31].

For the paraxial case, they did not set limits, as is required by the diffraction theories, and if attention is brought to the brief history review we presented at the beginning, in each step of the development of the diffraction theories a key element has always been the aperture (obstacle) that blocks the light field propagation. If we do not restrict our solutions of the Helmholtz wave equation we are not talking about diffraction and the results we obtain will be erroneous as is the ref case [31].

Moreover, when the authors analyzed the case of the nonparaxial case, the Rayleigh-Sommerfeld equation they applied was this one

$$E(r,\varphi,z) = \left(\frac{-ikz}{2\pi}\right)\frac{\exp(ik\rho)}{\rho^2}\int_0^{\infty}\int_0^{2\pi} E_0(r_0,\varphi_0,0) \times \exp\left\{\frac{ik}{2\rho}\left[r_0^2 - 2r_0 r\cos(\varphi_0-\varphi)\right]\right\} r_o dr_0 d\varphi_0$$

where $\rho = z + (x^2 + y^2)/2z$. A simple revision of any optics textbook [4, 11] would show us this equation is not the non-paraxial diffraction integral, therefore the result obtained is incorrect. This is evident even if we ignore the method they used because for this case they also did not apply limits and from our history review we know that the Rayleigh-Sommerfeld solution is an exact solution to the Helmholtz equation, so their result should have been the Bessel beam unaltered since no limits in the diffraction integral means the propagation is done through free-space where mathematically the Bessel beam is invariant.

The examples presented here are evidence of the theoretical gaps that surround the Bessel beams, and the flawed interpretations of the results as a consequence, thus it is desirable to have a definite theory of these and expand on their focusing characteristics to prove these beam-light structures can be focused.

The aim of this work is then to present an extensive and comprehensive review of the concepts required to fully understand the nature of the Bessel beams and their focusing features, among these concepts, we present a revision of the D'Alembert formula of the wave equations and an exhaustive description of the diffraction theory and paraxial optical beams. All with the purpose of proving the Bessel beams can be focused, and examining a focused apertured Bessel beam with the use of two apodization functions: the Super-Gaussian beam and the Flattened Gaussian beam, and simultaneously providing a complete 3D characterization of the evolution of a focused Bessel beam based on a geometrical approach.

This work is structured in the following manner. In Chapter 2, we recall D'Alembert solution to the wave equation, which is formed by the sum of two waves traveling in opposite directions. Additionally to the cartesian coordinate system, the solution is derived for the spherical and cylindrical coordinate systems, proving that the general solution to the wave equation is the same for every case. Further, we make this result evident when we explain the decomposition of any wave trajectory in fundamental plane waves.

Chapter 3 is addressed to show a particular solution to the wave equation is the harmonic wave, one that, likewise, can be written in the three main coordinate systems. We examine the relation the phase of the wavefunction has with the wavefront and attention is drawn to the harmonic cylindrical wave solution for the case of a wavefunction with dependence on the radial and z coordinates, whose wavefronts behave as two traveling conical functions.

The work continues in Chapter 4 by exploring the fundamental scalar diffraction theories, the first section considers the Rayleigh-Sommerfeld diffraction integral, their mathematical derivation, and the necessary conditions for their existence, among these we have the Sommerfeld's radiation condition, which explains that in order for the diffracted field to exist no sources from infinite should be considered. Moreover, we show how the Fresnel diffraction integral is an approximation of the RS integral formula and as such, the same conditions apply to it which is often ignored in literature. The most striking result of this section is the clarification it does about the diffraction phenomenon, by recalling that ultimately diffraction is produced by an element that modifies the amplitude or phase of the wave propagating, the elements include but are not limited to apertures and obstacles, and as such, transverse limits are required when studying the propagation of wave fields through an optical system. The second part of this chapter involves the mathematical procedure performed to obtain the paraxial Helmholtz wave equation and two of the most well-known solutions, the Gaussian beam and the Laguerre-Gaussian beam. At the end, we discuss the validity of the paraxial approximation and acknowledge the inconsistencies these approximations can cause.

The last chapter investigates the focusing characteristics of Gaussian beams and Bessel beams. Here one of the main features of a diffracted wavefield is introduced, the focal shift. We give a detailed explanation of this effect and an illustrative example to explain this shift of the position of maximum intensity with respect to the focal plane is due to the diffraction produced by an aperture (or obstacle) and that the point of maximum intensity reached by the Bessel beam during propagation is not related to it. The second half of the chapter studies in great detail the conical-wave formalism of the Bessel beam [25], this approach is used to characterize the focused Bessel beam, i.e. the Bessel beam propagation is described through its longitudinal axial intensity behavior and its transversal profile evolution through the propagation axis, which explains that due to Bessel beams being formed by the interference of traveling conical waves, its focusing characteristics are different from the other beams like Gaussian beams, but nevertheless they can be focused as well.

Then, two apodization functions are presented, the Super Gaussian beam and the Flattened Gaussian beam, these functions smooth the oscillations of the intensity on axis of the propagating beam and prove once again that a Bessel beam can be focused. For this part,

we employ Parseval's theorem to ensure energy conservation when assigning the values of the parameters of the two apodization functions, however, the energy loss is unavoidable due to diffraction effects that we explain in detail. Nevertheless, the Super Gaussian function provides results closer to the ones obtained when working with an apertured Bessel beam while at the same time reducing the contrast of the oscillations. But the Flattened Gaussian beam demonstrates that the smaller the focal length considered, the smaller the oscillations obtained for some cases. Finally, we obtain two expressions for the evolution of the Bessel beam passing through a lens using a geometrical optics approach and characterize the focusing characteristics, moreover these expressions obtained are written in controllable parameters and as such they could be of aid in experiments.

At the end of the work, a short discussion of the results is given.

Chapter 2

Propagating Electromagnetic Waves

The basis for any study about light waves is the wave equation, and as such this chapter is focused on deriving the general solutions to it in three coordinate systems.

2.1 The Wave Equation

Maxwell's equations in matter describe the state of free electric charges and currents, as well as electric and magnetic dipoles, that exist within the medium, and to achieve this the appropriate constitutive equations are required. These constitutive equations, $\mathbf{D}$ and $\mathbf{B}$, encapsulate the character of the medium [32].

$$\mathbf{D} = \epsilon_0 \mathbf{E} + \mathbf{P} \tag{2.1}$$

$$\mathbf{B} = \mu_0 \mathbf{H} + \mu_0 \mathbf{M} \tag{2.2}$$

The electric displacement $\mathbf{D}$, describes the response of the free charges and the bound charges to the electric field, and its relationship with the electric field $\mathbf{E}$ depends on the electric properties of the medium which are characterized by the polarization density $\mathbf{P}$. Similarly, the equation that relates the magnetic induction $\mathbf{B}$ and the magnetic field $\mathbf{H}$ describes the magnetic properties of the medium characterized by the magnetization density $\mathbf{M}$ [33].

Taking into consideration these relations Maxwell's equations read:

$$\nabla \times \mathbf{E} = -\frac{\partial \mathbf{B}}{\partial t} \tag{2.3}$$

$$\nabla \times \mathbf{H} = \frac{\partial \mathbf{D}}{\partial t} + \mathbf{J} \tag{2.4}$$

$$\nabla \cdot \mathbf{D} = \rho_f \tag{2.5}$$

$$\nabla \cdot \mathbf{B} = 0 \tag{2.6}$$

where $\mathbf{J}$ is the current equation described by Ohm's Law and ρ_f is the volume density of the electric free charge.

Based on the previous equations and considering nonmagnetic media, i.e. $\mathbf{M}$ is zero, the equation for the electric field $\mathbf{E}$ can be obtained by taking the curl of Eq. (2.3) and the time derivative of Eq. (2.4) using the fact that the order of differentiation with respect to time or space can be reversed [34].

$$\nabla \times (\nabla \times \mathbf{E}) = \nabla \times [-\frac{\partial \mathbf{B}}{\partial t}] = -\frac{\partial}{\partial t}(\nabla \times \mathbf{B}) = -\mu_0 \frac{\partial}{\partial t}(\nabla \times \mathbf{H}) \tag{2.7}$$

$$\frac{\partial}{\partial t}(\nabla \times \mathbf{H}) = \frac{\partial}{\partial t}\left[\frac{\partial \mathbf{D}}{\partial t} + \mathbf{J}\right] = \frac{\partial}{\partial t}\left[\epsilon_0 \frac{\partial \mathbf{E}}{\partial t} + \frac{\partial \mathbf{P}}{\partial t} + \mathbf{J}\right] \tag{2.8}$$

By substituting Eq. (2.8) into (2.7) we obtain

$$\nabla \times (\nabla \times \mathbf{E}) - \epsilon_0 \frac{\partial^2 \mathbf{E}}{\partial t^2} = \frac{\partial}{\partial t}\left[\frac{\partial \mathbf{P}}{\partial t} + \mathbf{J}\right] \tag{2.9}$$

The previous equation can be modified depending on the characteristics of the medium. The terms on the right are source terms that depend on the presence of polarization charges and currents. Now in the very specific case of a source-free medium, that is it contains no charges or currents, Maxwell's equations read as:

$$\nabla \times \mathbf{E} = -\frac{\partial \mathbf{B}}{\partial t} \tag{2.10}$$

$$\nabla \times \mathbf{H} = \frac{\partial \mathbf{D}}{\partial t} \tag{2.11}$$

$$\nabla \cdot \mathbf{D} = 0 \tag{2.12}$$

$$\nabla \cdot \mathbf{B} = 0 \tag{2.13}$$

With $\mathbf{D} = \epsilon\mathbf{E}$ and $\mathbf{B} = \mu\mathbf{H}$, where the scalar quantity $\epsilon = \epsilon_0(1+\chi)$ is the electric permittivity of the medium and μ is the magnetic permeability of the medium.

For this kind of medium Eq.(2.9) transforms into

$$\nabla \times (\nabla \times \mathbf{E}) - \epsilon_0 \frac{\partial^2 \mathbf{E}}{\partial t^2} = 0 \tag{2.14}$$

and using the vector identity

$$\nabla \times (\nabla \times \mathbf{V}) = \nabla(\nabla \cdot \mathbf{V}) - \nabla^2 \mathbf{V} \tag{2.15}$$

alongside with Eq.(2.12), we obtain the wave equation

$$\nabla^2 \mathbf{E} = \frac{1}{v^2} \frac{\partial^2 \mathbf{E}}{\partial t^2} \tag{2.16}$$

where

$$v = \frac{1}{\sqrt{\epsilon\mu}} \tag{2.17}$$

Eq. (2.17) is the speed of light of the electric field propagating in the medium.

If we follow similar steps but this time taking the curl of Eq. (2.4) and the time derivative of Eq. (2.3)

$$\begin{aligned} \nabla \times (\nabla \times \mathbf{H}) = \nabla \times [\frac{\partial \mathbf{D}}{\partial t} + \mathbf{J}] = \frac{\partial}{\partial t}(\nabla \times \mathbf{D}) + \nabla \times \mathbf{J} \\ = \epsilon_0 \frac{\partial}{\partial t}(\nabla \times \mathbf{E}) + \nabla \times \left[\frac{\partial \mathbf{P}}{\partial t} + \mathbf{J}\right] \end{aligned} \tag{2.18}$$

$$\frac{\partial}{\partial t}(\nabla \times \mathbf{E}) = \frac{\partial}{\partial t}\left[-\frac{\partial \mathbf{B}}{\partial t}\right] = -\frac{\partial^2 \mathbf{B}}{\partial t^2} \tag{2.19}$$

and once again substituting one equation into the other we obtain

$$\nabla \times (\nabla \times \mathbf{B}) + \epsilon_0\mu_0 \frac{\partial^2 \mathbf{B}}{\partial t^2} = \mu_0 \nabla \times \left[\frac{\partial \mathbf{P}}{\partial t} + \mathbf{J}\right] \tag{2.20}$$

And if once more we consider a medium for which Maxwell's equations are reduced to Eq. (2.10)-(2.13) the Eq. (2.20) transforms into

$$\nabla^2\mathbf{B} = \frac{1}{v^2}\frac{\partial^2\mathbf{B}}{\partial t^2} \tag{2.21}$$

Notice that a similar wave equation to Eq. (2.16) is obtained for the magnetic induction $\mathbf{B}$.

Let us now find a general solution for the wave equation Eq.(2.16). First, we consider a wavefunction in the form [35]

$$\mathbf{E} = \mathbf{E}(\mathbf{r}\cdot\widehat{\mathbf{u}}, t) \tag{2.22}$$

where $\widehat{\mathbf{u}}$ is a unit vector with a fixed direction.

Notice that at a given position $\mathbf{r}$(x,y,z) the scalar product from Eq.(2.22) reads as:

$$\mathbf{r}\cdot\widehat{\mathbf{u}} = xu_x + yu_y + zu_z \tag{2.23}$$

by definition, it represents the product of the projection of $\mathbf{r}$ along the direction of $\widehat{\mathbf{u}}$.

We can write the dot product as

$$\mathbf{r}\cdot\widehat{\mathbf{u}} = s \tag{2.24}$$

where s describes a trajectory, because, for each point laying on the trajectory, we have a vector $\mathbf{r}$ and $\widehat{\mathbf{u}}$ whose dot product is equal to a constant and so all these constant make up the complete trajectory.

It is easy to see that Eq.(2.22) represents a plane wave since at each instant of time the field is constant over each of the planes perpendicular to $\widehat{\mathbf{u}}$.

Next, applying the chain rule we can obtain the following relations [35]

$$\frac{\partial}{\partial x} = u_x\frac{\partial}{\partial s}, \quad \frac{\partial}{\partial y} = u_y\frac{\partial}{\partial s}, \quad \frac{\partial}{\partial z} = u_z\frac{\partial}{\partial s} \tag{2.25}$$

thus

$$\nabla^2\mathbf{E} = \frac{\partial^2\mathbf{E}}{\partial x^2} + \frac{\partial^2\mathbf{E}}{\partial y^2} + \frac{\partial^2\mathbf{E}}{\partial z^2} = (u_x^2 + u_y^2 + u_z^2)\frac{\partial^2\mathbf{E}}{\partial s^2}$$

$$\nabla^2\mathbf{E} = \frac{\partial^2\mathbf{E}}{\partial s^2} \tag{2.26}$$

Substituting this differential equation into Eq. (2.16) it can be rewritten as a one-dimensional partial differential equation, i.e.

$$\frac{\partial^2 \mathbf{E}}{\partial t^2} - v^2 \frac{\partial^2 \mathbf{E}}{\partial s^2} = 0 \tag{2.27}$$

To solve Eq.(2.27) we define the new variables ξ and η

$$\begin{aligned} \xi &= s - vt \\ \eta &= s + t \end{aligned} \tag{2.28}$$

Then by the chain rule, we obtain

$$\frac{\partial^2 \mathbf{E}}{\partial s^2} = \frac{\partial^2 \mathbf{E}}{\partial \xi^2} + 2\frac{\partial^2 \mathbf{E}}{\partial \xi \partial \eta} + \frac{\partial^2 \mathbf{E}}{\partial \eta^2} \tag{2.29}$$

$$\frac{\partial^2 \mathbf{E}}{\partial t^2} = v^2 \left[\frac{\partial^2 \mathbf{E}}{\partial \xi^2} - 2\frac{\partial^2 \mathbf{E}}{\partial \xi \partial \eta} + \frac{\partial^2 \mathbf{E}}{\partial \eta^2} \right] \tag{2.30}$$

Thus, the partial differential equation (2.27) is transformed into

$$-4v^2 \frac{\partial^2 \mathbf{E}}{\partial \xi \partial \eta} = 0 \tag{2.31}$$

Since the velocity can't be zero, the previous equation is reduced to

$$\frac{\partial^2 \mathbf{E}}{\partial \xi \partial \eta} = 0 \tag{2.32}$$

To solve this partial differential equation we integrate first with respect to ξ and then with respect to η

$$\int \frac{\partial^2 \mathbf{E}}{\partial \epsilon \partial \eta} d\epsilon = g(\eta)$$

$$\Rightarrow \int \frac{\partial \mathbf{E}}{\partial \eta} d\eta = \int g(\eta) d\eta + \mathbf{E}_2(\epsilon) = \mathbf{E}_1(\eta) + \mathbf{E}_2(\epsilon)$$

which gives as result

$$\mathbf{E}(\mathbf{r}, t) = \mathbf{E}_1(\eta) + \mathbf{E}_2(\epsilon) \tag{2.33}$$

where $\mathbf{E}_1$ and $\mathbf{E}_2$ are any twice differentiable functions.

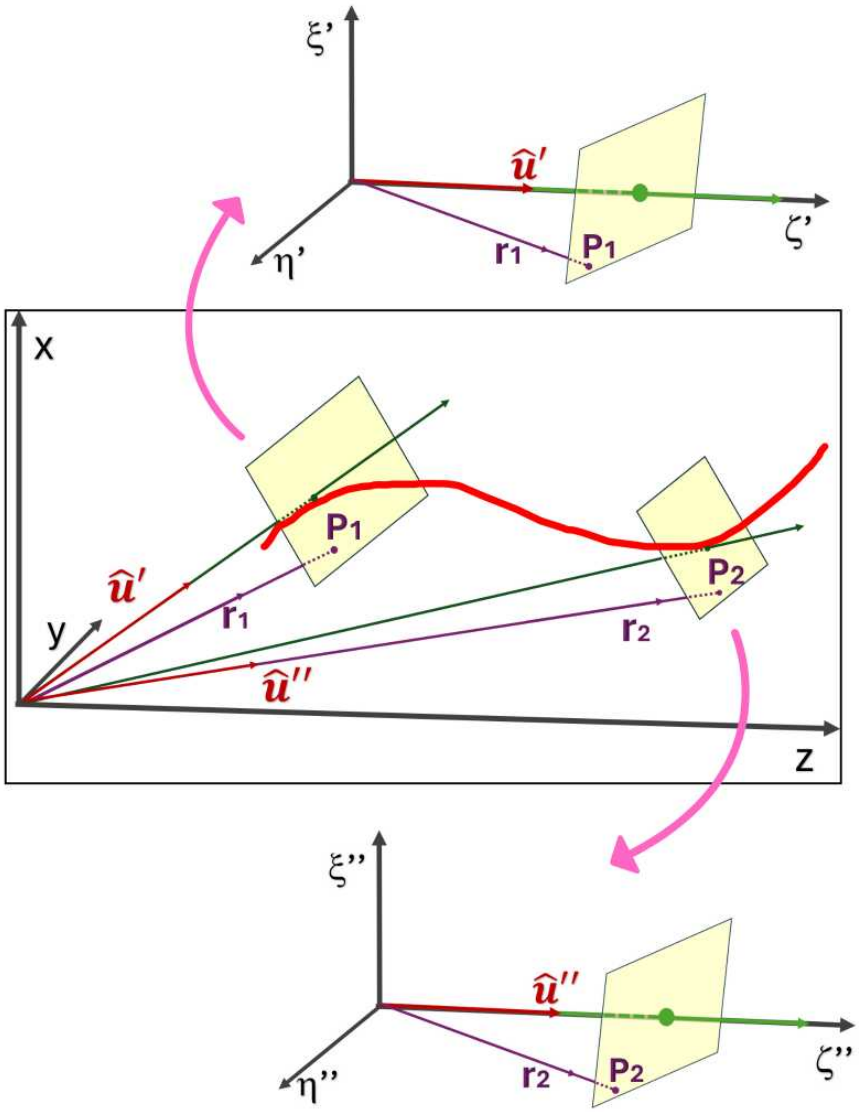

FIGURE 2.1: Graphic representation of an arbitrary trajectory s and its decomposition into plane waves.

Going back to the original variables the solution takes the form

$$\mathbf{E}(\mathbf{r},t) = \mathbf{E}_1(\mathbf{r}\cdot\widehat{\mathbf{u}} - vt) + \mathbf{E}_2(\mathbf{r}\cdot\widehat{\mathbf{u}} + vt) \tag{2.34}$$

Hence, the solution to Eq. (2.16) is the sum of two arbitrary functions that represent traveling waves in opposite directions. This solution was found by d'Alembert in 1747 [36].

What makes this result so relevant is the fact that so far we have not made assumptions about the direction of the unitary vector $\widehat{\mathbf{u}}$, and the vectorial format of Eq. (2.26) allows us to see the traveling-wave nature of the wavefunction in any trajectory s. Moreover, notice that it is possible to find a reference frame in which locally and instantly the field can be approximated by a plane traveling wave. In Figure (2.1) we illustrate this, the red line in the diagram at the middle represents a trajectory S. For each point over this trajectory, we can make a change of the variables and by doing so we are "changing" the reference frame to one where the angle between the propagation axis and the perpendicular plane to this point is zero, this procedure can be repeated for any trajectory and thus the solution found in Eq.(2.34) is valid consistently.

This last part is further proved in the next subsections, where it is show that Eq. (2.34) can be used to represent traveling waves in different geometries.

2.1.1 Wave Equation in Spherical Coordinates

For the case of the wave equation in spherical coordinates, we remember the definition of the Laplacian in spherical coordinates.

$$\nabla^2\mathbf{E} = \frac{1}{r^2}\frac{\partial}{\partial r}r^2\frac{\partial}{\partial r}\mathbf{E} + \frac{1}{r^2\sin\vartheta}\frac{\partial}{\partial\vartheta}\left(\sin\vartheta\frac{\partial\mathbf{E}}{\partial\vartheta}\right) + \frac{1}{r^2\sin^2\vartheta}\frac{\partial^2\mathbf{E}}{\partial\varphi^2} \tag{2.35}$$

With a little mathematical manipulation, it can be rewritten as:

$$\nabla^2\mathbf{E} = \frac{1}{r}\frac{\partial^2}{\partial r^2}(r\mathbf{E}) + \frac{1}{r^2\sin\vartheta}\frac{\partial}{\partial\vartheta}\left(\sin\vartheta\frac{\partial\mathbf{E}}{\partial\vartheta}\right) + \frac{1}{r^2\sin^2\vartheta}\frac{\partial^2\mathbf{E}}{\partial\varphi^2} \tag{2.36}$$

If we consider only radially symmetric solutions the Laplacian is reduced to

$$\nabla^2\mathbf{E} = \frac{1}{r}\frac{\partial^2}{\partial r^2}(r\mathbf{E}) \tag{2.37}$$

so the wave equation of Eq. (2.16) takes the form [35]

$$\frac{1}{r}\frac{\partial^2}{\partial r^2}(r\mathbf{E}) - \frac{1}{v^2}\frac{\partial^2\mathbf{E}}{\partial t^2} = 0$$

$$\frac{\partial^2}{\partial r^2}(r\mathbf{E}) - \frac{1}{v^2}\frac{\partial^2}{\partial t^2}(r\mathbf{E}) = 0 \tag{2.38}$$

Replacing the variable r by ρ and r$\mathbf{E}$ by $\mathbf{E}'$ the Eq. (2.38) reads

$$\frac{\partial^2 \mathbf{E}'}{\partial \rho^2} - \frac{1}{v^2}\frac{\partial^2 \mathbf{E}'}{\partial t^2} = 0 \tag{2.39}$$

we can notice this is essentially the same partial differential equation obtained in Section 2.1 so its solution must be similar

$$\mathbf{E}(r,t) = \frac{\mathbf{E_1'}(r-vt)}{r} + \frac{\mathbf{E_2'}(r+vt)}{r} \tag{2.40}$$

Eq. (2.40) is the sum of two arbitrary functions $\mathbf{E_1'}$ and $\mathbf{E_2'}$ that represent two traveling waves in opposite directions with the difference that in this case, these traveling waves are spherical waves, one diverging from the origin and the other converging towards the origin, both propagating with a velocity v.

2.1.2 Wave Equation in Cylindrical Coordinates

For the case of the wave equation in cylindrical coordinates, we are unable to find two arbitrary functions as an exact solution so instead we use a different approach to find a solution, more specifically we use the method of separation of variables. But first, we define the Laplacian in cylindrical coordinates as

$$\nabla^2\mathbf{E} = \frac{1}{r}\frac{\partial}{\partial r}\left(r\frac{\partial \mathbf{E}}{\partial r}\right) + \frac{1}{r^2}\frac{\partial^2 \mathbf{E}}{\partial \varphi^2} + \frac{\partial^2 \mathbf{E}}{\partial z^2} \tag{2.41}$$

where $x = r\cos\varphi$, $x = r\sin\varphi$ and $z = z$.

Once again we suppose a case with a wavefunction with radial symmetry so the wavefront represents a circular cylinder centered on the z-axis and having infinite length.

Thus, the wave equation reads as

$$\frac{1}{r}\frac{\partial}{\partial r}\left(r\frac{\partial \mathbf{E}}{\partial r}\right) - \frac{1}{v^2}\frac{\partial^2 \mathbf{E}}{\partial t^2} = 0 \tag{2.42}$$

To separate the spatial and time variables we suppose a solution of the form

$$\mathbf{E}(r,t) = R(r)T(t)\widehat{\mathbf{e}} \tag{2.43}$$

where $\widehat{\mathbf{e}}$ represents an unitary vector in the direction of $\mathbf{E}$.

Substituting it into Eq.(2.42) we obtain

$$\frac{T(t)}{r}\frac{\partial}{\partial r}\left(r\frac{\partial R(r)}{\partial r}\right) - \frac{R(r)}{v^2}\frac{\partial^2 T(t)}{\partial t^2} = 0 \tag{2.44}$$

diving by $R(r)T(t)$ and multiplying by v^2

$$\frac{v^2}{R(r)r}\frac{\partial}{\partial r}\left(r\frac{\partial R(r)}{\partial r}\right) - \frac{1}{T(t)}\frac{\partial^2 T(t)}{\partial t^2} = 0 \tag{2.45}$$

So the equality holds the term dependent on r and the one on t must be both equal to the same constant, that we conveniently make ω^2

$$\frac{1}{T(t)}\frac{\partial^2 T(t)}{\partial t^2} = -\omega^2 \tag{2.46}$$

$$\frac{v^2}{R(r)r}\frac{\partial}{\partial r}\left(r\frac{\partial R(r)}{\partial r}\right) = -\omega^2 \tag{2.47}$$

Solving Eq. (2.46) we obtain

$$T(t) = A\exp(-i\omega t) \tag{2.48}$$

Mathematically manipulating the Eq. (2.47) and remembering $k = \omega/v$ leads to

$$\frac{1}{R(r)r}\frac{\partial}{\partial r}\left(r\frac{\partial R(r)}{\partial r}\right) = -k^2 \tag{2.49}$$

$$\frac{1}{R(r)r}\left(\frac{\partial R(r)}{\partial r} + r\frac{\partial^2 R(r)}{\partial r^2}\right) - k^2 = 0 \tag{2.50}$$

$$r\left(\frac{\partial R(r)}{\partial r} + r\frac{\partial^2 R(r)}{\partial r^2}\right) - r^2k^2R(r) = 0 \tag{2.51}$$

we obtain the well-known Bessel equation whose general solution is the Hankel functions

$$R(r) = BJ_0(kr) \pm iCN_0(kr) \tag{2.52}$$

were J_0 and N_0 are the Bessel function of the first kind and the Neumann function (or Bessel function of the second kind) respectively, and B and C are constants. So using the asymptotic representations [37] of both functions and making $B = C = D$, where D is a constant, we can approximate the general solution as

$$R(r) \approx D\sqrt{\frac{2}{\pi r}}\exp(\pm ikr) \tag{2.53}$$

rewriting the last equation with the constant $A' = \sqrt{2/\pi}$ we have

$$R(r) \approx A^{'}\left(\frac{\exp(ikr)}{\sqrt{r}} + \frac{\exp(-ikr)}{\sqrt{r}}\right) \tag{2.54}$$

Finally, putting together Eq.(2.48) and (2.54) we get the solution of the wave equation in cylindrical coordinates Eq. (2.42).

$$\mathbf{E}(r,t) \approx A^{'}\left(\frac{\exp[i(kr-\omega t)]}{\sqrt{r}} + \frac{\exp[i(-kr-\omega t)]}{\sqrt{r}}\right) \tag{2.55}$$

$$\mathbf{E}(r,t) \approx A^{'}\left(\frac{\exp[ik(r-vt)]}{\sqrt{r}} + \frac{\exp[-ik(r+vt)]}{\sqrt{r}}\right) \tag{2.56}$$

This solution represents the sum of cylindrical waves traveling at velocity v in opposite directions.

We conclude the general solution of the wave equation (Eq.(2.16)) is formed by the sum of two waves traveling in opposite directions regardless of the coordinate system we work on. Next chapter, we analyze a particular solution of the wave equation.

Chapter 3

Harmonic Electromagnetic Waves in Open Free Space

In this chapter we study the propagation of light in open free space, that is, no transverse limitations in space are considered.

3.1 Helmholtz Equation and some fundamental solutions.

A particular solution of the wave equation Eq. (2.16) is a plane harmonic wave provided that $v = w/k$. This particular solution can be written as a complex exponential expression [38].

$$\mathbf{E}(\mathbf{r}, t) = \mathbf{E}(\mathbf{r})\exp(-i\omega t) \tag{3.1}$$

In this form, this equation receives the name of the complex wavefunction. The space-dependent part $\mathbf{E}(\mathbf{r})$ is the complex amplitude of the wave.

Some other special harmonic waves are the spherical waves and the cylindrical waves, the main difference between these types depends on the spatial coordinates used to represent the complex amplitude [39].

Before going further into the particulars of these fundamental solutions it is worth mentioning that the complex amplitude can be written as $\mathbf{E}(\mathbf{r}) = \mathbf{A}(\mathbf{r})\exp[iW(\mathbf{r})]$, where $\mathbf{A}(\mathbf{r})$ is an amplitude function and the argument of the exponential represent the wavefront. It

makes sense to generalize the complex amplitude of the harmonic wave this way when we remember that by definition the wavefront is a surface of constant phase, i.e. the phase of the wavefunction gives us the shape of the wavefront. For a planar wave, the phase is uniform in a plane orthogonal to the propagation direction, meanwhile, for a spherical wave, the phase varies quadratically (in the paraxial regime) with transverse displacement from the propagation axis [40], these examples will be clearer in the next subsections.

Now by substituting Eq. (3.1) into the wave equation Eq. (2.16) we obtain an equation for the complex amplitude called the **Helmholtz equation**.

$$\nabla^2\mathbf{E} + k^2\mathbf{E} = 0 \tag{3.2}$$

where k is the wavenumber. In the following subsections we present solutions to this equation in three coordinate systems.

3.1.1 Harmonic Plane Waves

The simplest solution of the Helmholtz equation Eq. (3.2) is found in Cartesian coordinates [33]

$$\mathbf{E}(\mathbf{r}) = \mathbf{A}\exp(i\mathbf{k}\cdot\mathbf{r}) \tag{3.3}$$

where $\mathbf{A}$ is the complex amplitude and $\mathbf{k} = k\widehat{\mathbf{u}} = (k_x, k_y, k_z)$ where $\widehat{\mathbf{u}}$ is an unitary vector and k is the magnitude of the wavevector which means $k^2 = k_x^2 + k_y^2 + k_z^2$. It is straightforward to see that in this case, the phase of the wave is the plane equation.

$$\mathbf{k}\cdot\mathbf{r} = k_x x + k_y y + k_z z = \text{constant} \tag{3.4}$$

This equation represents planes perpendicular to the wavevector $\mathbf{k}$, so the wavefronts are planar. Thus, with this complex amplitude, the harmonic plane wave solution takes the form of

$$\mathbf{E}(\mathbf{r}, t) = \mathbf{A}\exp[-ik(\widehat{\mathbf{u}}\cdot\mathbf{r} + \omega t)] \tag{3.5}$$

which represents a traveling plane wave in the direction of the wavevector. But last chapter we verified that the general solution of the wave equation in any coordinate system is of the form Eq. (2.34), which translated to the harmonic plane wave solution tells us that the particular solution of the Helmholtz equation, and therefore to the wave equation, is actually of the form

$$\mathbf{E}(\mathbf{r},t) = \mathbf{A}\exp[-ik(\widehat{\mathbf{u}}\cdot\mathbf{r}+\omega t)] + \mathbf{B}\exp[-ik(\widehat{\mathbf{u}}\cdot\mathbf{r}-\omega t)] \tag{3.6}$$

In short, the general solution of the three-dimensional Helmholtz equation in cartesian coordinates is the sum of two plane harmonic waves traveling in opposite directions.

So we have just established that the harmonic wave is a solution of the Helmholtz equation, one kind of harmonic wave is the one just described, the plane wave, but another kind, it is the spherical wave or cylindrical wave, these kinds of waves can be constructed from the superposition of planar waves propagating at different angles, as we explained in Chapter 1 with the Fig. 2.1.

This decomposition into plane waves that we can make for any wave resides in the fact that a generalized coordinate system consists of a family of three surfaces whose equations in terms of the Cartesian coordinates are $\varepsilon_1(x,y,z)$ = constant, $\varepsilon_2(x,y,z)$ = constant and $\varepsilon_3(x,y,z)$ = constant. The points of intersection of these surfaces are the coordinates points, and in each point for orthogonal systems, there are three mutually perpendicular unit vectors $\widehat{\mathbf{u_1}}$, $\widehat{\mathbf{u_2}}$ and $\widehat{\mathbf{u_3}}$ which are used to describe the wavefunction. In Cartesian coordinates, it is easy to see that the three mutually perpendicular surfaces are the planes: x = constant, y = constant and z = constant [41], which from what we have learned so far represent the wavefront shape of the harmonic plane wave (Eq.(3.6)), this last part is obvious to see. However, it is not as simple to identify these surfaces, and therefore the shape of the wavefronts, in other coordinate systems so we shall discuss some characteristics of the most used orthogonal coordinates in a real 3-dimensional space.

3.1.2 Harmonic Spherical Waves

For the case of **spherical polar coordinates**, the three mutually perpendicular surfaces of constant coordinate are [42]:

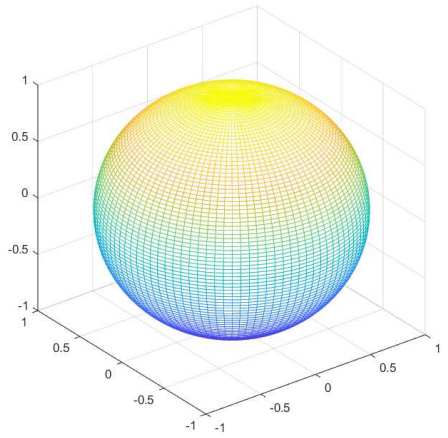

(A) Concentric sphere

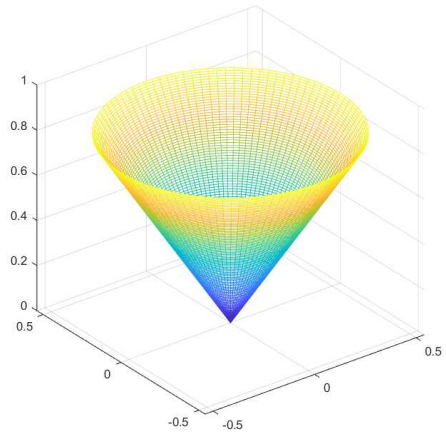

(B) Right circular cone

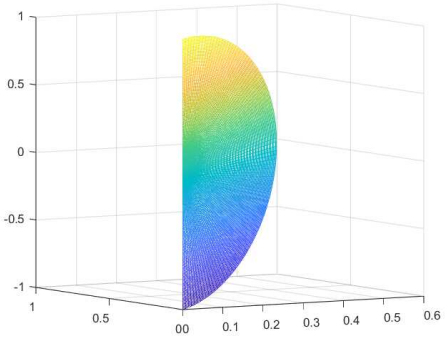

(C) Half-disc

FIGURE 3.1: Spherical coordinates surfaces

(1) a concentric sphere of radius r centered at the origin

$$r = (x^2 + y^2 + z^2)^{\frac{1}{2}} = \text{constant} \tag{3.7}$$

$$0 \leq r \leq \infty \tag{3.8}$$

(2) a circular cone of opening angle θ with respect to z and centered in the origin

$$\theta = \arccos\left(\frac{z}{r}\right) = \text{constant} \tag{3.9}$$

$$0 \leq \theta \leq \pi \tag{3.10}$$

(3) a plane half disc through the z (polar) axis at an angle φ measured from the x

direction

$$\varphi = \arctan\left(\frac{y}{x}\right) = \text{constant} \tag{3.11}$$

$$0 \leq \varphi \leq 2\pi \tag{3.12}$$

the intersection of these three planes describes any point **r** of this coordinate system. Each surface is illustrated in Figure 3.1.

In subsection 2.1.1 we established that the general solution for the wave equation in spherical coordinates is the sum of two spherical waves thus a particular solution would be

$$E(r,t) = A\left(\frac{\exp[i(kr-\omega t)]}{r} + \frac{\exp[i(-kr-\omega t)]}{r}\right) \tag{3.13}$$

which represents two spherical harmonic waves, one diverging from the origin and the other converging into it, this is now better understood from Figure 3.1a, because the phase from both traveling waves in Eq.(3.13), excluding the temporal part, depends only on the radial coordinate which is equivalent to having a spherical wavefront.

3.1.3 Harmonic Cylindrical Waves

In the case of **circular cylindrical coordinates** the three surfaces are [43]:

(1) a right-circular cylinder with the z-axis as the common axis

$$r = (x^2 + y^2)^{\frac{1}{2}} = \text{constant} \tag{3.14}$$

$$0 \leq r \leq \infty \tag{3.15}$$

(2) a half-plane through the z-axis at an angle φ measured from the x direction

$$\varphi = \arctan\left(\frac{y}{x}\right) = \text{constant} \tag{3.16}$$

$$0 \leq \varphi \leq 2\pi \tag{3.17}$$

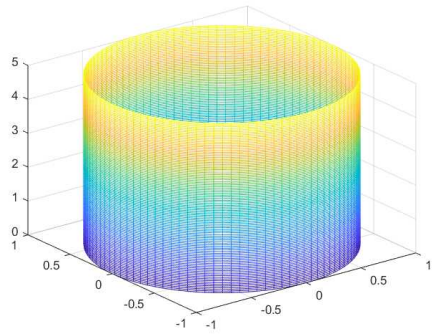

(A) Right-circular cylinder

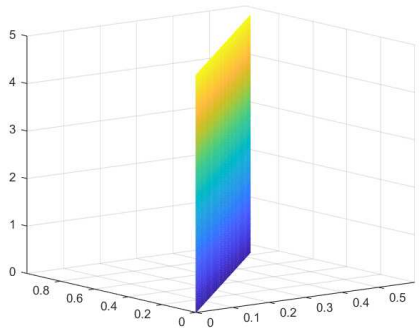

(B) Half-plane

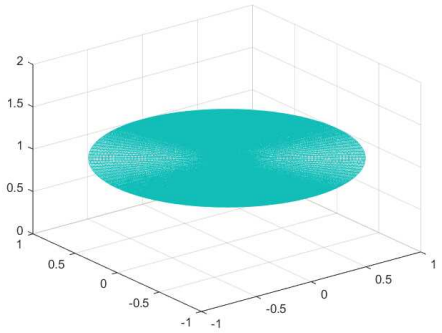

(C) Plane parallel to the x-y plane

FIGURE 3.2: Cylindrical coordinates surfaces

(3) a plane parallel to the x-y plane, as in the Cartesian system

$$z = z \tag{3.18}$$

$$-\infty \leq z \leq \infty \tag{3.19}$$

and analogously to spherical coordinates, the point of intersection of these planes describes each point of this coordinate system. Each surface is illustrated in Figure 3.2.

The relation the phase has with the shape of the surface with which the wave propagates in space will be relevant in Chapter 5, when we describe the wavefronts that lead to the formation of the Bessel beams, for now, we limit to showing the surfaces of constant phase we obtain by mixing the coordinates of the cylindrical system.

If we consider the phase is written in terms of the three coordinates, i.e. the phase takes the form $\exp\left[-i\Phi_{rz\varphi}(r,z,m)\right]$ where $\Phi_{rz\varphi}(r,z,m) = k_r r + k_z z + m\varphi$ then the wavefront is

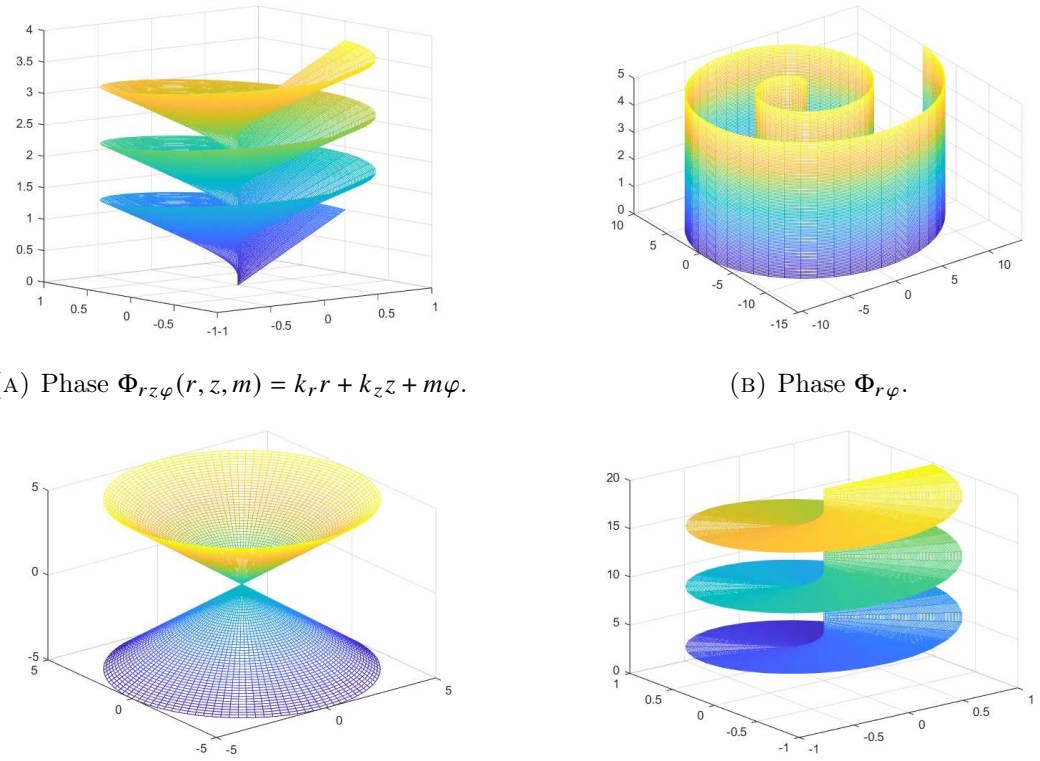

(A) Phase $\Phi_{rz\varphi}(r, z, m) = k_r r + k_z z + m\varphi$.

(B) Phase $\Phi_{r\varphi}$.

(C) Phase Φ_{rz}.

(D) Phase $\Phi_{\varphi z}$.

FIGURE 3.3: Wavefronts result of the mixing of the cylindrical coordinates in the phase of the wave.

approximated to spiraling cones (Figure 3.3a). But if the phase only depends on the radial and azimuthal coordinates ($\mathbf{\Phi}_{r\varphi}$) then the wavefront resembles a wrapped tortilla (Figure 3.3b), while if it depends on the radial r and z coordinate ($\mathbf{\Phi}_{rz}$) the wavefront will take the form of an up and down cone (Figure 3.3c), and for a dependency on the azimuthal φ and z coordinate ($\mathbf{\Phi}_{\varphi z}$) the wavefront looks like a spiraling ramp (Figure 3.3d).

Now, for the cylindrical coordinate system in subsection 2.1.2 we obtained Eq.(2.56), which analogously to the plane and spherical coordinate case represents the sum of two coaxial circular cylinders filling all space and traveling toward or away from an infinite source [44] (see Figure 3.2a). But with what we have learned so far we can consider a more general case, one with a wavefunction whose wavefront is written in terms of the radial r

and z coordinate. For this case, the wave equation reads as

$$\frac{1}{r}\frac{\partial}{\partial r}\left(r\frac{\partial \mathbf{E}}{\partial r}\right)+\frac{\partial^2 \mathbf{E}}{\partial z^2}-\frac{1}{v^2}\frac{\partial^2 \mathbf{E}}{\partial t^2}=0 \tag{3.20}$$

To separate the spatial and time variables we suppose a solution of the form

$$\mathbf{E}(r,t)=R(r)Z(z)T(t)\widehat{\mathbf{e}} \tag{3.21}$$

where $\widehat{\mathbf{e}}$ represents an unitary vector in the direction of $\mathbf{E}$.
Substituting it into Eq.(3.20) we obtain

$$\frac{T(t)}{r}\frac{\partial}{\partial r}\left(r\frac{\partial R(r)}{\partial r}\right)+R(r)T(z)\frac{\partial^2 Z(z)}{\partial z^2}-\frac{R(r)}{v^2}\frac{\partial^2 T(t)}{\partial t^2}=0 \tag{3.22}$$

diving by $R(r)T(t)Z(t)$ and multiplying by v^2

$$\frac{v^2}{R(r)r}\frac{\partial}{\partial r}\left(r\frac{\partial R(r)}{\partial r}\right)+\frac{v^2}{Z(z)}\frac{\partial^2 Z(z)}{\partial z^2}-\frac{1}{T(t)}\frac{\partial^2 T(t)}{\partial t^2}=0 \tag{3.23}$$

for this equality to hold, the spatial and temporal term must be both equal to the same constant, that we conveniently make ω^2

$$\frac{1}{T(t)}\frac{\partial^2 T(t)}{\partial t^2}=-\omega^2 \tag{3.24}$$

$$\frac{v^2}{R(r)r}\frac{\partial}{\partial r}\left(r\frac{\partial R(r)}{\partial r}\right)+\frac{v^2}{Z(z)}\frac{\partial^2 Z(z)}{\partial z^2}=-\omega^2 \tag{3.25}$$

Solving Eq. (3.24) we obtain

$$T(t)=A\exp(-i\omega t) \tag{3.26}$$

Mathematically manipulating Eq. (3.25) and remembering that $k=\omega/v$

$$\frac{1}{R(r)r}\frac{\partial}{\partial r}\left(r\frac{\partial R(r)}{\partial r}\right)+\frac{v^2}{Z(z)}\frac{\partial^2 Z(z)}{\partial z^2}=-k^2 \tag{3.27}$$

Now, we repeat the mathematical procedure of splitting and equating the differential equation to a constant, but for this case, we conveniently rewrite k as $k^2=k_r^2+k_z^2$, so we

have

$$\frac{1}{R(r)r}\left(\frac{\partial R(r)}{\partial r}+r\frac{\partial^2 R(r)}{\partial r^2}\right)+k_r^2=0 \tag{3.28}$$

$$\frac{1}{Z(z)}\frac{\partial^2 Z(z)}{\partial z^2}+k_z^2=0 \tag{3.29}$$

It is clear to notice Eq. (3.29) is the same as Eq.(3.24) thus the result is the same

$$Z(z)=A'\exp(-ik_z z) \tag{3.30}$$

In the case of Eq.(3.28), we rewrite it in the following form

$$r\left(\frac{\partial R(r)}{\partial r}+r\frac{\partial^2 R(r)}{\partial r^2}\right)+r^2k_r^2R(r)=0 \tag{3.31}$$

and we obtain the well-known Bessel equation whose general solution is the Hankel functions

$$R(r)=BJ_0(k_r r)\pm iCN_0(k_r r) \tag{3.32}$$

were J_0 and N_0 are the Bessel function of the first kind and the Neumann function (or Bessel function of the second kind) respectively, and B and C are constants. And similar to what we did in Section 2.1.2 we use the asymptotic representations of both functions and approximate the general solution as

$$R(r)\approx D\left(\frac{\exp(ik_r r)}{\sqrt{r}}+\frac{\exp(-ik_r r)}{\sqrt{r}}\right) \tag{3.33}$$

where $D=\sqrt{2/i\pi}$.

Finally putting together Eqs.(3.26), (3.30) and (3.33) we get the solution of the wave equation in cylindrical coordinates Eq. (3.20) as

$$\mathbf{E}(r,t)\approx A'\left(\frac{\exp[i(k_r r+k_z z-\omega t)]}{\sqrt{r}}+\frac{\exp[i(-k_r r-k_z z-\omega t)]}{\sqrt{r}}\right) \tag{3.34}$$

Notice the phase depends on the coordinates r and z, and from Fig.3.3c, we know the wavefront will then take the form of a cone, moreover the temporal part of the phase tells

us we have two conical wavefronts are traveling in opposite directions. This result will be expanded on in Chapter 5.

Now we can have a better visualization of the wavefronts of the harmonic traveling waves solutions to the Helmholtz equation in other coordinate systems which as we mentioned in Chapter 1 will come in hand later.

Chapter 4

Origin of diffraction and Paraxial Approximation.

As we mentioned at the beginning of this work, we cannot talk about the propagation of light without talking about diffraction which is why this chapter is a revisitation of the scalar diffraction theory and the paraxial optical beams.

4.1 Rayleigh-Sommerfeld Diffraction Theory

The last two chapters have revolved around solving the Helmholtz equation by finding fundamental solutions like harmonic waves in different coordinate systems and while it was not explicitly stated we have been considering initial boundary conditions at infinity. In this section we will focus on the solution when we apply finite initial boundary conditions, this is done through the use of integral mathematical methods. The initial boundary conditions represent an aperture (or obstacle), an element essential to talk about diffraction as we will see in this chapter consequently before proceeding further, it seems wise to give a classification of the kind of apertures based on their transmissivity profile of light.

Apertures can be hard or soft ones, the first one refers to those that either fully transmit or fully block the light, examples of these are the binary apertures such as the circular aperture. The second kind is the type where the transition of light has a gradual spatial variation; an example is a Gaussian aperture where a Gaussian function describes the transmissivity

profile. Soft apertures can help to avoid or mitigate the effects of diffraction [45]. Another classification for apertures refers to their geometric borders, these can be finite or semi-infinite, the latter refers to apertures that are open from one side. For the rest of the chapter and in the next ones we will focus only on finite apertures.

Now that we have established the aperture as the starting point to delve into the diffraction subject, it is understandable we will require the Green Theorem to build the diffraction theory because this theorem tells us:

Let E(P) and G(P) be any two complex-valued functions of position evaluated on the point P, and let S be a closed surface surrounding a volume V. If E, G, and their first and second partial derivatives are single-valued and continuous within and on S, then we have [46]

$$\iiint_{V'} \left(E\nabla^2 G - G\nabla^2 E\right) dv = \iint_{S'} \left(E\frac{\partial G}{\partial n} - G\frac{\partial E}{\partial n}\right) ds \tag{4.1}$$

where $\frac{\partial}{\partial n}$ signifies a partial derivative in the outward normal direction at each point on S. To use this theorem in the solution of diffraction problems it is necessary to make the

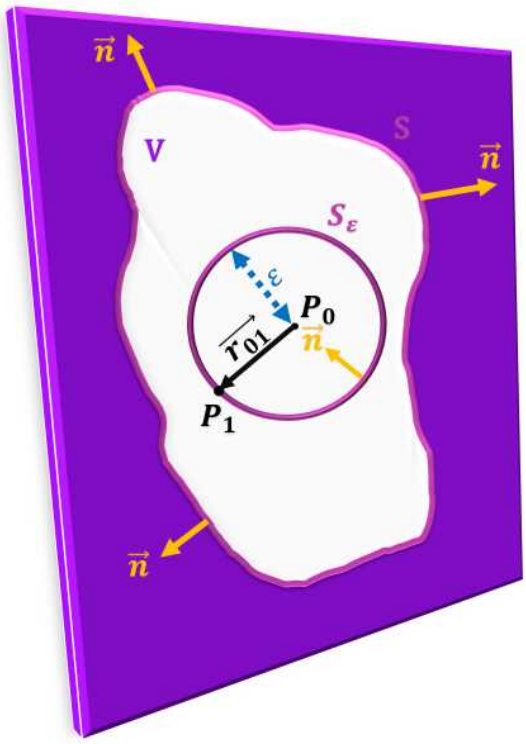

FIGURE 4.1: Arbitrary surface S that surrounds the point P_0 at where we want to find the optical field.

appropriate selection of the auxiliar function G and closed surface S.

Kirchoff's formulation to find the optical field at an observation point P_0 surrounded by an arbitrary surface S chooses as the auxiliar function a spherical wave centered at P_0

$$G(P_1) = \frac{\exp(ikr_{01})}{r_{01}} \tag{4.2}$$

To ensure the function G and its derivates are continuous as the theorem requires the discontinuity at P_0 is excluded by enclosing this point with a small spherical surface S_ϵ of radius ϵ, as shown in Figure 4.1. So the volume of integration V is the one lying between the surfaces S and S_ϵ, and the surface of integration is the sum of these two surfaces, that is $S' = S + S_\epsilon$.

Notice that we have used the letter E in our definition of the Green theorem because it represents the wavefunction (or wavefield) we are trying to find and as such we have assumed this function E satisfies the Helmholtz equation. In the case of the function G, this is a spherical wave so within the volume V it also satisfies the Helmholtz equation, which means that

$$\nabla^2 E = -k^2 E \tag{4.3}$$

$$\nabla^2 G = -k^2 G \tag{4.4}$$

We substitute these relations into the left-hand side of Green's theorem

$$\iiint_{V'} \left(E\nabla^2 G - G\nabla^2 E\right) dv = -\iiint_{V} \left(EGk^2 - GEk^2\right) dv = 0 \tag{4.5}$$

Thus the right-hand side of the Green theorem is reduced to:

$$\iint_{S+S_\epsilon} \left(E\frac{\partial G}{\partial n} - G\frac{\partial E}{\partial n}\right) ds = 0 \tag{4.6}$$

$$\Rightarrow -\iint_{S_\epsilon} \left(E\frac{\partial G}{\partial n} - G\frac{\partial E}{\partial n}\right) = \iint_{S} \left(E\frac{\partial G}{\partial n} - G\frac{\partial E}{\partial n}\right) \tag{4.7}$$

Now Eq.(4.2) it is our auxilar function for a general point P_1 on $S^{'}$ so we have

$$\frac{\partial G(P_1)}{\partial n} = \cos(\vec{n}; \vec{r_{01}}) \left(ik - \frac{1}{r_{01}}\right) \frac{\exp(ikr_{01})}{r_{01}} \tag{4.8}$$

where $\cos(\vec{n}; \vec{r_{01}})$ represents the cosine of the angle between the vectors $\vec{n}$ and $\vec{r_{01}}$. For the case of the point P_1 being inside the surface S_ϵ then $\cos(\vec{n}; \vec{r_{01}}) = -1$ because the normal of this surface points towards the center of it.

Thus when $r_{01} = \epsilon$ we have

$$G(P_1) = \frac{\exp(ik\epsilon)}{\epsilon} \quad \Rightarrow \quad \frac{\partial G(P_1)}{\partial n} = \left(\frac{1}{\epsilon} - ik\right)\frac{\exp(ik\epsilon)}{\epsilon} \tag{4.9}$$

When we substitute Eq. (4.9) into the left-hand side of Eq. (4.7) and take the limit as ϵ approaches zero we obtain

$$\begin{aligned} &\lim_{\epsilon\to 0}\iint_{S_\epsilon}\left(E\frac{\partial G}{\partial n} - G\frac{\partial E}{\partial n}\right)ds \\ &\quad = \lim_{\epsilon\to 0} 4\pi\epsilon^2\left[E(P_0)\left(\frac{1}{\epsilon} - ik\right)\frac{\exp(ik\epsilon)}{\epsilon} - \frac{\partial E(P_0)}{\partial n}\frac{\exp(ik\epsilon)}{\epsilon}\right] \\ &\quad = 4\pi E(P_0) \end{aligned} \tag{4.10}$$

Equating this result to the right-hand side of Eq.(4.7) and using the auxiliar function Eq.(4.2) gives as a result

$$E(P_0) = \frac{1}{4\pi}\iint_S\left[\frac{\exp(ikr_{01})}{r_{01}}\frac{\partial E}{\partial n} - E\frac{\partial}{\partial n}\left(\frac{\exp(ikr_{01})}{r_{01}}\right)\right]ds \tag{4.11}$$

This equation is called the **Integral Theorem of Helmholtz and Kirchhoff** and its relevance in the scalar diffraction theory resides in the fact it describes the field at a point P_0 as the result of the contributions on any closed surface that surrounds it.

Next, we apply this integral theorem to the case of a wave disturbance coming from a source located at a point P_2 at the left of an opaque screen and aperture, the objective is to find the field in a point P_0 on the right side of the aperture, this is illustrated in Figure 4.2. To do so it is important to choose a convenient surface that surrounds the point P_0 like the theorem requires, in this instance Kirchhoff's theory proposes a closed surface will be formed by two parts, a plane surface, S_1, lying directly behind the opaque screen, and a closed spherical cap, S_2, of radius R and centered at the observation point P_0. So the total surface S is simply the sum of S_1 and S_2. Thus, the Integral Theorem of Helmholtz and

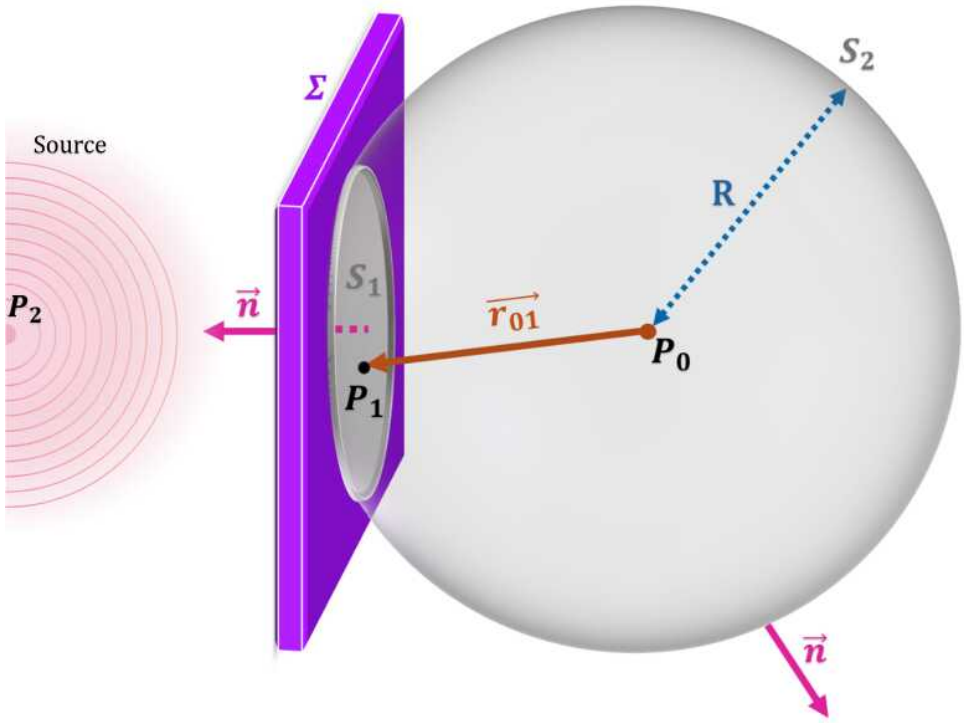

FIGURE 4.2: Surface S consisting of two parts, S_1 and S_2, proposed by Kirchhoff's theory.

Kirchhoff takes the form [47]

$$E(P_0) = \frac{1}{4\pi} \iint_{S_1+S_2} \left[G \frac{\partial E}{\partial n} - E \frac{\partial G}{\partial n} \right] ds \tag{4.12}$$

where the auxiliar function is still a spherical wave like Eq. (4.2). For a point on S_2 we have that

$$G = \frac{\exp(ikR)}{R} \quad \Rightarrow \quad \frac{\partial G}{\partial n} = \left(ik - \frac{1}{R} \right) \frac{\exp(ikR)}{R} \tag{4.13}$$

If we consider a large R then the normal derivate of G can be approximated by

$$\frac{\partial G}{\partial n} \approx ikG \tag{4.14}$$

Consequently, we rewrite the integral over the surface S_2 as

$$\frac{1}{4\pi} \iint_{S_2} \left[G \frac{\partial E}{\partial n} - E \frac{\partial G}{\partial n} \right] ds = \int_{\Omega} G \left[\frac{\partial E}{\partial n} - ikE \right] R^2 d\omega \tag{4.15}$$

where we made a change of variables from Cartesian to Spherical $ds = R^2 \sin\theta d\varphi d\omega = R^2 d\omega$ and used the solid angle Ω subtended by S_2 at P_0.

The existence of this integral is assured if $|RG| < \infty$, on that account for the integral to vanish over S_2 as $R \to \infty$ the following condition must be met

$$\lim_{R\to\infty} R\left[\frac{\partial E}{\partial n} - ikE\right] = 0 \tag{4.16}$$

this condition is known as *Sommerfeld radiation condition*, and it tells us the integral will vanish exclusively for outgoing waves on S_2, as opposed to incoming waves for which the integral might not be zero for large R. In other words, the field on P_0 depends entirely on the source P_2 located on the left side of the aperture and not on sources that come from the right side of the aperture, that is infinity sources do not contribute to the field.

This interpretation is related to the causality principle because by definition causality refers to the influence one event (cause) has on another (effect) and the dependence between both of them, in this case, the cause is the field at the aperture and the effect is the phenomenon of diffraction that the integral Theorem of Helmholtz and Kirchhoff describes.

Taking into consideration the Sommerfeld radiation condition the integral over S_2 vanishes and the Eq. (4.12) is reduced to an integral exclusively over S_1 [48].

$$E(P_0) = \frac{1}{4\pi}\iint_{S_1}\left[G\frac{\partial E}{\partial n} - E\frac{\partial G}{\partial n}\right] ds \tag{4.17}$$

Now this integral is fundamental to the diffraction theory because it describes the diffracted field once it has passed through the aperture and this last part is key because most literature fails to give a precise definition of the diffraction phenomenon when ultimately this phenomenon is the result of an element, be this an aperture, an obstacle, a film, a crystal, a spatial light modulator, etc., that modifies the amplitude and/or the phase of a propagating wave. Here we are only concerned with elements that modify the amplitude, more specifically apertures.

The diffraction integral Eq. (4.17) provides the value of the amplitude distribution of the diffracted field caused by the aperture at some point in the propagation axis. However, there are conditions to ensure this integral exists and is valid which simultaneously will ensure that

the diffracted field calculated with the integral is accurate, these are

1. The scalar theory holds.

2. Both E and G satisfy the Helmholtz wave equation.

3. The Sommerfeld radiation condition is satisfied.

Notice the last condition tells us that any diffracted field can not be infinite because infinite sources do not contribute to the integral Eq. (4.17), this is of relevance because this integral is the basis of the diffraction theory, taking it as a starting point one can arrive to the Rayleight-Sommerfeld (RS) diffraction integral and the Fresnel-Kirchhoff (FK) diffraction integral depending of the approximations considered, furthermore, from the RS and FK diffraction integrals an expression for the Huygens-Fresnel principle is obtained, and thus for the Fresnel and Fraunhoffer integrals. Therefore, the conditions presented here for the validity of the diffraction integral are conditions necessary for the validity of these posterior approximations as well. When the origin of the diffraction integrals is ignored it can lead to erroneous interpretations of the results obtained with them.

4.1.1 First and Second Rayleigh-Sommerfeld Solutions

Following Sommerfeld formulation of diffraction, the boundary conditions are either E or $\frac{\partial E}{\partial n}$ are zero on all the surface S_1, but not both at the same time contrary to the Kirchhoff boundary conditions in which both are zero and leads to a mathematical inconsistency [48]. Additionally, the KF theory makes paraxial approximations regarding the size of the aperture and observation plane, and the distance between them, which can lead in certain cases to inaccurate results as we will see in Section 4.1.2.

For the auxiliar function in the RS theory, the existence of a second point source is proposed, this second source is located at P_0' which is the mirror image of the point source at position P_0 on the opposite side of the aperture, as illustrated in Figure 4.3, both sources have the same wavelength λ but there is a phase difference of π between them. So the Green's function is given by [48]

$$G_-(P_1) = \frac{\exp(ikr_{01})}{r_{01}} - \frac{\exp(ikr'_{01})}{r'_{01}} \tag{4.18}$$

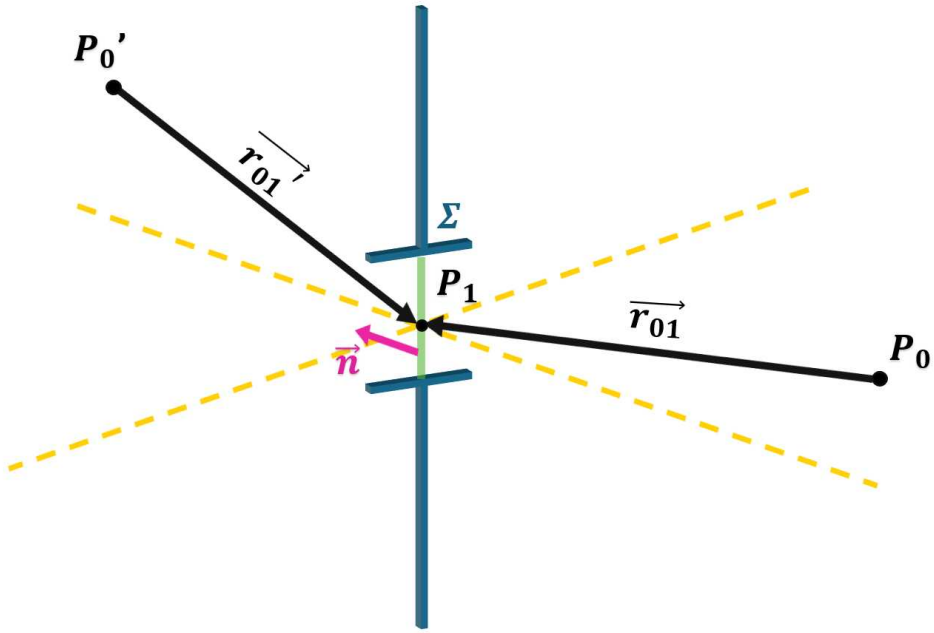

FIGURE 4.3: Sommerfeld's auxiliary function consisting of two mirroring points.

It is easy to see that at position P_1, the auxiliar function Eq. (4.18) is zero because $r_{01} = r'_{01}$, and the boundary condition applied is that E vanishes over all the surface S_1 except for the plane aperture Σ, so the integral of Eq. (4.17) takes the form

$$E_I(P_0) = -\frac{1}{4\pi}\iint_{\Sigma} E\frac{\partial G_-}{\partial n}ds \tag{4.19}$$

This integral is called the *first Rayleigh-Sommerfeld solution.*

Equation (4.18) is not the only possible Green's function, an alternative option is

$$G_+(P_1) = \frac{\exp(ikr_{01})}{r_{01}} + \frac{\exp(ikr'_{01})}{r'_{01}} \tag{4.20}$$

in this case, the normal derivative is zero across the screen and aperture, and the boundary condition is $\frac{\partial E}{\partial n} = 0$ on all the surface S_1 except at the plane aperture Σ thus we the field is

$$E_{II}(P_0) = \frac{1}{4\pi}\iint_{\Sigma} G_+\frac{\partial E}{\partial n}ds \tag{4.21}$$

This is the *second Rayleigh-Sommerfeld solution.*

We can rewrite both solutions in terms of the exponential function [49], first, we calculate the normal derivative of G_-

$$\begin{aligned}\frac{\partial G_-(P_1)}{\partial n} =& \cos(\vec{n},\vec{r}_{01})\left(ik-\frac{1}{r_{01}}\right)\frac{\exp(ikr_{01})}{r_{01}} \\ &-\cos\left(\vec{n},\vec{r'}_{01}\right)\left(ik-\frac{1}{r'_{01}}\right)\frac{\exp(ikr'_{01})}{r'_{01}}\end{aligned} \tag{4.22}$$

We notice from Figure 4.3 that P_1 is located on the aperture Σ and right in the middle of both sources so we have that $r_{01} = r'_{01}$ and $\cos(\vec{n},\vec{r}_{01}) = -\cos\left(\vec{n},\vec{r'}_{01}\right)$, hence the normal derivative takes the form

$$\frac{\partial G_-(P_1)}{\partial n} = 2\cos(\vec{n},\vec{r}_{01})\left(ik-\frac{1}{r_{01}}\right)\frac{\exp(ikr_{01})}{r_{01}} \tag{4.23}$$

If we assume that $r_{01} >> \lambda$ then

$$\frac{\partial G_-(P_1)}{\partial n} = 2ik\cos(\vec{n},\vec{r}_{01})\frac{\exp(ikr_{01})}{r_{01}} \tag{4.24}$$

we substitute this result into the first solution Eq.(4.19) to obtain

$$E_I(P_0) = -\frac{1}{i\lambda}\iint_\Sigma E(P_1)\cos(\vec{n},\vec{r}_{01})\frac{\exp(ikr_{01})}{r_{01}}ds \tag{4.25}$$

For the second solution, it is straightforward to see from Eq.(4.20) that on P_1 and under the condition of $r_{01} >> \lambda$ we have that

$$G_+(P_1) = 2\frac{\exp(ikr_{01})}{r_{01}} \tag{4.26}$$

Consequently, the second solution can be rewritten as

$$E_{II}(P_0) = \frac{1}{2\pi}\iint_\Sigma \frac{\exp(ikr_{01})}{r_{01}}\frac{\partial E(P_1)}{\partial n}ds \tag{4.27}$$

In the literature, we can find numerous examples of the usage of these Rayleigh-Sommerfeld solutions to solve diffraction problems, one example is briefly presented in the following

subsection.

4.1.2 Diffraction produced by an arbitrary aperture

The Rayleigh-Sommerfeld integrals presented last section provide exact solutions however they tend to be complicated to solve analytically which is why reducing them can be very useful.

If we consider an incident plane wave of amplitude E_0 on the aperture and use polar coordinates, then the Eq.(4.25) can be rewritten as:

$$E(x,y,z) = \frac{E_0 z}{2\pi} \iint_{\Sigma} \left(\frac{1}{r} - ik\right) \frac{\exp(ikr)}{r} dr d\varphi \tag{4.28}$$

The key point now is to use as the origin of the polar coordinates, the projection of the observation point on the plane of the aperture, with this and integrating by parts it yields [50]:

$$\begin{aligned} E(x,y,z) = &- \frac{E_0 z}{2\pi} \int \left[\exp\left(ikR_{max}(\varphi)\right)\left(\frac{1}{R_{max}(\varphi)}\right)\right] d\varphi \\ &+ \frac{E_0 z}{2\pi} \int \left[\exp\left(ikR_{min}(\varphi)\right)\left(\frac{1}{R_{min}(\varphi)}\right)\right] d\varphi \end{aligned} \tag{4.29}$$

where $R_{max}(\varphi)$ and $R_{min}(\varphi)$ are the maximum and minimum values of r, the distance between a point in the aperture and the location point of the observation point projected on the origin plane, for a given value of φ, respectively. For the integration limits for the variable φ there are two cases, one where the projection on the origin plane of the observation point falls inside the aperture, for this case $R_{max}(\varphi) = \sqrt{z^2 + c^2(\varphi)}$ and $R_{min}(\varphi) = z$, where $c(\varphi)$ is the distance from the projection point to the border of the aperture. The other case considers the projection points falling outside the aperture, here the border of the aperture is divided into two curves: C_{max} and C_{min} where one is the side of the border closer to the projection point and the other is the side of the border further apart from the projection point respectively.

The integral Eq.(4.29) gives the diffracted field produced by an arbitrary aperture by reducing the 2-D integral Rayleight-Sommerfeld solution into a 1-D parametric integration over the perimeter of the aperture, it has proved to be easier to solve and give exact results

for on-axis and off-axis cases [50]. But the relevance of the integral Eq.(4.29) dwells on the fact the integral depends on a parameter φ that characterizes the border of the aperture which further establishes that the diffracted field depends on the geometry of the aperture.

Now, before taking this matter further, a simple example of what we are trying to highlight in this section is none other than the well-known Babinet's principle, it tells us the diffraction pattern in the far field of an aperture and its complementary aperture is the same[51]. This arises when we consider the function of a complementary aperture f_c and we write it as

$$f_c(x, y) = 1 - f(x, y) \tag{4.30}$$

where $f(x, y)$ is the function of the aperture (or obstacle). The Fourier Transform, which will be explained better in the next section, is applied to Eq.(4.30) to obtain

$$\begin{aligned} \mathfrak{F}[f_c(x, y)] &= \mathfrak{F}[1] - \mathfrak{F}[f(x, y)] \\ &= \delta(u, v) - \mathfrak{F}[f(x, y)] \end{aligned} \tag{4.31}$$

So the square of the modulus of the Fourier transform for points different from zero is

$$|\mathfrak{F}[f_c(x, y)]|^2 = |\mathfrak{F}[f(x, y)]|^2 \tag{4.32}$$

This result proves that the intensity of the diffraction pattern of the aperture and its complementary in the far field is the same and notice that the one feature they share is the geometrical shape of their border, this is fundamentally the same result Eq.(4.29)gives, the diffraction pattern depends on the shape of the border of the aperture (or obstacle), which subsequently agrees with the concept that any element that modifies the amplitude of a propagating wave produces diffraction.

It has been proved too that Babinet's principle gives an exact result, the same as the Rayleigh-Sommerfeld diffraction integral [52]. An illustrative example can be found when calculating the intensity of Poisson's spot. When instead of using the Rayleigh-Sommerfeld integral the Fresnel-Kirchhoff integral is applied the result fails to converge.

The field at a point on the propagation axis is for the Rayleigh-Sommerfeld integral yields

$$E(0,0,z) = E_0 \frac{z}{r_0} \exp(ikr_0) \tag{4.33}$$

and for the Fresnel-Kirchhoff the result is [52]

$$E(0,0,z) = E_0 \frac{1}{2}\left(1 + \frac{z}{r_0}\right)\exp(ikr_0) - E_0 \frac{1}{2}\exp[ik(r \to \infty)] \tag{4.34}$$

where in both $r_0 = \sqrt{z^2 + a^2}$ and a represents the radius of the circular obstacle at the $z = 0$ plane. So we notice when $a = 0$, that is there is no obscuration, both results should be the unaltered plane wave $E_0 \exp(ikz)$ which is not the case for Eq.(4.34). To eliminate the diverging term the Babinet's principle is required. For this case we consider the plane wave to be the result of the sum of the diffraction pattern of the obstacle and the diffraction pattern of its complementary aperture: $U_{ob} + U_{ap} = E_0 \exp(ikz)$. Thus $U_{ob} = E_0 \exp(ikz) - U_{ap}$ which yields

$$E(0,0,z) = E_0 \frac{1}{2}\left(1 + \frac{z}{r_0}\right)\exp(ikr_0) \tag{4.35}$$

Notice Eq.(4.35) will be a plane wave in the absence of an obstacle but the inconsistency this time involves the boundary condition, it does not satisfy the Kirchhoff boundary condition however this matter is beyond the scope of this section. We can conclude from this analysis that in some cases the Rayleigh-Sommerfeld integral leads to accurate descriptions of the diffracted field while the Fresnel-Kirchhoff integral fails to do so.

Nevertheless, both of these integrals even after reducing them can still be difficult to solve for many practical cases which is why in the next section, we will explore in detail the diffraction integrals most used in the literature.

4.2 Fresnel and Fraunhoffer diffraction

So far we have described the diffraction phenomenon through the Rayleigh-Sommerfeld solutions but the use of simpler expressions can be helpful, which is why in this section we introduce the Fresnel and Fraunhoffer approximations.

But first, it is important to establish the Huygens-Fresnel principle which states that each point on a wavefront generates a spherical wave. The envelope of these secondary waves (or "edge-waves") constitutes the new wavefront and their superposition constitutes the wave in another plane [53]. Figure 4.4 illustrates this, where the "edge-waves" are generated on the plane (x', y') with each point of the diffracting aperture Σ as their source and the superposition of these results into the diffracted field that lies on the plane (x,y) parallel to (x', y'). Mathematically this principle can be stated as Eq.(4.25) with a positive sign [54].

$$E_I(P_0) = \frac{1}{i\lambda}\iint_{\Sigma} E(P_1)\cos\theta\frac{\exp(ikr_{01})}{r_{01}}ds \tag{4.36}$$

where we defined the argument of the cosine as θ. If we explicitly write the cosine term as

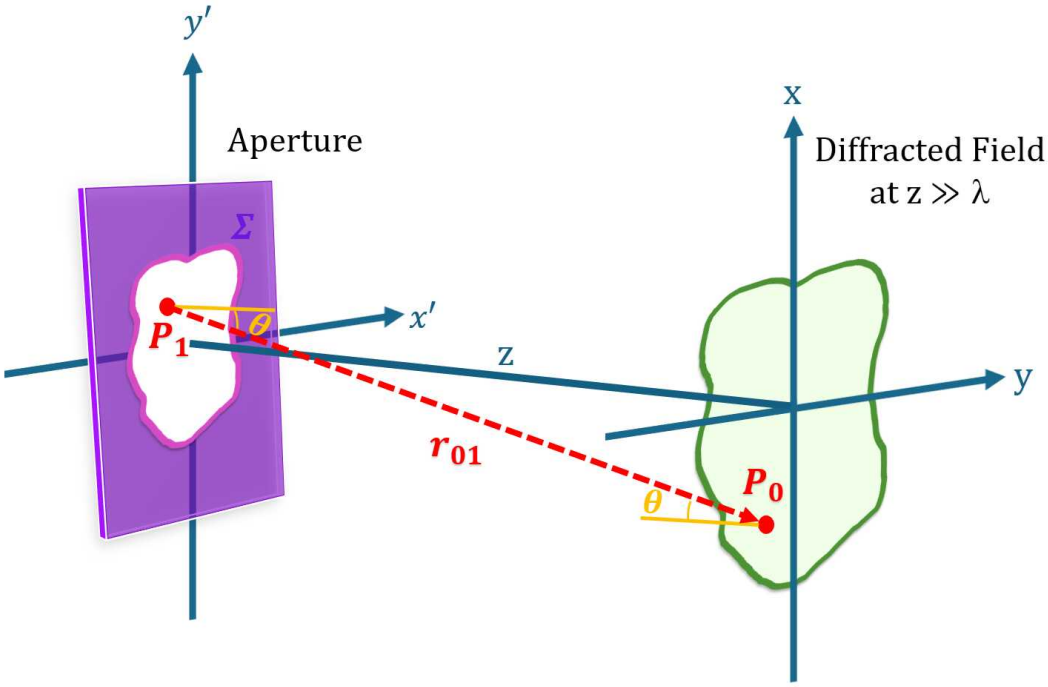

FIGURE 4.4: The diffraction field at $z \gg \lambda$ is the result of the superposition of the "edge-waves" generated by the aperture.

$\cos\theta = z/r_{01}$ and express the wave field in its corresponding coordinates then the principle can be rewritten as

$$E(x,y,z) = \frac{z}{i\lambda}\iint_{\Sigma} E(x',y',z=0)\frac{\exp(ikr_{01})}{r_{01}^2}ds \tag{4.37}$$

where

$$r_{01} = \sqrt{z^2 + (x - x')^2 + (y - y')^2} \tag{4.38}$$

Now the Fresnel approximation mentioned earlier is applied to this distance r_{01}, to do so we take out z from the square root

$$r_{01} = z\sqrt{1 + \left(\frac{x - x'}{z}\right)^2 + \left(\frac{y - y'}{z}\right)^2} \tag{4.39}$$

and if we suppose the observation points are close to the axis z but far away enough from the aperture i.e.

$$z >> \lambda;\ \theta < \frac{1}{2} \quad \Rightarrow \quad z >> \max\left[x', \eta \mid x', \eta \in \Sigma\right] \tag{4.40}$$

then we can use the Taylor expansion to approximate the Eq. (4.39) to

$$r_{01} \approx z\left[1 + \frac{1}{2}\left(\frac{x - x'}{z}\right)^2 + \frac{1}{2}\left(\frac{y - y'}{z}\right)^2\right] \tag{4.41}$$

The term r_{01} appears in the argument of the exponent multiplied by k, which happens to be a large number with a length value around 10^7, and we know phase shifts as little as a fraction of radian change the value of the exponential function so to diminish the error as much as possible we substitute the approximation Eq.(4.41) into the exponent, however for the r_{01} that appears in the denominator the error will be small even if we drop all the quadratic terms and leave only the z. Once we have taken into consideration this the integral equation takes the form

$$E(x, y, z) = \frac{z}{i\lambda}\iint_{-\infty}^{\infty} E(x', y', z = 0)\frac{\exp\left\{ikz\left[1 + \frac{1}{2}\left(\frac{x-x'}{z}\right)^2 + \frac{1}{2}\left(\frac{y-y'}{z}\right)^2\right]\right\}}{z^2}dx'dy' \tag{4.42}$$

Notice the limits of the integral are changed because now the information about the geometry of the aperture is contained in the field $E(x', y', z = 0)$. With some algebraic manipulations, we rewrite the integral Eq.(4.42) as [54]

$$E(x, y, z) = \frac{\exp(ikz)}{i\lambda z}\iint_{-\infty}^{\infty} E(x', y', z = 0)\exp\left\{\frac{ik}{2z}\left[(x - x')^2 + (y - y')^2\right]\right\}d\xi d\eta \tag{4.43}$$

this integral equation is known as the *Fresnel diffraction integral*.

If we expand the quadratic factor of the exponent the Fresnel integral takes the following form

$$E(x,y,z) = \frac{\exp(ikz)}{i\lambda z}\exp\left[i\frac{k}{2z}(x^2+y^2)\right]\iint_{-\infty}^{\infty}\left\{E(x',y',z=0)\exp\left[i\frac{k}{2z}\left(x'^2+y'^2\right)\right]\right\} \times \exp\left[-\frac{ik}{z}\left(xx'+yy'\right)\right]dx'dy' \tag{4.44}$$

Eq. (4.44) allows us to see more clearly that the Fresnel diffraction integral is the Fourier transform of a product of the complex field on the plane of the aperture and a quadratic phase exponential.

Another useful approximation to the diffraction integral is done when the exponential term with the quadratic phase is either eliminated or neglected [55]. There are two paths to arrive at the same expression for this approximation, the first one is to consider the optic field $E(x',y')$ is incident on a thin lens located at $z=0$ and calculate the diffracted field at the focal plane $z=f$. The lens adds a quadratic phase term defined as

$$p_{lens}(x',y') = \exp\left[-i\frac{k}{2f}(x'^2+y'^2)\right] \tag{4.45}$$

We introduce this term into the integral Eq. (4.44) and it is straightforward to see the two quadratic terms cancel so we obtain the following integral equation:

$$E(x,y) = \frac{\exp(ikf)}{i\lambda f}\exp\left[i\frac{k}{2f}(x^2+y^2)\right]\iint_{-\infty}^{\infty}E(x',y')\exp\left[-\frac{ik}{z}\left(xx'+yy'\right)\right]dx'dy' \tag{4.46}$$

The other path is to consider distances z large enough such that $z \gg x'^2+y'^2$, this is considered the far-field region, and this allows to approximate the quadratic phase exponential inside the integral Eq. (4.44) to unity and thus obtain a simpler expression

$$E(x,y,z) = \frac{\exp(ikz)}{i\lambda z}\exp\left[i\frac{k}{2z}(x^2+y^2)\right]\iint_{-\infty}^{\infty}E(x',y',z=0)\exp\left[-\frac{ik}{z}\left(xx'+yy'\right)\right]dx'dy' \tag{4.47}$$

Notice how both Eq.(4.46) and (4.47) represent a Fourier transform in Cartesian coordinates of the kernel $E(x',y',)$. Equation (4.46) is called the *Fraunhofer diffraction integral* mean-

while Eq. (4.47) is the *Fraunhofer approximation*. However, the last one becomes the same as Eq.(4.46) when $z = f$. The main difference between the two of them is that Eq.(4.46) is exact and Eq.(4.47) is not, for it to be exact the distances z considered have to satisfy the condition [55]

$$z \gg \frac{k(x'^2 + y'^2)_{max}}{2} \tag{4.48}$$

where $(x'^2 + y'^2)_{max}$ is the maximum value of the radio $(x'^2 + y'^2)$ that contributes to the integral. If we define the Rayleigh length $L_D = ka^2/2$ where for this case $a = (x'^2+y'^2)_{max}$ then we can conclude the Fraunhofer approximation will give accurate enough results provided it is evaluated for distances z larger than the Rayleigh length.

The intent of presenting both approaches is to expand the understanding we have of the Fraunhofer integral. The Fraunhofer approximation tells us that the diffracted field calculated with the integral Eq. (4.47) is an approximation that will maintain its transversal shape within the far-field region, in other words, the only major change on the diffracted field as it propagates will be the spreading of its profile, provided the distance z is larger than the Rayleigh length.

For its part, the Fraunhofer diffraction integral Eq. (4.46) gives us the exact diffracted field calculated at the focal plane of a lens once the field has passed through it. Ultimately, both are the same, because in the literature is common to refer to these "far-field" distances z where the diffracted field is found as "infinite" so the role of the lens is to "pull" the field from infinite and locate it at the focal plane, hence both integrals yield look-alike diffracted pattern.

In sum, the Fresnel diffraction integral is used to obtain the field diffracted by an aperture (or obstacle) at $z = 0$ for points within the near-field region ($0 < z < L_D$) and the Fraunhofer diffraction integral calculates the diffracted field at the focal point of a lens located at the right side of the aperture ($z > 0$).

A well-known example of the usage of the Fraunhofer integral is found when calculating the diffracted field of a circular aperture. For this case, we consider a plane wave with

amplitude equal to unity passing through a circular aperture that we represent as

$$U(\rho_\varepsilon) = \text{circ}\left(\frac{\rho_\varepsilon}{a}\right)$$

We are using polar coordinates due to the geometry of the aperture, so $\rho' = \sqrt{x'^2 + y'^2}$ and a is the ratio of the circular aperture. As we concluded from Eqs. (4.46) and (4.47) the field U(ρ) is the result of a Fourier transform, i.e.

$$U(\rho) = \exp\left[i\frac{k}{2z}\rho^2\right]\mathscr{F}\{U(\rho')\}$$

where $\mathscr{F}$ represents the Fourier transform in polar coordinates which yields

$$U(\rho) = \left(\frac{\pi a^2}{2\lambda z}\right)\exp\left[i\frac{k}{2z}\rho^2\right]\frac{J_1\left(\frac{ka\rho}{2z}\right)}{\left(\frac{ka\rho}{2z}\right)} \tag{4.49}$$

and so the intensity of the diffracted field on the observation plane is of the form [55]

$$I(\rho) = |U(\rho)|^2 = \left(\frac{\pi a^2}{2\lambda z}\right)^2\left[\frac{J_1\left(\frac{ka\rho}{2z}\right)}{\left(\frac{ka\rho}{2z}\right)}\right]^2 \tag{4.50}$$

We mentioned previously that when using Eq.(4.47) the field obtained will keep its transverse shape and with this example, we can explicitly see what we meant by that. Notice the intensity distribution is always a Bessel function J_1 scaled by z, this tells us the form of the diffraction pattern does not change but the larger the distance z, the bigger the spreading of the diffracted field will be.

To find the exact value we evaluate the result for $z = f$ and we obtain

$$I(\rho) = |U(\rho)|^2 = \left(\frac{\pi a^2}{2\lambda f}\right)^2\left[\frac{J_1\left(\frac{ka\rho}{2f}\right)}{\left(\frac{ka\rho}{2f}\right)}\right]^2 \tag{4.51}$$

This function takes the name of the English mathematician, George Biddell Airy, who first derived it, and it is known as an *Airy disk* which is shown in Figure 4.5. It is clear to see

Eqs.(4.50) and (4.51) are basically the same, this is what we meant when we mentioned the Fraunhoffer approximation and exact integral produce the same diffracted pattern.

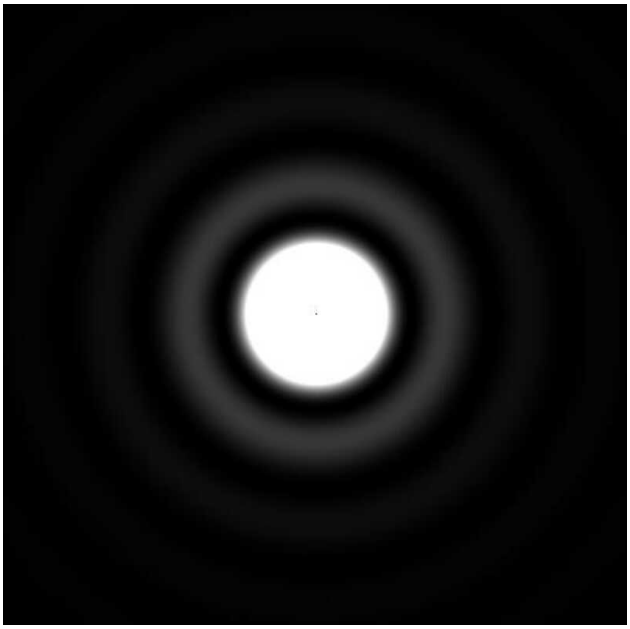

FIGURE 4.5: Airy disk

The radius of the Airy disk is given by the first zero of the Bessel function J_1 which yields:

$$3.83 = \frac{ka\rho_A}{2f}$$

When we solve for ρ_A we obtain

$$\rho_A = (3.83)\frac{2f}{ka} \approx 1.22\left(\frac{\lambda f}{a}\right)$$

In the next chapter, we will use the diffraction integrals presented here but before that, it is necessary to discuss the features of the paraxial optical beams and present some examples of these, which will help us better understand the concept of light beam.

4.3 Paraxial Optical Beams

From Chapter 3 we recall the complex amplitude can be written as $\mathbf{E}(\mathbf{r}) = \mathbf{A}(\mathbf{r})\exp[iW(\mathbf{r})]$, so for the case of a plane wave traveling in the z direction it takes the form

$$E(\mathbf{r}) = A(\mathbf{r})\exp(-ikz) \tag{4.52}$$

Where $A(\mathbf{r})$ represents a slowly varying complex function, we refer to a slow variation when within a distance of a wavelength $\lambda = 2\pi/k$ we have that $\Delta A << A$. Eq.(4.52) is then what we know as a paraxial wave and when substituted into the Helmholtz equation Eq.(3.2) we obtain

$$\left(\frac{\partial^2 A}{\partial x^2} + \frac{\partial^2 A}{\partial y^2}\right) - 2ik\frac{\partial A}{\partial z} + \frac{\partial^2 A}{\partial z^2} = 0 \tag{4.53}$$

But A varies slowly with z so when $z \approx \lambda$ we have that [56]

$$\Delta A \approx \frac{\partial A}{\partial z}\lambda \quad \Rightarrow \quad \frac{\partial A}{\partial z} << \frac{A}{\lambda} \quad \Rightarrow \quad \frac{\partial A}{\partial z} << kA \tag{4.54}$$

It is logical to assume the derivative of $\partial A/\partial z$ also varies slowly which means

$$\frac{\partial^2 A}{\partial z^2} << k^2 A \tag{4.55}$$

This inequality allows us to neglect the second derivative term in the Eq.(4.53) and obtain

$$\left(\frac{\partial^2 A}{\partial x^2} + \frac{\partial^2 A}{\partial y^2}\right) - 2ik\frac{\partial A}{\partial z} = 0 \tag{4.56}$$

Which is known as the *Paraxial Helmholtz equation*. The simplest solution to this equation is the paraboloidal wave. Other well-known solution is the Gaussian beam, also called the "fundamental mode" [16], and the Laguerre-Gaussian beam, the following sections will center around these two beams.

But before that, we normalize the paraxial Helmholtz equation to find the Gaussian beam complex amplitude, the normalization is not necessary but it allows us to work with dimensionless variables which makes the derivation far easier as we shall see.

First, we propose new variables

$$x' = \frac{x}{w_0}, \; y' = \frac{y}{w_0} \tag{4.57}$$

and by the chain rule, we have the following relations

$$\frac{\partial}{\partial x} = \frac{1}{w_0}\frac{\partial}{\partial x'} \quad \Rightarrow \quad \frac{\partial^2}{\partial x^2} = \frac{1}{w_0^2}\frac{\partial^2}{\partial x'^2} \tag{4.58}$$

$$\frac{\partial}{\partial y} = \frac{1}{w_0}\frac{\partial}{\partial y'} \quad \Rightarrow \quad \frac{\partial^2}{\partial y^2} = \frac{1}{w_0^2}\frac{\partial^2}{\partial y'^2} \tag{4.59}$$

Substituting these into Eq.(4.56)

$$\frac{1}{w_0^2}\left(\frac{\partial^2}{\partial x'^2} + \frac{\partial^2}{\partial y'^2}\right)A + 2ik\frac{\partial A}{\partial z} = 0$$

$$\left(\frac{\partial^2}{\partial x'^2} + \frac{\partial^2}{\partial y'^2}\right)A + 2ikw_0^2\frac{\partial A}{\partial z} = 0 \tag{4.60}$$

And to simplify this equation even more we use the definition of Rayleight length $L_D = ka^2/2$ we gave in Section 4.2 to define $\zeta = z/L_D$ with $a = w_0$. Additionally we define $E = E_0 A$ where $|A| = 1$ at $z = 0$. With all these into consideration, the paraxial equation is reduced to the form

$$\frac{1}{4}\left(\frac{\partial^2}{\partial x'^2} + \frac{\partial^2}{\partial y'^2}\right)E + i\frac{\partial E}{\partial \zeta} = 0 \tag{4.61}$$

This equation is the *normalized paraxial Helmholtz wave equation*. From here on when we use the paraxial wave equation we might change the denotation of the variables to facilitate the mathematical derivations, however, we will specify if we are working with the conventional paraxial Helmholtz wave equation Eq.(4.56) or the normalized one Eq. (4.61).

4.3.1 Gaussian Beams

To find the expression for the amplitude distribution of a Gaussian beam we start with the paraxial normalized Helmholtz wave equation Eq.(4.61) with a different notation.

$$-i\frac{\partial E}{\partial z} + \frac{1}{4}\left(\frac{\partial^2 E}{\partial x^2} + \frac{\partial^2 E}{\partial y^2}\right) = 0 \tag{4.62}$$

and propose the ANSATZ [16, 57]

$$E(x, y, z) = \exp\left[-i\left(P(z) + \frac{x^2 + y^2}{2Q(z)}\right)\right] \tag{4.63}$$

where $P(z)$ and $Q(z)$ are for now arbitrary complex functions, to find their analytic expressions we start with the following initial condition

$$|E(x, y, 0)|^2 = \exp\left(-\frac{x^2 + y^2}{2}\right) \tag{4.64}$$

After the corresponding derivations of Eq.(4.62) and substitutions into the paraxial Helmholtz equation, we obtain

$$\frac{x^2 + y^2}{2Q^2}\left(Q' - \frac{1}{2}\right) - (x^0 + y^0)\left(P' + \frac{i}{2Q}\right) = 0 \tag{4.65}$$

It is well known that the subspace (1, x, x^2, ...) is a linearly independent base so for Eq.(4.65) to be satisfied, each term between parenthesis should be equal to zero which gives us as result.

$$Q'(z) = \frac{1}{2}\,,\; P'(z) = -\frac{i}{2Q} \tag{4.66}$$

With the use of the initial condition we can find the value of Q because

$$E(x, y, 0) = \exp\left(-\frac{x^2 + y^2}{2}\right) = \exp\left(-i\frac{x^2 + y^2}{2Q}\right) \quad \Rightarrow \quad Q(z = 0) = i \tag{4.67}$$

To find the explicit expressions for Q and P we integrate Eqs. (4.66). For the case of Q, it is easy to see we have

$$Q(z) = \frac{z}{2} + i \tag{4.68}$$

Where we used Eq.(4.67), with this result we can rewrite the exponential as

$$\exp\left(-i\frac{x^2+y^2}{2Q}\right) = \exp\left[-i\frac{x^2+y^2}{2}\left(\frac{1}{\frac{z}{2}\left(1+\frac{4}{z^2}\right)} - \frac{i}{\frac{z^2}{4}+1}\right)\right] \tag{4.69}$$

For the case of P(z) the integration yields

$$iP(z) = \ln\left(1 - \frac{iz}{2}\right) \tag{4.70}$$

we rewrite the complex argument of the natural algorithm in the polar form.

$$-iP = -\ln\left[\sqrt{1+\left(\frac{z}{2}\right)^2}\exp\left(-i\arctan\left(\frac{z}{2}\right)\right)\right] \tag{4.71}$$

and finally obtain

$$\exp(-iP) = \left(\sqrt{1+\left(\frac{z}{2}\right)^2}\right)^{-1}\exp\left(-i\arctan\left(\frac{z}{2}\right)\right) \tag{4.72}$$

Putting together Eq. (4.69) and (4.72) we have the expression for a *Gaussian beam normalized amplitude distribution*

$$E(\mathbf{r}) = E_0\mathfrak{A}(z)\exp[-i\Phi(z)]\exp\left(\frac{-i(x^2+y^2)^2}{2R(z)}\right)\exp\left(-\frac{(x^2+y^2)^2}{2w^2(z)}\right) \tag{4.73}$$

or alternatively

$$E(\mathbf{r}) = E_0\mathfrak{A}(z)\exp[-i\Phi(z)]\exp\left(\frac{-ir^2}{2R(z)}\right)\exp\left(-\frac{r^2}{2w^2(z)}\right) \tag{4.74}$$

with $r^2 = (x^2+y^2)^2$ and where the parameters are defined by

$$w^2(z) = 1 + \frac{z^2}{4} \tag{4.75}$$

$$\Phi(z) = \arctan\left(\frac{z}{2}\right) \tag{4.76}$$

$$R(z) = \frac{z}{2}\left[1+\left(\frac{4}{z^2}\right)^2\right] \tag{4.77}$$

$$\mathfrak{A}(z) = \frac{1}{\sqrt{1+\frac{z^2}{4}}} \tag{4.78}$$

We emphasize once again that we are considering normalized variables for this subsection.

As we mentioned at the beginning of this section, the Gaussian beam is a solution to the paraxial Helmholtz equation but not the only one, an alternative solution can be obtained when we consider cylindrical coordinates instead of cartesian, and the result is the well-known Laguerre-Gaussian beams. The following subsection focus on these.

4.3.2 Gaussian beams in cylindrical coordinates: Laguerre-Gaussian

To find the Laguerre-Gaussian amplitude distribution we will use once again the normalized paraxial Helmholtz equation now in cylindrical coordinates.

$$\frac{\partial^2 U}{\partial \rho^2} + \frac{1}{\rho}\frac{\partial U}{\partial \rho} + \frac{1}{\rho^2}\frac{\partial^2 U}{\partial \phi^2} + i4\frac{\partial U}{\partial z} = 0 \tag{4.79}$$

The proposed ANSATZ is of the form [58]

$$U(\mathbf{r}) = F\left[\frac{\rho}{w(z)}\right] G(\phi) E(\mathbf{r}) \exp[i\alpha(z)] \tag{4.80}$$

where $E(\mathbf{r})$ is a Gaussian beam defined by Eq.(4.74).

After the corresponding derivation process of Eq.(4.80) we substitute in Eq.(4.79) to obtain

$$\begin{aligned}\frac{1}{F}\frac{\partial^2 F}{\partial \rho^2} + \frac{1}{E}\frac{\partial^2 E}{\partial \rho^2} + \frac{2}{FE}\frac{\partial E}{\partial \rho}\frac{\partial F}{\partial \rho} + \frac{1}{\rho}\left[\frac{1}{F}\frac{\partial F}{\partial \rho} + \frac{1}{E}\frac{\partial E}{\partial \rho}\right] \\ + \frac{1}{\rho^2 G}\frac{\partial^2 G}{\partial \phi^2} + 4i\left[\frac{1}{E}\frac{\partial E}{\partial z} + \frac{1}{F}\frac{\partial F}{\partial z}\right] - 4\frac{\partial \alpha}{\partial z} = 0\end{aligned} \tag{4.81}$$

But we know the Gaussian beam satisfies the paraxial Helmholtz equation so the sum of the terms that depend solely upon $E(r)$ are equal to zero. The expression is then reduced to

$$\frac{1}{F}\frac{\partial^2 F}{\partial \rho^2} + \frac{2}{FE}\frac{\partial E}{\partial \rho}\frac{\partial F}{\partial \rho} + \frac{1}{\rho}\left[\frac{1}{F}\frac{\partial F}{\partial \rho}\right] + \frac{1}{\rho^2 G}\frac{\partial^2 G}{\partial \phi^2}\frac{\partial \alpha}{\partial z} + \frac{4i}{F}\frac{\partial F}{\partial z} - 4\frac{\partial \alpha}{\partial z} = 0 \tag{4.82}$$

Now we define a new variable

$$\varrho = \rho/w \tag{4.83}$$

and with the use of the chain rule of differentiation, we obtain the following relations

$$\frac{\partial}{\partial \rho} = \frac{1}{w}\frac{\partial}{\partial \varrho} \tag{4.84}$$

$$\frac{\partial F}{\partial z} = \frac{\partial \varrho}{\partial z}\frac{\partial F}{\partial \varrho} = -\frac{\varrho}{2R}\frac{\partial F}{\partial \varrho} \tag{4.85}$$

Notice the second term of the differential equation Eq.(4.82) still has a dependency to $E(r)$ so we proceed to find the derivative of the function.

$$\frac{\partial E}{\partial \rho} = -\frac{\varrho}{w}\left(\frac{iw^2}{R} - 1\right)E \tag{4.86}$$

We substitute Eq.(4.86) and use the relations Eq.(4.84) and (4.85) to rewrite the differential equation, which yields

$$\frac{1}{w^2 F}\frac{\partial^2 F}{\partial \varrho^2} - \frac{2}{F}\left(\frac{iw^2}{R} - 1\right)\frac{\varrho}{w^2}\frac{\partial F}{\partial \varrho} + \frac{1}{\varrho F}\frac{1}{w^2}\frac{\partial F}{\partial \varrho} - \frac{2i\varrho}{RF}\frac{\partial F}{\partial \varrho} + \frac{1}{\varrho^2 G}\frac{2}{\omega^2}\frac{\partial^2 G}{\partial \phi^2} - 4\frac{\partial \alpha}{\partial z} = 0 \tag{4.87}$$

By multiplying by w^2 and canceling the equal term we finally obtain

$$\frac{\varrho}{F}\frac{\partial^2 F}{\partial \varrho^2} - \frac{2\varrho}{F}\frac{\partial F}{\partial \varrho} + \frac{1}{\varrho F}\frac{\partial F}{\partial \varrho} + \frac{1}{\varrho^2 G}\frac{\partial^2 G}{\partial \phi^2} - 4w^2\frac{\partial \alpha}{\partial z} = 0 \tag{4.88}$$

Now to solve it we separate the differential equation into terms that solely depend on one variable and solve each one individually.

For the term dependant of α we set it equal to a constant C and so its solution is

$$\alpha(z) = \frac{C}{2}\arctan\left(\frac{z}{2}\right) \tag{4.89}$$

For the term dependant on ϕ we set it equal to a constant $-m_2$ where m is an integer and the solution G is

$$G(\phi) = A_m \exp(im\phi) + B_m \exp(-im\phi) \tag{4.90}$$

To solve the differential equation first, we equal Eq.(4.88) to $(-C - m^2)$ and notice it can be further reduced to the following expression

$$\frac{\partial^2 F}{\partial \varrho^2} + \left[\frac{1}{\varrho} - 2\varrho\right]\frac{\partial F}{\partial \varrho} + \left[C - \frac{m^2}{\varrho^2}\right]F = 0 \tag{4.91}$$

what follows is to make the coordinate transform $y = \varrho^2$ and rewrite once again Eq.(4.91) in the following way

$$y\frac{\mathrm{d}^2 F}{\mathrm{d}y^2} + (1-y)\frac{\mathrm{d}F}{\mathrm{d}y} + \frac{1}{4}\left[C - \frac{m^2}{y}\right]F = 0 \tag{4.92}$$

It is straightforward to see the differential equation (4.92) has a singular point at $y = 0$ which happens to be also a regular point this means we can apply the Frobenius method to solve it. The proposed solution is thus of the form

$$F(y) = \sum_{k=0}^{\infty} a_k y^{k+s} \tag{4.93}$$

The indicial equation gives $s = \pm m/2$ for $a_0 \neq 0$, and if we choose as the only regular solution at the origin the positive root then we can define a function H(y) that reads as

$$H(y) = y^{m/2}F(y) \tag{4.94}$$

Once we rewrite the differential equation Eq.(4.92) in terms of this new function we obtain

$$yH'' + (m+1-y)H' + \left(\frac{1}{4}C - \frac{m}{2}\right)H = 0 \tag{4.95}$$

Eq. (4.95) is the Laguerre's differential equation and its solution is the Laguerre polynomials $L_n^m(y)$, so putting together the Eqs. (4.89), (4.90) and the $L_n^m(y)$ polynomials back in the original coordinates the result of the normalized paraxial Helmholtz equation in cylindrical coordinates is [58]

$$U_n^m(\mathbf{r}) = \sqrt{\frac{2n!}{\pi\omega_0^2(n+m)!}}\left(\frac{\sqrt{2}\rho}{\omega(z)}\right)^m L_n^m\left(\frac{2\rho^2}{\omega^2(z)}\right)\exp(im\Phi)\exp(i\alpha(z))E(\mathbf{r}) \tag{4.96}$$

with $n = C/4 - m/2$ and so $\alpha(z) = (2n+m)\arctan\left(\frac{z}{2}\right)$, and the first term is a normalization

term to ensure the energy is finite and equal to 1.

Equation (4.96) is a solution to the paraxial Helmholtz wave equation and it is called a Laguerre-Gaussian beam (LG beam). It shares similar properties with the Gaussian beam because as we can notice this beam has the same parameters $w(z)$ and $R(z)$ defined in Section 4.3.2, which tells us under free space propagation or transformation by lens a beam of higher order like the LG beam will remain as a mode of the same order [16], exactly like it happens with a Gaussian beam.

4.3.3 Validity and inconsistencies of the paraxial approximation

Throughout this chapter, we have employed the paraxial approximation, and it was instrumental in the derivation of the Paraxial Helmholtz wave equation, which is why it is important to briefly talk about the region of validity of this approximation.

We have mentioned in Chapter 2 that any optical beam can be represented as the superposition of plane waves traveling at different angles with respect to the propagation axis. So if for simplicity we consider a 2-D case then we can write a plane wave traveling at angle θ to the z-axis as [59]

$$\begin{aligned} E(x,z) &= \exp\left[-ikx\sin\theta - ikz\cos\theta\right] \\ &= A(x,z)\exp[-ikz] \end{aligned} \tag{4.97}$$

where the amplitude A(x,z) is defined as

$$A(x,z) = \exp\left[-ikx\sin\theta - ikz(1-\cos\theta)\right] \tag{4.98}$$

to evaluate the validity of the paraxial approximation we shall apply it to the amplitude A(x,z) and rewrite it in the form

$$A(x,z) = \exp\left[-ik\theta x + ik\frac{\theta^2}{2}z\right] = \exp\left[-ik\left(x\theta - \frac{\theta^2}{2}z\right)\right] \tag{4.99}$$

Now we perform the corresponding first and second derivatives that appear in the paraxial

Helmholtz Eq. (4.56)

$$2ik\frac{1}{A}\frac{\partial A}{\partial z} \approx k^2\theta^2 \tag{4.100}$$

$$\frac{1}{A}\frac{\partial^2 A}{\partial x^2} \approx -k^2\theta^2 \tag{4.101}$$

If we remember the second derivative is related to the curvature of a path [60] then the second derivative of Eq.(4.101) can provide us with information about the magnitude of the angle θ.

$$\frac{1}{A}\frac{\partial^2 A}{\partial z^2} \approx -\frac{k^2\theta^4}{4} \tag{4.102}$$

We notice the right side of the Eq.(4.102) is smaller than Eqs. (4.100) and (4.101) by the ratio $\theta^2/4$ and to ensure this ratio is much smaller than one i.e. we stay under the limits of the paraxial approximations, we need that the next inequality is fulfilled

$$\theta < \frac{1}{2} \text{ radians} \tag{4.103}$$

With this, we guarantee that the $\frac{\partial^2 A}{\partial z^2}$ will be an order of magnitude smaller than either of the other terms [59], or in other words that the magnitude of the wave vector inclination angle will fall under the paraxial approximation.

Another path to verify the limits of the validity of the paraxial approximation is to center our attention on the beam radius function, the one given by the normalized Eq. (4.75), the minimum is found at the $z = 0$ plane, which is called beam waist and it increases monotonically with z and from the Figure 4.6 we can make the following approximation

$$\tan\theta_{MAX} = \frac{1 + \frac{z^2}{4}}{z} \tag{4.104}$$

and for $z \to \infty$ we will have

$$\tan\theta_{MAX} \approx \frac{1}{2} \approx \theta_{MAX} \tag{4.105}$$

which once again confirms the limits of the paraxial approximation. Moreover, for distances z much larger than the Rayleigh length the evolution of $w(z)$ will be linear with z [61], that is $w(z) \approx z\ \theta_{MAX}$, which from Eq. (4.105) translates to $w(z) \approx \frac{z}{2}$ and this is nothing more

than the asymptote to Eq.(4.75) which is perfectly illustrated in the Figure 4.6.

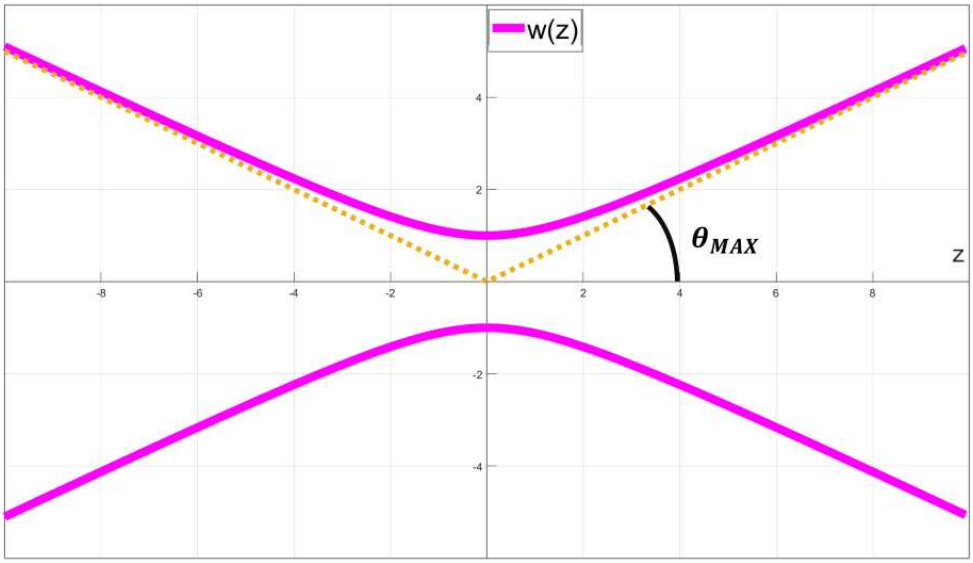

FIGURE 4.6: The Gaussian beam width. The yellow dotted line represents the asymptote to w(z).

However, even if we stay under the paraxial approximation we will find inconsistencies that sometimes can lead to inexact results, for example, if we once again pay attention to the function of the waist beam we will notice it represents the equation of hyperbole while the wavefronts of the Gaussian beam are represented by a paraboloidal equation which can be approximated by spheres under the paraxial approximation [61]. This is of relevance because hyperboles and paraboles (or spheres) are not perpendicular and if the direction of the energy flux density (hyperbole) is not perpendicular to the wavefronts (parabole) then one of the results of the electromagnetic theory in vacuum space (Eqs. (2.10 - 2.13)) is contradicted which tells the Poynting vector points in the propagation direction of the wave [62].

In most cases we can ignore this contradiction and the use of the paraxial approximation will provide accurate enough results. Still, we must be careful and not lose sight of the fact we are working ultimately with an approximation.

Chapter 5

Focusing Gaussian beams and Bessel beams

We have finally arrived at the main chapter of this work in which we explain the nature of the Bessel beams, and how their formation as interference of conical waves impacts the way they behave after passing through a converging thin lens. But first, we present in detail one last effect related to diffraction, the focal shift.

5.1 Focused fields and focal shift.

Born and Wolf studied the diffraction of a spherical monochromatic wave that passes through a circular aperture and converges towards the axial focal point, they did so through the Debye integral and established that the maximum irradiance of the diffracted field is found at the focal plane [63]. In this plane the field takes the form of the Airy disk which is expected from the Fraunhofer diffraction theory, as it was shown in the Section 4.2. However, Goubau, van Nie and Kogelnik [17, 64, 18] found that when focusing a Gaussian beam the maximum irradiance point does not correspond to the geometrical focus but to a point closer to the aperture which contradicts the established before.

The Debye integral is an approximation done to the Huygens-Fresnel integral which does not consider the nature of the aperture. Its boundary conditions are based on the Kirchhoff diffraction theory, which is why later Li and Wolf [65] showed that the Debye integral may not

always describe the diffracted field with enough accuracy as the Huygens-Fresnel treatment would do it, they found that for the case of an angular semi-aperture smaller than 45° the condition for the Debye treatment to be valid is to have the Fresnel number of the circular aperture to be larger than unity. Even further, they showed that this shift in the location of the maximum intensity with respect to the focal plane of a focused wave depends only on the Fresnel number of the aperture and it was called *focal shift* [66].

Their analysis draws from the Huygens-Fresnel principle applied to a general case of monochromatic, uniform, converging spherical wave, diffracted at an aperture of radius a in an opaque screen. Figure 5.1 shows the spherical wave being focused at an aperture, F is the geometrical focus, O is the origin, and P is an arbitrary point along the axis not too close to the aperture.

For this analysis two assumptions are necessary

$$a \gg \lambda \text{ and } \left(\frac{a}{f}\right) \gg 1 \tag{5.1}$$

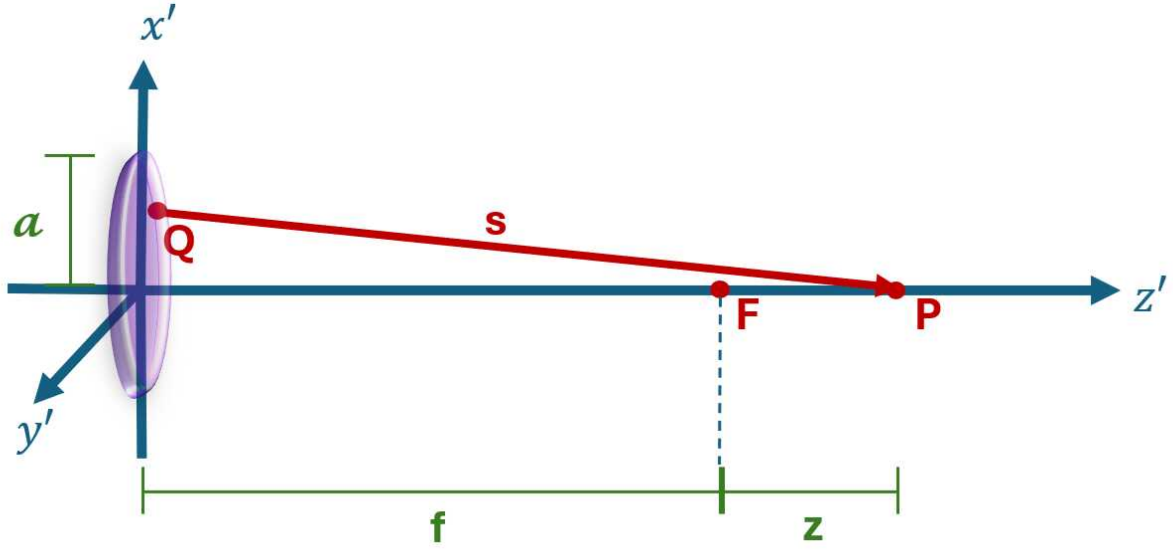

FIGURE 5.1: Schematic diagram of a converging spherical wave being focused after passing through an aperture of radius a.

The field at the point P is

$$E(P) = -\left(\frac{ik}{2\pi}\right)\frac{A\exp(-ikf)}{f}\iint_S \frac{\exp(iks)}{s}dS \tag{5.2}$$

Notice this integral is the Huygens-Fresnel principle defined by Eq.(4.36) with $E(P_1)$ being a converging spherical wave and $\cos\theta \approx 1$ because we are considering small angles (paraxial approximation) according to Eq. (5.1).

In Eq.(5.2) $s = \overline{QP}$ is the distance between the points P and Q, Q lies over the spherical wavefront product of the diffraction caused by the aperture, and it is defined as

$$s = [\rho^2 + (f + z - z')^2]^{1/2} \tag{5.3}$$

where

$$\rho^2 = x'^2 + y'^2 \tag{5.4}$$

is the square of the distance of the point Q from the z'-axis.

After some mathematical manipulation and the usage of the assumptions Eq.(5.1) the distance s can be approximated to

$$s \approx \left[(f+z)^2 - \left(\frac{z}{f}\right)\rho^2\right]^{1/2} \tag{5.5}$$

Thus the integral Eq.(5.2) takes the form

$$E(P) = -\left(\frac{ikA}{2\pi}\right)\frac{\exp(-ikf)}{f}\int_0^a\int_0^{2\pi}\frac{\exp\left\{ik\left[(f+z)^2 - \left(\frac{z}{f}\right)\rho^2\right]^{1/2}\right\}}{\left[(f+z)^2 - \left(\frac{z}{f}\right)\rho^2\right]^{1/2}}\rho d\rho d\phi \tag{5.6}$$

where ϕ is the azimuthal angle in the aperture plane. This integral can be solved with a

simple change of variable, and the explicit result for the field E(P) is

$$E(P) = -A\frac{\exp(-ikf)}{z} \times \left\{ \exp\left[ik(f+z)\left(1-\left(\frac{a}{f+z}\right)^2 \frac{z}{f}\right)^{1/2}\right] - \exp\left[ik(f+z)\right]\right\} \tag{5.7}$$

The expression Eq. (5.7) can be further simplified provided that the analysis is restricted to points P whose distance from the aperture is no less than $0.4f$ [66], therefore the field E(P) is reduced to

$$E(P) = A\frac{\exp(ikz)}{z}\left\{\exp\left[-\frac{1}{2}ik\left(\frac{z}{f}\right)\frac{a^2}{f+z}\right]-1\right\} \tag{5.8}$$

At the beginning of this section, we mentioned the Fresnel number of the aperture N is associated with the focal shift, so a definition of the Fresnel number is needed, namely

$$N_a = \frac{a^2}{\lambda f} \tag{5.9}$$

Now, before moving forward is necessary to state that Eq.(5.9) is a general expression for the Fresnel number. For example, if we consider the case of a Gaussian aperture then a will take the value of the waist of the Gaussian function i.e. $a = w$, which results in the Fresnel number of the Gaussian beam

$$N_w = \frac{w^2}{\lambda f} \tag{5.10}$$

Continuing with the mathematical derivation it is useful to rewrite argument of the Eq.(5.8) as follows

$$\begin{aligned} E(P) &= A\frac{\exp(ikz)}{z}\left\{\exp\left[-\left(\frac{i}{2}\right)\frac{a^2}{\lambda f}\left(2\pi\frac{z}{f+z}\right)\right]-1\right\} \\ &= A\frac{\exp(ikz)}{z}\left\{\exp\left[-\left(\frac{i}{2}\right)\left(2\pi N_a\frac{z}{f+z}\right)\right]-1\right\} \\ &= A\frac{\exp(ikz)}{z}\left\{\exp\left[-\left(\frac{i}{2}\right)u_N\right]-1\right\} \end{aligned} \tag{5.11}$$

where u_N is defined as

$$u_N = 2\pi N_a\frac{z}{f+z} \tag{5.12}$$

With Eq. (5.12) it is easier to show the relationship between the Fresnel number and the focal shift, and it is straightforward to obtain the expression for z in terms of u_N which will be useful later

$$z = \frac{u_N}{2\pi N_a - u_N} f \tag{5.13}$$

with both of these definitions Eq. (5.12) and (5.13), we may rewrite the expression for the field on point P as

$$E(P) = A\left(\frac{2\pi N_a - u_N}{f u_N}\right) \exp\left(\frac{ikf u_N}{2\pi N_a - u_N}\right) \left[\exp\left(-\frac{i}{2} u_N\right) - 1\right] \tag{5.14}$$

Now as was mentioned, the focal shift manifests as an apparent displacement of the point of maximum intensity from the geometrical focal point so to verify this we need to center our attention on the intensity of the field E(P)

$$I(P) = |E(P)|^2 \tag{5.15}$$

Substitution of the Eq.(5.14) into Eq.(5.15) gives as a result

$$I(P) = I_0 \left(1 - \frac{u_N}{2\pi N_a}\right)^2 \left[\frac{\sin\left(\frac{u_N}{4}\right)}{\left(\frac{u_N}{4}\right)}\right]^2 \tag{5.16}$$

where

$$I_0 = \left(\frac{\pi a^2 |A|}{\lambda f^2}\right)^2 \tag{5.17}$$

is the intensity at the geometrical focus F.

Additionally, it is well known that to find the point of maximum intensity along the axis one must find the roots of the derivative of the expression for the intensity, i.e.

$$\frac{\mathrm{d}I}{\mathrm{d}z} \equiv \frac{\mathrm{d}I}{\mathrm{d}u_N} \frac{\mathrm{d}u_N}{\mathrm{d}z} = 0 \tag{5.18}$$

Equation (5.18) is then satisfied for the solutions of any of the following three equations [66]:

$$\left(1 - \frac{u_N}{2\pi N_a}\right) = 0 \tag{5.19}$$

$$\frac{\sin\left(\frac{u_N}{4}\right)}{\left(\frac{u_N}{4}\right)} = 0 \tag{5.20}$$

$$\frac{\tan\left(\frac{u_N}{4}\right)}{\left(\frac{u_N}{4}\right)} = 1 - \frac{u_N}{2\pi N} \tag{5.21}$$

The Eq. (5.19) is never zero for any value of u_N, but we find the roots of Eq.(5.20) at the points:

$$u_N = \pm 4m\pi, \quad m = 1, 2, 3, ... \tag{5.22}$$

At these points, we found a minimum of intensity. For its part, Eq.(5.21) is a transcendental function, so to find the roots of the equation it is required to plot the two functions and locate the intersection points which is what we illustrate in Figure 5.2, the blue curve represents the function on the left side of the Eq.(5.21) and the orange line its right side.

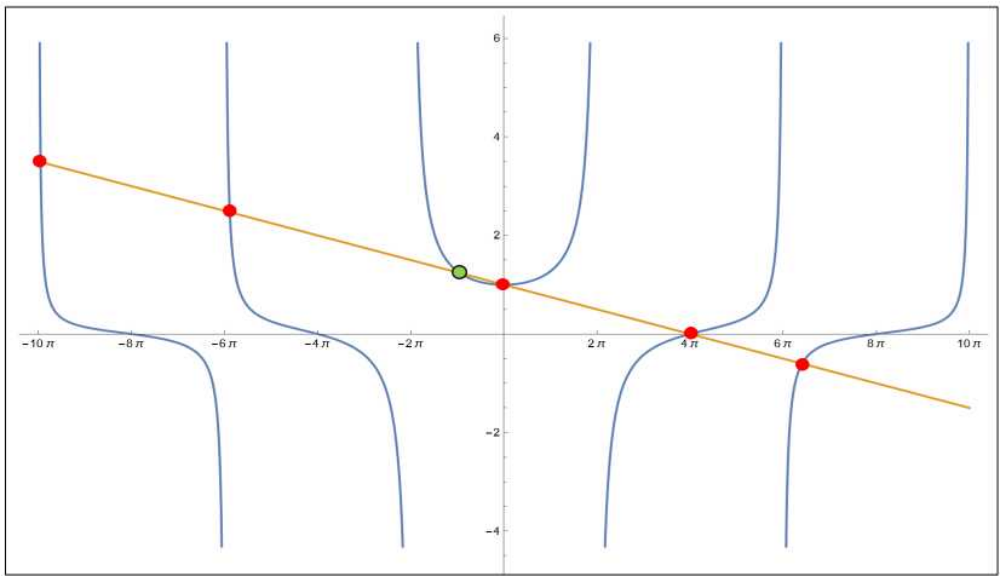

FIGURE 5.2: Roots of the transcendental function. The blue line is the function on the left side of the equation and the orange line represents its right side.

From Figure 5.2 we observe we have a root between each of the values given by Eq.(5.22), this tells us the roots of the transcendental function represents the maximal points of intensity. The greatest maximum intensity is located at the position u_N in the range $-2\pi < u_N < 0$ [66], marked by the green dot in Figure 5.2. The value of this green point can be found for different Fresnel numbers and using the expression for z defined in Eq.(5.13) we can calculate the value of the focal shift and its dependence with the Fresnel number, which is shown in

Figure 5.3. Figure 5.3 shows that when $N_a \leq 3$ the relative focal shift is bigger than 10% of

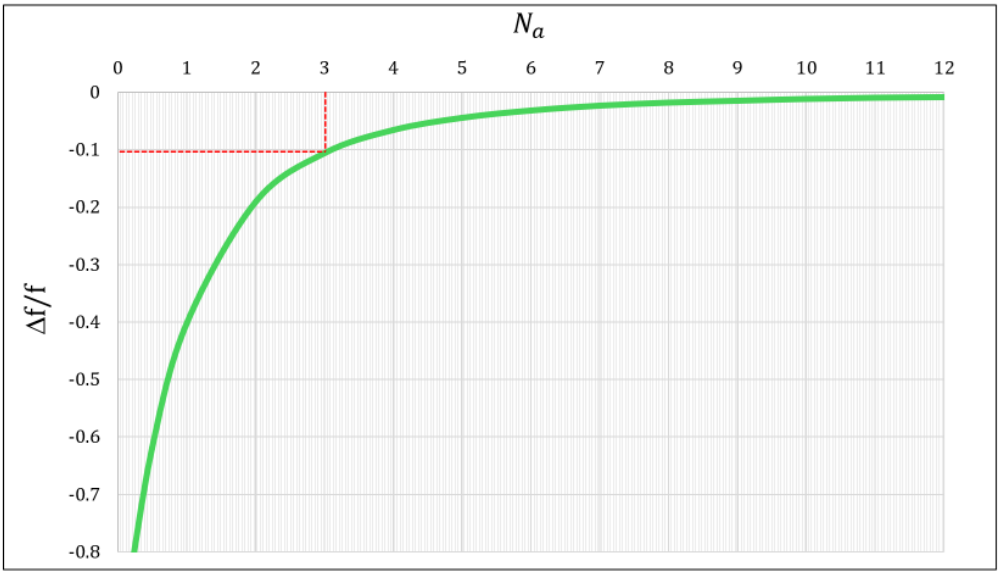

FIGURE 5.3: The relative focal shift $\Delta f/f$ vs. the Fresnel number of the aperture.

f, and as the Fresnel number increases this focal shift decreases. This tells us for very large Fresnel numbers the difference in intensity at the geometrical focus and the "real" focus is minimal. However, the main result of this analysis is the confirmation that the existence of the focal shift is a result of the aperture size, because if $a \to \infty$, i.e. no aperture, then the focal shifts tend to zero, as expected.

With the purpose of providing an expression to calculate the focal shift, we present an approximation done for small values of u_N.

For small values of u_N the Taylor series expansion of the tangent can be applied here

$$\tan\left(\frac{u_N}{4}\right) \approx \frac{u_N}{4} + \frac{1}{3}\left(\frac{u_N}{4}\right)^3 \tag{5.23}$$

Then when it is substituted in the transcendental Eq.(5.21) and solved for u_N it is found that the point on the axis where the intensity is maximum is

$$u'_N \approx -\frac{24}{\pi N} \tag{5.24}$$

This value is substituted in Eq. (5.13) to find the value of the focal shift, the reason why we

rename this specific value of z as Δf

$$z|_{u'_N} = \Delta f \quad \Rightarrow \quad \Delta f \approx -\frac{f}{1+\frac{\pi^2 N_a^2}{12}} \tag{5.25}$$

Notice that regardless of the value of the Fresnel number N the focal shift is always negative which tells us the shift is always towards the aperture. This formula calculates the focal shift of a focused spherical wave with enough accuracy for apertures whose Fresnel number N_a is greater than 12 [66] and it is very similar to the one found for the case of a focused Gaussian beam as we will see in the next section.

Additionally, emphasis on three important facts used to find the focal shift expression should be made, first, converging spherical waves were considered, two, we were concerned with finding the the diffracted field at a point P around the geometrical focal plane and three, we used the maximum intensity to find the position of the displacement. These three points are of relevance because if we look at Eq.(5.16) we will understand we calculated the diffraction pattern of the spherical wave that has passed through an aperture (lens) and then we were interested in the point where this diffraction pattern reached its maximum intensity, that is, the focal shift is related to the point where the diffracted field distribution is maximum and consequently, this displacement is a consequence of diffraction.

Another study about focused beams found a technique based on the Fourier transform to calculate the focal shift and applied it to annular beams and came to the same conclusion about the focal shift being always towards the aperture and its dependency on the value of the Fresnel number N_a with the addition that for annular beams the value of the ratio of the central obscuration plays a role too, more precisely if this ratio increases then the focal shift increases too [67], which further proves the focal shift as a diffraction related effect because it depends on the shape of the aperture.

5.2 Relation of Gaussian beams and ABCD Q-parameter

To study the transformations of a Gaussian beam when transmitted through an optical system it is often used the parameter Q and the ABCD matrix law.

In Chapter 4 we found the parameter Q when we obtained the amplitude distribution of a Gaussian beam and the definitions for its parameters that describe the beam properties such as the waist beam w(z) and radius R(z).

However, before proceeding to explain the ABCD method it is inevitable to clarify that from here on we will not be using the normalized definitions of the parameters because as we explained in the previous chapter while it has been proven to be easier to mathematically manipulate the expression in their normalized versions, there are circumstances where the problem gives results that are more directly understood using the standard definitions, which happens to be the case here.

5.2.1 Focusing of Gaussian beams: ABCD method

The ABCD law relates the Q-parameters of an incident (Q_1) and transmitted (Q_2) Gaussian beam through an optical system described by the transmission matrix ABCD [16], i.e.

$$Q_2 = \frac{AQ_1 + B}{CQ_1 + D} \tag{5.26}$$

Where A, B, C, D are the elements of the matrix. This equation describes the effects an optical paraxial system has on a Gaussian beam. For this section, we are interested in the effects of a thin lens of focal length f on Gaussian beams.

Figure 5.4 illustrates the case we will analyze, the incident Gaussian beam has a Q-parameter Q_1 which can be written as

$$\frac{1}{Q_1} = \frac{1}{R_1} - i\frac{\lambda}{\pi w_1^2 n} \tag{5.27}$$

If we consider the distance d_1 is the position where $R_1 \to \infty$, that is where the wavefront of the beam is plane then

$$\frac{1}{Q_1} = -i\frac{\lambda}{\pi w_1^2 n} = \frac{1}{iL_{D1}} \tag{5.28}$$

where $L_{D1} = \pi n w_1^2/\lambda$. With the use of the ABCD matrix method we can find the Q-parameter

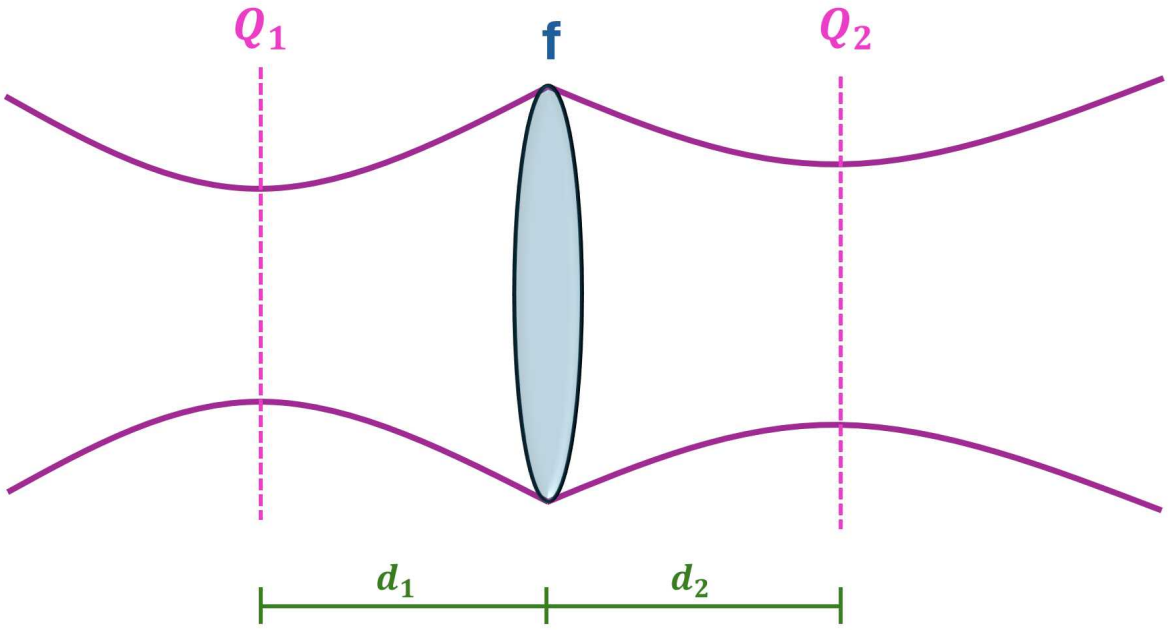

FIGURE 5.4: Diagram of a Gaussian beam transmitted through a thin lens of focal length f.

of the transmitted Gaussian beam (Q_2) when we consider the matrix to be

$$\begin{bmatrix} A & B \\ C & D \end{bmatrix} = \begin{bmatrix} 1 & d_2 \\ 0 & 1 \end{bmatrix} \begin{bmatrix} 1 & 0 \\ -\frac{1}{f} & 1 \end{bmatrix} \begin{bmatrix} 1 & d_1 \\ 0 & 1 \end{bmatrix} \tag{5.29}$$

The expression for Q_2 is found with the use of Eqs. (5.28) and (5.29):

$$Q_2 = \frac{ACL_{D1}^2 + BD + iL_{D1}}{(L_{D1}C)^2 + D^2} \tag{5.30}$$

To ensure the position d_2 marks the point of the minimum waist of the transmitted Gaussian beam, i.e. the position where the beam is focused, we need the real part of Eq.(5.30) to be zero. This condition leads us to the expression:

$$L_{D1} = -\frac{BD}{AC} \tag{5.31}$$

where according to Eq.(5.29), $A = 1-d_2/f$, $B = d_1+d_2-(d_1d_2/f)$, $C = -1/f$ and $D = 1-d_1/f$.

If we solve Eq.(5.31) for $d_2 - f$ we obtain

$$d_2 - f = \frac{(d_1 - f)f^2}{L_{D1}^2 + (d_1 - f)^2} \tag{5.32}$$

which represents the position of the minimum waist we were looking for. From Eq.(5.32), we can obtain the expression for the value of the transmitted beam waist

$$w_2^2 = \frac{w_1^2 f^2}{L_{D1}^2 + (d_1 - f)^2} \tag{5.33}$$

Eq. (5.32) is the same result H. Kogelnik found in 1965 [18], and it gives us the position of the waist of the transmitted Gaussian beam w_2 in terms of the distance the incident Gaussian beam is from the lens and the focal length of the latter.

If we consider the input Gaussian beam has its waist at the lens position, i.e. $d_1 = 0$ and use Eq.(5.32) to obtain the relative distance between the point where the Gaussian beam is focused and the geometrical focal point, we have that:

$$d_2 - f = \frac{-f^3}{L_{D1}^2 + (d_1 - f)^2} \tag{5.34}$$

It is straightforward to see the value of d_2 is then

$$d_2 = \frac{f}{1 + \left(\frac{L_{D1}}{f}\right)^2} = \frac{f}{1 + (\pi n N_w)^2} \tag{5.35}$$

Notice the denominator is always a positive quantity and because we are considering distances here the Eq.(5.35) tells us the Gaussian beam is not focused at the geometrical focal plane of the lens but at the shorter distance and closer to the lens, that is, Eq.(5.35) is the focal shift of a Gaussian beam obtained with the use of the ABDC method. Further, note we have written L_{D1} in terms of the Fresnel number of the Gaussian beam Eq. (5.10) to explicitly show the focal shift obtained in Section 5.1 (Eq. (5.25))is indeed similar to the one obtained here.

Other approaches to this subject can be made by taking the Hyugens-Fresnel integral

as a starting point and instead of using the Q-parameter the attention is centered on the apertures, this approach provides a more general analysis of the problem and highlights once again the focal shift is due to the presence of apertures, soft or hard, which is why the following section is dedicated to this subject.

5.2.2 Focal shift of a Gaussian beams.

Focal shift on-axis.

In Section 5.1, we established the definition and analytical expression of the focal shift, but for this section, we center our attention on the particular case of the focal shift experimented by an apertured Gaussian beam.

The process of finding the analytical expression is analogous to the general case in Section 5.1 with the obvious difference that the field that emerges from the focusing lens is expressed as a monochromatic Gaussian beam

$$E(\rho, z) = A \exp\left(-\frac{\rho^2}{w^2(z)}\right) \frac{\exp(ikf)}{f} \tag{5.36}$$

where the periodic time-dependent factor has been omitted and the last term represents the spherical converging wave created by the focusing lens. The waist of the beam is located in the plane of the lens.

The field is inserted into the Huygens-Fresnel integral Eq.(4.36) to find the diffracted field at an arbitrary point P on the propagation axis around the focal plane

$$E(P) = -\left(\frac{ik}{2\pi}\right) \frac{A\exp(-ikf)}{f} \iint_S \exp\left(-\frac{\rho^2}{w^2}\right) \frac{\exp(iks)}{s} dS \tag{5.37}$$

where similarly to Section 5.1, s is the distance between the point Q on the reference plane and the P the observation point along the axis (see Figure 5.1), defined as

$$s = [\rho^2 + (f + z - z')^2]^{1/2} \tag{5.38}$$

where

$$\rho^2 = x'^2 + y'^2 \tag{5.39}$$

is the square of the distance of the point Q from the z'-axis. The expression for s can be approximated for paraxial waves to [68]

$$s \approx \left[(f+z)^2 - \left(\frac{z}{f}\right)\rho^2 \right]^{1/2} \tag{5.40}$$

Further, Eq.(5.40) can be expanded into a power series:

$$s \approx (f+z)\left[1 - \frac{1}{2}\left(\frac{\rho}{f+z}\right)^2 \left(\frac{z}{f}\right) - \frac{1}{8}\left(\frac{\rho}{f+z}\right)^4 \left(\frac{z}{f}\right)^2 - ... \right] \tag{5.41}$$

However, two different approximations are considered for the second term that accompanies the Gaussian term in the integral Eq. (5.37). The s on the denominator is approximated by the first term of Eq. (5.41) and the s on the exponential function by the first two terms of the powers series.

For the approximation done in the denominator to be valid, the first term of the expansion has to be smaller than unity, which leads to the condition [68]:

$$z > -0.5f \tag{5.42}$$

This tells us, that the results we obtain with the first approximation are accurate for points P whose distance from the focal plane is at least half of the focal length and not closer than that.

For the second approximation, the following condition must be met to ensure it is valid:

$$\left| \frac{k}{8}\left(\frac{\rho}{f+z}\right)^4 \left(\frac{z}{f}\right)^2 \right| \ll 2\pi \tag{5.43}$$

which rewritten in terms of the Fresnel number of the aperture (Eq.(5.9)) yields:

$$\left(\frac{a}{f}\right)^2 \ll \frac{8}{N_a}\left[\frac{\left|1+\frac{z}{f}\right|^3}{\left(\frac{z}{f}\right)^2}\right] \tag{5.44}$$

But the paraxial wave approximation marks that of $(a/f)^2 \ll 1$, so the equation we need to solve to obtain the range of validity of the second approximation is

$$1 = \frac{8}{N_a}\left[\frac{\left(1+\frac{z}{f}\right)^3}{\left(\frac{z}{f}\right)^2}\right] \tag{5.45}$$

where we have already considered $z > -f$, we solve Eq.(5.45) numerically and find a solution $K(N_a)$ that depends on the Fresnel number. The plot of this function is presented in Figure 5.5, alongside the line $z/f = -0.5$ from Eq.(5.42). So the second condition to ensure the

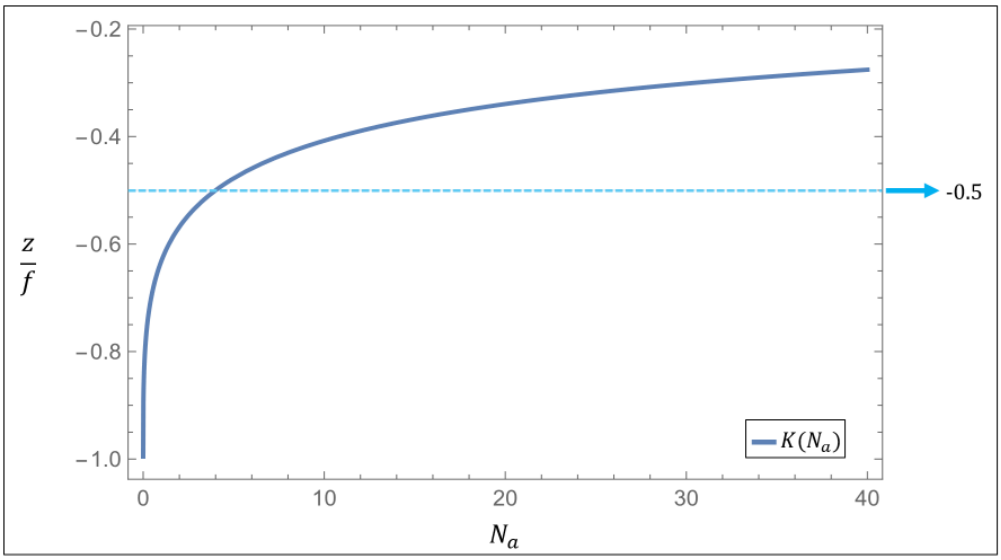

FIGURE 5.5: The region of validity is the space above both of the curves, specified by the Eqs.(5.42) and (5.45).

results we obtain with the approximations are accurate is

$$z \geq K(N_a) f \tag{5.46}$$

Thus provided the inequalities of Eq.(5.42) and (5.46) hold and after long calculations, it is possible to find the field on the P on-axis [68]

$$E(P) = iA\left(\frac{\pi N_a - u}{f}\right)\exp\left(ikf\frac{u}{\pi N_a - u}\right)\frac{\exp(-\alpha - iu) - 1}{\alpha + iu} \tag{5.47}$$

where N is the Fresnel number of the aperture defined in Eq.(5.9) and α is the coefficient of truncation of the Gaussian beam

$$\alpha = \left(\frac{a}{w}\right)^2 \tag{5.48}$$

and u is a dimensionless parameter dependent on the variable z, analogous to Eq.(5.12).

$$u(z) = \frac{\pi N_a z}{f + z} = \frac{u_N}{2} \tag{5.49}$$

The intensity at the point P will be [68]

$$I(P) = I(F)\left(1 - \frac{u}{\pi N_a}\right)^2 \frac{\alpha^2}{\alpha^2 + u^2}\frac{\cosh\alpha - \cos u}{\cosh\alpha - 1} \tag{5.50}$$

where

$$I(F) = \left(\frac{\pi|A|}{f}\right)^2 [1 - \exp(-\alpha)]^2 N_w^2 \tag{5.51}$$

represent the intensity at the lens plane and N_w is the Fresnel number of the waist of the incident Gaussian beam defined by Eq. (5.10).

In a similar way as in the case presented in Section 5.1, the mathematical procedure leads to a transcendental equation that can be solved numerically to find the location u_M of the principal maximum in intensity, substituting this principal root u_M into Eq.(5.49) the expression for the relative focal shift of the Gaussian beam case reads as [68]

$$\Delta f = f\frac{u_M}{\pi N_a - u_M} \tag{5.52}$$

To better analyze the correlation between the focal shift and the Fresnel numbers it is useful

to redefine the coefficient of truncation as

$$\alpha = \frac{N_a}{N_w} \tag{5.53}$$

this will allow us to examine two limiting cases, the first one happens when $\alpha \gg 1$ which translates to

$$N_a \gg N_w \tag{5.54}$$

From the definitions of both Fresnel numbers, it is straightforward to see this inequality happens when the radius of the aperture is larger than the waist of the Gaussian beam, which is referred to as weak truncation. For this case, the focal shift depends majorly on the Fresnel number of the beam.

Additionally, for this case, the focal shift of the Gaussian beam can take the following form [68]

$$\Delta f = -\frac{f}{1 + \pi^2 N_w^2} \tag{5.55}$$

which happens to be basically the same as Eq.(5.25).

The opposite case is when $\alpha \ll 1$ and then we have

$$N_a \ll N_w \tag{5.56}$$

for this case the waist of the Gaussian beam is larger than the aperture radius, this is called strong truncation, and contrary to the previous case the focal shift will depend mainly on the Fresnel number of the aperture. When the waist w tends to infinity we obtain the same case presented in Section 5.1.

In summary, we calculated the diffracted field of a Gaussian field that has passed through an aperture (lens) and then found the point of maximum intensity because once again, diffraction produces a focal shift and this effect is the relative displacement of the diffracted pattern with respect to the geometric focal point. The question that arises now is if this focal shift happens for beams whose propagation axis is tilted.

Focal shift of tilted off-axis of beams.

The focal shift is present in off-axis cases as well, and it also depends on the Fresnel numbers, as expected. This means that regardless of the focusing set-up used, the amplitude distribution of the beam, or the tilt angle if one beam has the same Fresnel number as another they are both going to suffer the same focal shift [69].

If we consider an off-axis focusing, monochromatic beam with an amplitude distribution given by a real function $p(r_0, \phi_0)$ we can find the intensity distribution along a tilted chief axis characterized by the variable θ. For this approach, the scalar paraxial approximation was used, and the Fresnel diffraction formula for this case yields [69]

$$I(z) = \left[\frac{2\pi}{\lambda f(z+f)}\right]^2 \left|\int_0^\infty t(r_0) \exp\left[-2\pi \frac{z}{2\lambda f(z+f)} r_0^2\right] r_0 dr_0\right|^2 \tag{5.57}$$

where z denotes the on-axis coordinate and

$$t(r_0) = \frac{1}{2\pi} \int_{-\pi}^{\pi} p_r(r_0, \phi_0) \exp\left[-i2\pi r_0 \frac{\sin\alpha}{\lambda} \sin(\phi_1 + \phi_0)\right] d\phi_0 \tag{5.58}$$

with

$$p(r_0, \phi_0) = p(r_0 \sin\phi_0, r_0 \cos\phi_0) \tag{5.59}$$

here $p(r_0, \phi_0)$ represents the amplitude distribution of the beam at the x_0-y_0 plane, for this formulation this function acts as the aperture function as well. The angle ϕ_0 and r_0 are the azimuthal and radial coordinates in circular coordinates of the reference place respectively, and ϕ_1 is the azimuthal coordinate that locates the focus point on the chief axis. This is illustrated in the Figure 5.6. To find an expression for the relative focal shift along the tilted axis with respect to the off-axis focal point the Eq.(5.57) is expanded into a Taylor series around the focal point from which it is possible to determine the position of maximum intensity which leads to the expression [69]:

$$\Delta f = -\frac{f}{\pi^2 N_g^2} \tag{5.60}$$

where the parameter N_g is referred to as the generalized Fresnel number whose main differ-

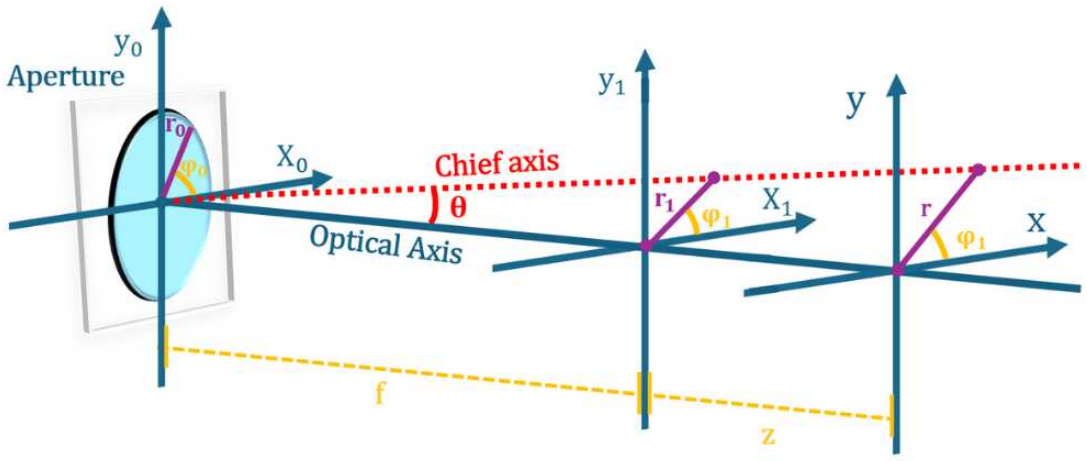

FIGURE 5.6: Schematic representation of the focusing set-up.

ence from the previous definitions is the use of the standard deviation of the function $t(\sqrt{r_0})$ denoted by σ

$$N_g = \frac{\sigma}{\lambda f} \tag{5.61}$$

where σ is given by

$$\sigma = \left[\frac{m_2}{m_0} - \left(\frac{m_1}{m_0}\right)^2\right]^{1/2} \tag{5.62}$$

with

$$m_n = 2\int_0^\infty t(r_0) r_o^{2n+1} dr_0 \tag{5.63}$$

From Eq.(5.60) it is evident the displacement produced by the focal shift is the same for beams with the same Fresnel number regardless of the focal point laying on-axis or off-axis, because the equation does not depend on the tilted factor θ. Additionally, notice from the definition of expression of the focal shift for off-axis cases that the negative sign confirms that the point of maximum irradiance along the chief axis is closer to the aperture, which was expected.

Now that we understand the concept of focal shift, we can move on to the definition of Bessel beams, and their focusing properties where we explain further how the effect of focal shift is not related to the maximum in intensity found when propagating this beam.

5.3 Bessel beams, description as traveling waves

In 1987, J. Durin presented a solution to the wave equation in free-space that represented what he called diffracted-free beams, the simplest one being the Bessel beam. He defined the amplitude of this kind of beam in the form [19]:

$$\begin{aligned} E(\mathbf{r},t) &= \exp\left[i(k_z z - \omega t)\right] \int_0^{2\pi} \exp\left[ik_r(x\cos\phi + y\sin\phi)\right] \frac{\mathrm{d}\phi}{2\pi} \\ &= \exp\left[i(k_z z - \omega t)\right] J_0(k_r \rho) \end{aligned} \tag{5.64}$$

Where $\rho^2 = x^2 + y^2$ and J_0 is the zeroth-order Bessel function of the first kind.

This Helmholtz wave equation solution is exact and considered to be impractical for real-life applications, as such, the study of Bessel beams is centered in the apertured kind. However, regardless of the transverse limitation applied to the Bessel function of zeroth-order, these beamlike waves undergo minimal spreading due to diffraction in comparison with other wave propagation like Gaussian beams [21, 70]. which is why the Bessel beams are still to this day referred to as "diffraction-free", but we will see that in reality, these beamlike waves are a result of the interference of fundamental waves and not per-see beams.

An interpretation of the Bessel beam that provides a complete formalism to explain the nature of the beamlike structure, it describes these beams as the superposition of fundamental solutions of the wave equation with cylindrical symmetry [25].

From Chapters 2 and 3 we know that to find the solution of the wave equation in cylindrical coordinates we use the method of separation of variables which leads to the Bessel differential equation of order zero for the variable r.

$$\frac{\mathrm{d}^2 H}{\mathrm{d}r^2} + \frac{1}{r}\frac{\mathrm{d}H}{\mathrm{d}r} + k_r^2 H = 0 \tag{5.65}$$

Whose general solution is the Hankel functions Eqs. (3.32) we represented in Section 3.1.3. Here we have conveniently changed the nomenclature from R(r) to H(r) in Eq. (5.65).

Most times only one of the two functions of the Hankel equation is considered as the solution, however, neither the Bessel function nor the Neuman function satisfies the Sommerfeld radiation condition, which as we explained in Chapter 4 states that no waves incoming from

infinite sources contribute to the field amplitude distribution. This tells us we can not use these solutions separately to describe the propagation of light and that the general solution to the wave equation is a linear combination of both equations, the Bessel and the Neuman. The main reason for many authors ignoring the second solution of the differential equation is the singularity at the origin ($r = 0$) as illustrated in Figure 5.7, but soon we will see this feature has a physical explanation. Furthermore, we also established in Section 3.1.3 that the general solution of the wave equation in cylindrical coordinates is the superposition of two conical traveling waves (see Eq. (3.34)). In other words, the correct solution of the wave equation in cylindrical coordinates must be the Hankel equations.

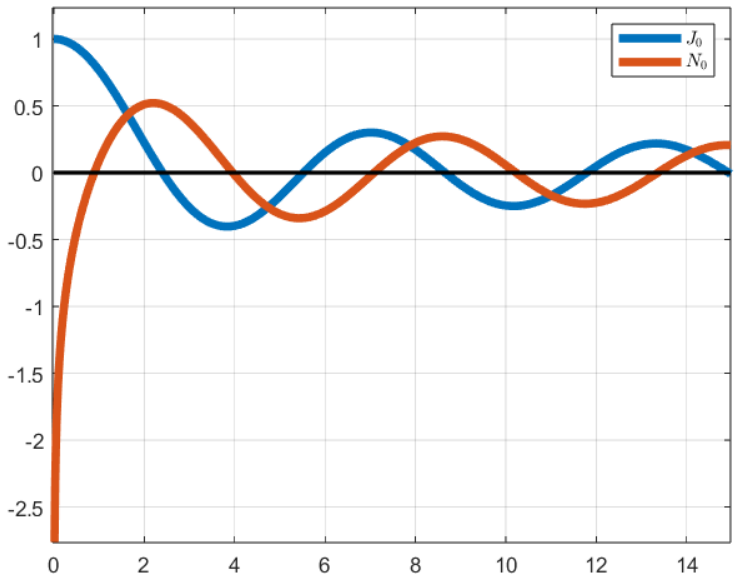

FIGURE 5.7: Bessel function of the first kind and second kind, both of order *0*.

In [25] the method of characteristics is used to obtain the characteristic surfaces to have a geometrical interpretation of the Hankel solutions because as we established in Chapter 3 these constant phase surfaces are related to the wavefronts of the beams.

The equation of characteristics surfaces associated with the wave equation in cylindrical coordinates is then

$$\left(\frac{\partial \varphi}{\partial r}\right)^2 + \left(\frac{\partial \varphi}{\partial z}\right)^2 - \frac{1}{v^2}\left(\frac{\partial \varphi}{\partial t}\right)^2 = 0 \tag{5.66}$$

In this case the phase φ has the value of $\varphi = \pm k_r r + k_z z - \omega t =$ constant so the Eq.(5.66) is

rewritten as

$$\left(\frac{\partial t}{\partial r}\right)^2 + \left(\frac{\partial t}{\partial z}\right)^2 = \frac{1}{v^2} \tag{5.67}$$

The solution of this equation is the conic surface $\varphi = r^2 + (z - z_0)^2 + v^2(t - t_0)^2 = 0$ and the vertex $(0,\ z_0,\ t_0)$ is the singular point of the surface. This result supports the fact that the wavefronts of the solutions of the wave equation in cylindrical coordinates are conic. So following the solution obtained through the method of separation of variables, the fundamental solutions of the wave equation with cylindrical symmetry are [25]

$$E_{out}(r, z, t) = [J_0(k_r r) + iN_0(k_r r)] \exp(ik_z z - i\omega t) \tag{5.68}$$

$$E_{in}(r, z, t) = [J_0(k_r r) - iN_0(k_r r)] \exp(ik_z z - i\omega t) \tag{5.69}$$

The nomenclature $E_{out}(r, z, t)$ and $E_{int}(r, z, t)$ represents an outgoing conic wave and an incoming wave respectively, both with its origin as the z-axis. This behavior is deduced from the method of characteristics which indicates a positive solution with an outward-pointing normal vector and a negative solution with an inward-pointing normal vector.

Notice that since the z-axis is the origin for both solutions, $E_{in}(r, z, t)$ becomes $E_{out}(r, z, t)$ after passing through it. As a result of keeping the complete general solution of the wave equation, the outgoing Hankel waves of Eqs. (5.68) and (5.69) satisfy the Sommerfeld radiation condition as $r \to \infty$ [25].

For the purpose of providing a physical explanation of the singularity that we talked about before we make the dependence on z zero ($k_z = 0$) and the attention is centered in the cylindrical case (r,t). Now the fundamental solution, the Hankel function, is formed by a non-singular term (Bessel function) and a singular one (Neumann function), as we mentioned at the start of the section the latter is often ignored under the statement of considering only "real" solutions however while it is correct to say any linear combination of the Bessel and Neuman functions is a solution to the wave equation, we are interested in the one given by Eqs.(5.68) and Eq.(5.69), which represent cylindrical wavefronts collapsing and being created at the longitudinal z-axis because the general solution must represent traveling waves, and it is precisely this source-sink duality of the solution which gives rise to the physical singularity

[25].

Additionally, taking into account the last part it is logical to assume the linear combination creates a region where the resulting standing waves exist, i.e. there is a region where the Hankel waves superpose. So when E_{in} and E_{out} are added the singular parts are canceled leaving only the Bessel function.

$$E_{in}(r,z,t) + E_{out}(r,z,t) = 2J_0(k_r r)\exp(ik_z z - i\omega t) \tag{5.70}$$

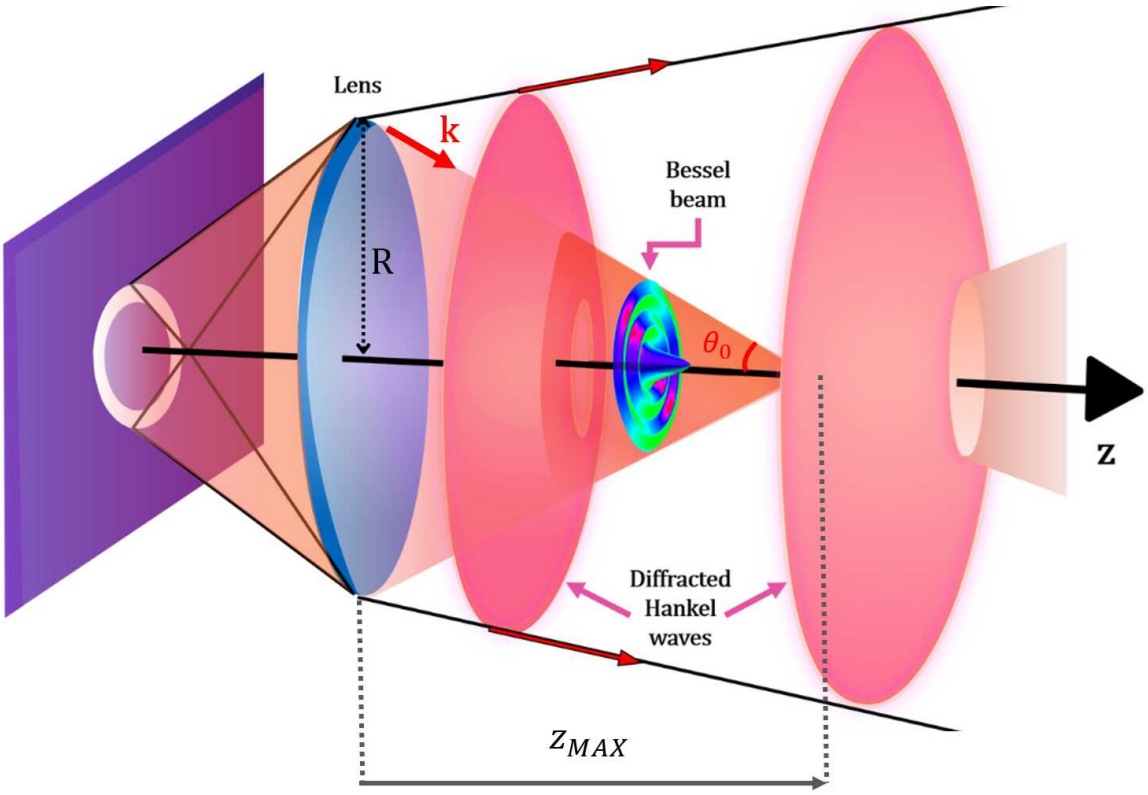

FIGURE 5.8: Esquematic diagram of the region of existence of the Bessel beam.

This equation tells us the Bessel beams are the result of the superposition of conic traveling waves. Another important result from Eq. (5.70) is the fact the incoming waves that form the solution should be produced at a finite distance from the z-axis in order to satisfy the Sommerfeld radiation condition and consequently, the Bessel beam must exist in a finite transverse $x-y$ space [25], contrary to what the general interpretation of the Bessel beams states.

Now, from a geometrical perspective, the conic nature of the traveling waves means the

interference region of both Hankel waves is conic and it is within this region where the Bessel beam exists which agrees well with the literature [19]. Outside this cone of interference, we have an outgoing diffracted Hankel wave as illustrated in Figure 5.8. The semi-angle of the cone of existence is given by $\tan\theta_0 = k_r/k_z$, and this value, as well as the radius aperture R of the generating system, describes the range of existence of the Bessel beam, that is $z_{MAX} = R/\tan\theta_0$ [19, 25]. Within the cone region, the light would appear to travel parallel to the optical axis z, since instantaneously it forms a transverse stationary wave in space [26].

However, we must not lose sight of the conical waves that created those standing waves, these are traveling in a direction dictated by the cone of wave vectors. This fact explains one of the apparently non-physical features that the Bessel beams have, the self-healing property, since the light that "self-reconstructs" was not blocked by the opaque object [26].

Further, from Figure 5.8 it is obvious the outgoing Hankel wave is subjected to diffraction, and the energy of the system is lost as a consequence. However, simulations have proved Bessel beams can be created with finite energy [25].

Lastly, this description of the Bessel beams helps us understand the propagation of apertured Bessel beams. The aperture function modulates the Hankel waves that constitute the beam, and this function is subjected to diffraction effects which will impact on the propagation of the conical waves. Outside the cone of existence, the outgoing Hankel wave will be modulated by the diffraction pattern of the aperture function, and within the cone, the diffraction pattern of the aperture function follows the path of the conical waves, i.e. we have a modulating function traveling along an off-axis direction.

5.3.1 Whittaker integral and propagation invariant beams: interference of conical waves.

Whittaker found that a solution of the Helmholtz wave equation that represents non-diffracting optical field can be written as a plane wave expansion [71]

$$E(x,y,z) = \exp(ik_z z)\int_{-\pi}^{\pi} A(\varphi)\exp\left[ik_t\left(x\cos\varphi + y\sin\varphi\right)\right]d\varphi \tag{5.71}$$

this equation is a reduced form of the integral Whittaker proposed, where $A(\varphi)$ is a complex function corresponding to the frequency spectrum where the set of wavevectors have the same angle $\theta_0 = \arctan(k_z/k)$ with respect to the propagation axis and the tips lie on a circular delta of radius k_r, for this reason it can be called the annular spectrum [29]. The annular spectrum is responsible for the transverse structure of the field when $A(\varphi) = \exp(im\varphi)$ the field E(x,y,z) is a mth-order Bessel beam $J_m\left(k_r r \exp(im\varphi)\right)$. If $A(\varphi) = 1$ then a Bessel function is obtained

$$J_0(x, y) = \int_{-\pi}^{\pi} \exp\left[ik_t\left(x\cos\varphi + y\sin\varphi\right)\right] d\varphi \tag{5.72}$$

This equation tells us the Bessel beam is formed by multiple tilted plane waves, and each wave vector of these plane waves lies on a cone, and when we spin the plane waves around the z-axis we obtain a conical wavefront [26] as illustrated in Figure 5.9a. This mathematical interpretation agrees with the stated in the previous section because then we can conclude the wave vectors form a cone with two conic wavefronts associated, one incoming and the other outgoing, this is illustrated in Figure 5.9b. In the last section, we explained why these traveling conical waves are fundamental when talking about the propagation of diffraction-free beams.

But to further explain this last part, we shall start with a simple example, the superposition of two tilted plane waves which results in a cosine interference pattern. This interference pattern presents a change of phase of π because we have dark and bright fringes. If we pay attention only to this pattern ignoring the plane waves that formed it we can consider it a "cosine beam" that propagates parallel to the z-plane and it is diffraction-free within a delimited region, but this interpretation is erroneous. The light is traveling following an off-axis direction, the plane waves are the ones propagating and the cosine beam is merely the interference of them, i.e. the cosine beam is a transverse stationary wave in space. This same logic is applied to the Bessel beam case and other families of invariant beams. In summary, the most important result of these two last sections is that Bessel beams are the result of the interference of two traveling conical waves.

At this point, one could say it has been proved enough that Bessel beams are not rig-

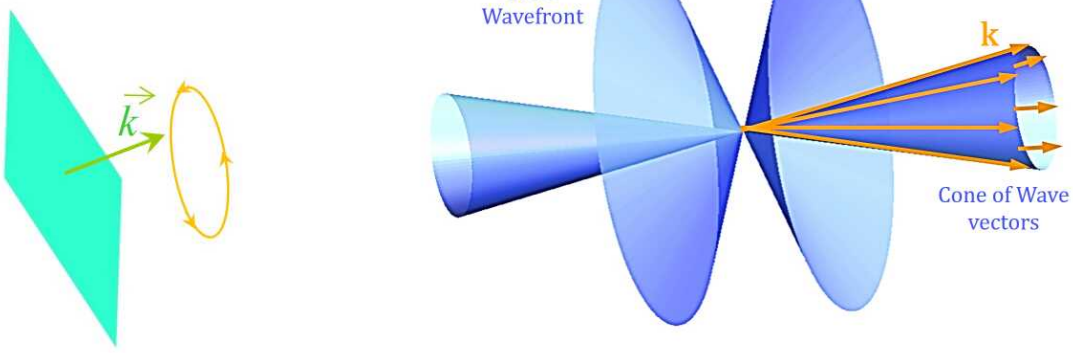

(A) Each plane has associated a wavevector whose tips lie on a circle.

(B) Rotating the wave vectors two conic surfaces are created, these represent the conical wave fronts.

FIGURE 5.9: Cone of wavevectors of the Bessel beam with its associated conic wavefronts.

orously speaking diffraction-free beams nonetheless the Bessel function is indeed a solution of the Helmholtz equation, the same as the Gaussian beam we talked about in Chapter 4 however we must talk about the reason behind the latter is affected by diffraction and not the former, at least mathematically speaking.

If we recall from Section 4.3.1 to find the amplitude distribution of the Gaussian beam Eq. (4.74) we established as an initial condition a Gaussian function Eq.(4.64), physically this represents an aperture, a soft one, and thus Gaussian beams suffer diffractive spreading because as we clarified in Section 4.1 the diffraction is produced by an aperture or obstacle.

In Durin's case when he proposed the Bessel beams as a solution to the Helmholtz equation no initial conditions were imposed, i.e. his solution is for free open space. Another well-known solution in free open space is the plane waves, as we saw in Chapter 3, which also happen to be considered of infinite energy as Durin himself stated, but analogous to what happens with Bessel beams, in both cases, this happens due to the lack of consideration about the limitations in space of the source, that is, Durin solved the Helmholtz equation without physical transversal limits. Additionally, he does not take into account the Rayleight-Sommerfeld radiation condition we explicated in Chapter 4, which tells us we cannot consider infinite sources. Thus, his mathematical result is not incorrect but calling this solution "diffraction-free" is. This erroneous interpretation of the Bessel beams is one of the examples

we referred to in Chapter 4 when we mentioned the importance of understanding the origin of the diffraction theories.

5.4 Focusing of Bessel beams.

Now that we have established Bessel beams in terms of constituent conical waves represented by Hankel functions and explained how the aperture function will modify these conic waves we will center our attention on the focusing characteristics of apertured Bessel beams.

When a Bessel beam passes through a lens the conical waves converge into a ring structure in the geometrical focal plane, as we will demonstrate in the first section of this chapter. Still, it has been proved before that if we follow the focusing evolution of the traveling conical waves it can be found a position behind the focal plane where the axial and transverse intensities of the beam reach a maximum value, this point can be viewed as a pseudo-focal point for the Bessel beams [28, 29, 30].

Furthermore, a geometrical approach can be applied to find the analytical expression for the position of the pseudo-focal point, the axial intensity, and the transverse magnification of the Bessel beam to have its complete tridimensional characterization.

5.4.1 Bessel beam at the focal plane.

While we cannot find analytically an expression that describes the propagation of a Bessel beam that has passed through a thin lens, we can find the diffracted field of the apertured Bessel function at the focal plane, which is what we will do next, but before doing that we present the normalization of the Fresnel integral we obtained in Section 4.2.

From Eq.(4.44) the standard Fresnel integral is

$$E(x,y,z) = \frac{\exp(ikz)}{i\lambda z}\exp\left[i\frac{k}{2z}(x^2+y^2)\right]\iint_{-\infty}^{\infty}\left\{E(x',y',z=0)\exp\left[i\frac{k}{2z}\left(x'^2+y'^2\right)\right]\right\} \times \exp\left[-\frac{ik}{z}\left(xx'+yy'\right)\right]dx'dy' \tag{5.73}$$

to normalize it we propose a new set of variables scaled to w and the Rayleigh lenght:

$$\xi = \frac{x'}{w},\ \eta = \frac{y'}{w},\ \zeta = \frac{z}{L_D} \tag{5.74}$$

and so the Eq.(5.73) can be rewritten as

$$\begin{aligned} E(\xi,\eta,\zeta) = \frac{\exp(i\kappa\zeta)}{i\pi\zeta}\exp\left[i\frac{1}{\zeta}(\xi^2+\eta^2)\right]\iint_{-\infty}^{\infty}\left\{E(\xi',\eta',0)\exp\left[i\frac{1}{\zeta}\left(\xi'^2+\eta'^2\right)\right]\right\} \\ \times\exp\left[-\frac{2i}{\zeta}\left(\xi\xi'+\eta\eta'\right)\right]d\xi' d\eta' \end{aligned} \tag{5.75}$$

where $\kappa = (kw/\sqrt{2})^2$.

Now, making the change to cylindrical coordinates is straightforward if we consider a radially symmetric light field and define the following variables

$$\rho = \xi^2+\eta^2,\ \xi = \rho\cos\varphi,\ \eta = \rho\sin\varphi \tag{5.76}$$

further we can use this integral of the Bessel function

$$\int_0^{2\pi}\exp[-i\alpha\cos(\varphi-\phi)]d\varphi = 2\pi J_0(\alpha) \tag{5.77}$$

Which leads to the reduced Normalized Fresnel Integral in cylindrical coordinates

$$E(\rho,\zeta) = \frac{-i}{\pi\zeta}\exp[i\kappa\zeta]\exp\left[\frac{i\rho^2}{\zeta}\right]\int_0^{\infty}E(\rho',0)\exp\left[\frac{i\rho'^2}{\zeta}\right]J_0(k_{rn}\rho')\rho' d\rho' \tag{5.78}$$

where $k_{rn} = 2\rho/\zeta$. Now if we remember Section 4.2, the Fresnel integral becomes the Fraunhofer diffraction integral when a lens is introduced, for that reason, we consider an incident field of the form:

$$E(\rho',0) = E_1'(\rho',0)\exp(-\frac{i\rho'^2}{f_N}) \tag{5.79}$$

where $f_N = f/L_D$ is the normalized focal length.

We substitute Eq.(5.79) into Eq.(5.78), and translate the variable ζ to the focal plane,

i.e. $\zeta = f_N$, to obtain the normalized Fraunhofer diffraction integral:

$$E(\rho, \zeta = f_N) = \frac{-i}{\pi f_N} \exp\left(\frac{i\kappa}{\zeta}\right) \exp\left(\frac{i\rho^2}{f_N}\right) \int_0^\infty E_1^{'}(\rho^{'}, 0) J_0\left(\frac{2\rho\rho^{'}}{f_N}\right) \rho^{'} d\rho^{'} \tag{5.80}$$

which analogously to Eq.(4.46) this integral represents a Hankel Transform.

If we define $k'_\rho = 2\rho/f_N$ we can rewrite last integral as

$$E(\rho, f_N) = \frac{-i}{\pi f_N} \exp(i\kappa\zeta) \exp\left(\frac{i\rho^2}{f_N}\right) \int_0^a E_1^{'}(\rho^{'}, 0) J_0(k'_\rho \rho^{'}) \rho^{'} d\rho^{'} \tag{5.81}$$

With Eq.(5.81) we can find the diffracted field of an apertured Bessel beam, but as we mentioned in Section 4.2 the information about the geometry of the aperture is contained in the field $E(\rho', 0)$ which we define as:

$$\begin{aligned} E'_1(\rho^{'}, 0) &= T\left(\frac{\rho'}{a}\right) J_n\left(\frac{a k'_T \rho^{'}}{a}\right) \\ &= \begin{cases} J_n\left(\frac{a k'_T \rho^{'}}{a}\right), & |\rho^{'}| < a \\ 0, & |\rho^{'}| > a \end{cases} \end{aligned} \tag{5.82}$$

We substitute Eq.(5.82) into Eq.(5.81), which yields

$$E(\rho, f_N) = \frac{-i}{\pi f_N} \exp(i\kappa\zeta) \exp\left(\frac{i\rho^2}{f_N}\right) \int_0^a J_n\left(\frac{a k'_T \rho'}{a}\right) J_0(k'_\rho \rho^{'}) \rho^{'} d\rho^{'} \tag{5.83}$$

We solve this integral by substitution, with the new variables being $p = \rho'/a$, $\kappa_T = a k'_T$, and $\beta = a k'_\rho$, this results in

$$E(\rho, f_N) = \frac{-i a^2}{\pi f_N} \exp(i\kappa\zeta) \exp\left(\frac{i\rho^2}{f_N}\right) \int_0^1 J_n\left(\kappa_T p\right) J_0(\beta p) p dp \tag{5.84}$$

For $n = 0$, i.e. the case of a Bessel beam of zeroth-order, the integral is reduced to

$$E(\rho, f_N) = \frac{-i a^2}{\pi f_N} \exp(i\kappa\zeta) \exp\left(\frac{i\rho^2}{f_N}\right) \int_0^1 J_0\left(\kappa_T p\right) J_0(\beta p) p dp \tag{5.85}$$

And using the formula integral [72], also called Lommel integral

$$\int_0^1 xJ_\nu(\alpha x)J_\nu(\beta x)dx = \frac{\beta J_{\nu-1}(\beta)J_\nu(\alpha) - \alpha J_{\nu-1}(\alpha)J_\nu(\beta)}{\alpha^2 - \beta^2} \tag{5.86}$$

and the Bessel function identity

$$J_{-m} = (-1)^m J_m(z) \tag{5.87}$$

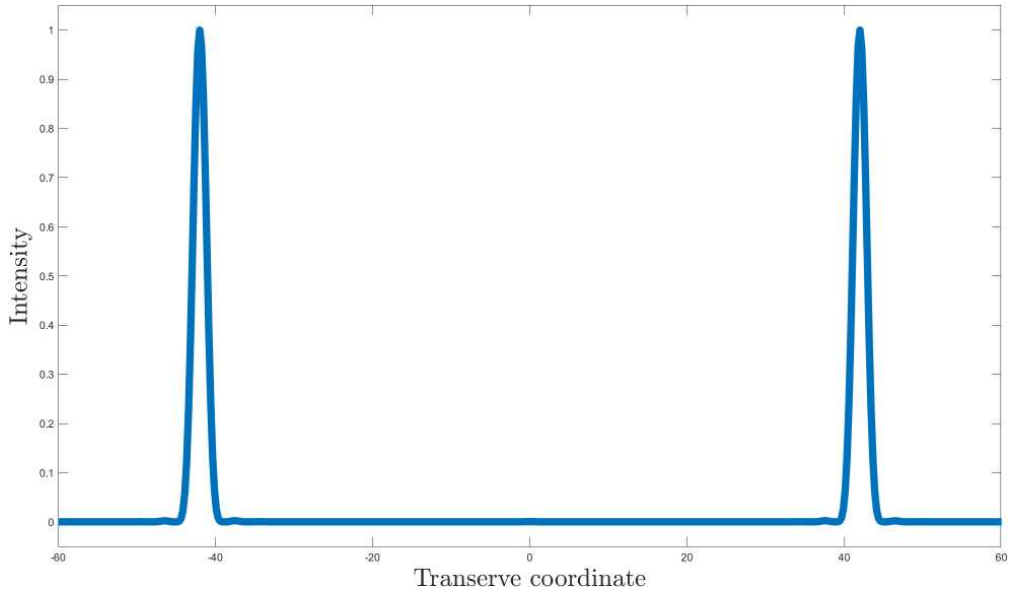

FIGURE 5.10: Transerve intensity profile at the focal plane of the apertured Bessel beam.

The intensity distribution of an apertured Bessel beam of zeroth-order at the focal plane is described by the equation:

$$E(\rho, f_N) = \frac{-ia^2}{\pi f_N}\exp(i\kappa\zeta)\exp\left(\frac{i\rho^2}{f_N}\right)\frac{\kappa_T J_1(\kappa_T)J_0(\beta) - \beta J_1(\beta)J_0(\kappa_T)}{\kappa_T^2 - \beta^2} \tag{5.88}$$

and the diffraction pattern is:

$$I(\rho) = \left(\frac{a^2}{\pi f_N}\right)^2\left[\frac{\kappa_T J_1(\kappa_T)J_0(\beta) - \beta J_1(\beta)J_0(\kappa_T)}{\kappa_T^2 - \beta^2}\right]^2$$

$$I(\rho) = \left(\frac{a}{\pi f_N}\right)^2\left[\frac{k'_T J_1(ak'_T)J_0(ak'_\rho) - k'_\rho J_1(ak'_\rho)J_0(ak'_T)}{(k'_T)^2 - (k'_\rho)^2}\right]^2 \tag{5.89}$$

where $k'_\rho = 2\rho/f_N$. In Figure 5.10 we show the transverse intensity profile described by Eq.(5.89), where the maxima points represent the annular ring we expected to obtain.

5.4.2 Focusing a Bessel-Gauss beam.

As an example of what we talked in Section 5.3 about how the aperture function modulates the Bessel beam we present an example, the Bessel-Gauss beam[73]. This kind of beam is a Bessel beam whose transverse profile is limited by a Gaussian function, the latter precisely working as an aperture. The transverse amplitude distribution of a Bessel-Gauss beam (BGB) can be written as:

$$p_r(r_0) = J_0(r_0 k \sin\theta) \exp\left[-\left(\frac{r_0}{w}\right)^2\right] \tag{5.90}$$

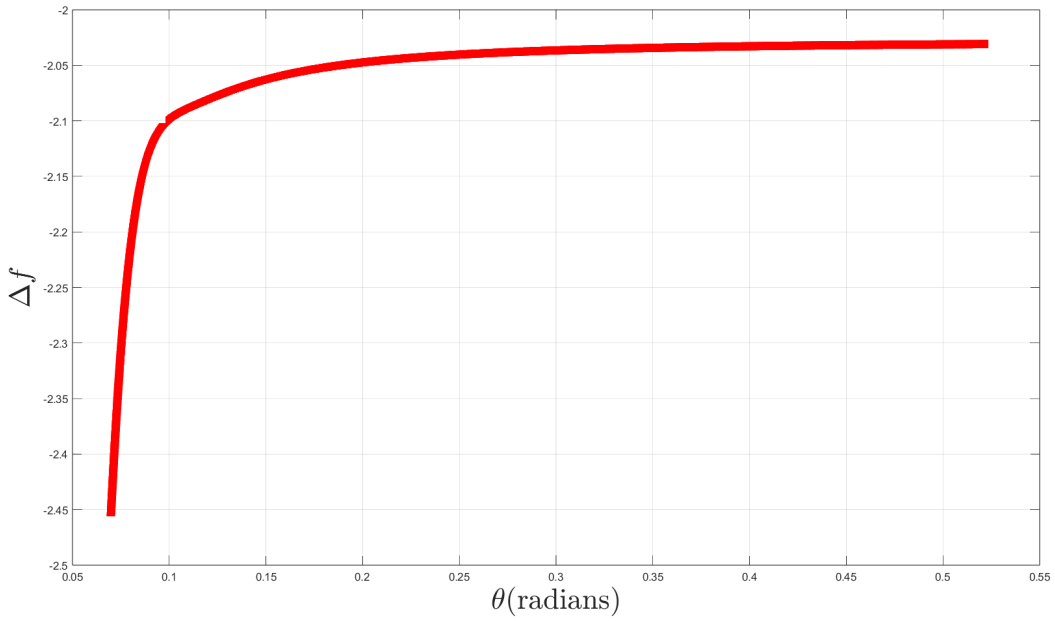

FIGURE 5.11: The relative focal shift of a Bessel-Gauss beam versus the θ coordinate that characterizes the tilted chief axis.

We know that the wave vectors of a Bessel beam lie on a cone, and for the BGB the propagation axis of the Gaussian beam lies on this same cone, which means the Gaussian beam follows an off-axis direction and it can be viewed as an off-axis focus case. The opening

of the tilted chief axis is given by θ.

We are interested with what happens once the BGB has passed through a thin converging lens, and to further explain the concept of focal shift, we analyze this displacement of the diffracted pattern and its dependence on the angle θ.

In Section 5.1 and 5.2.2 we concluded the focal shift depends of the Fresnel number of the light field, so first we present the generalized Fresnel number of the BGB [69]:

$$N_g = \frac{w^2}{\lambda f}\left(\frac{1}{2}\left[(\beta-2)^2 - \beta(\beta-3)\frac{I_1(\beta/2)}{I_0(\beta/2)}\right] - \frac{1}{4}\left[(\beta-2) - \beta\frac{I_1(\beta/2)}{I_0(\beta/2)}\right]^2\right)^{1/2} \tag{5.91}$$

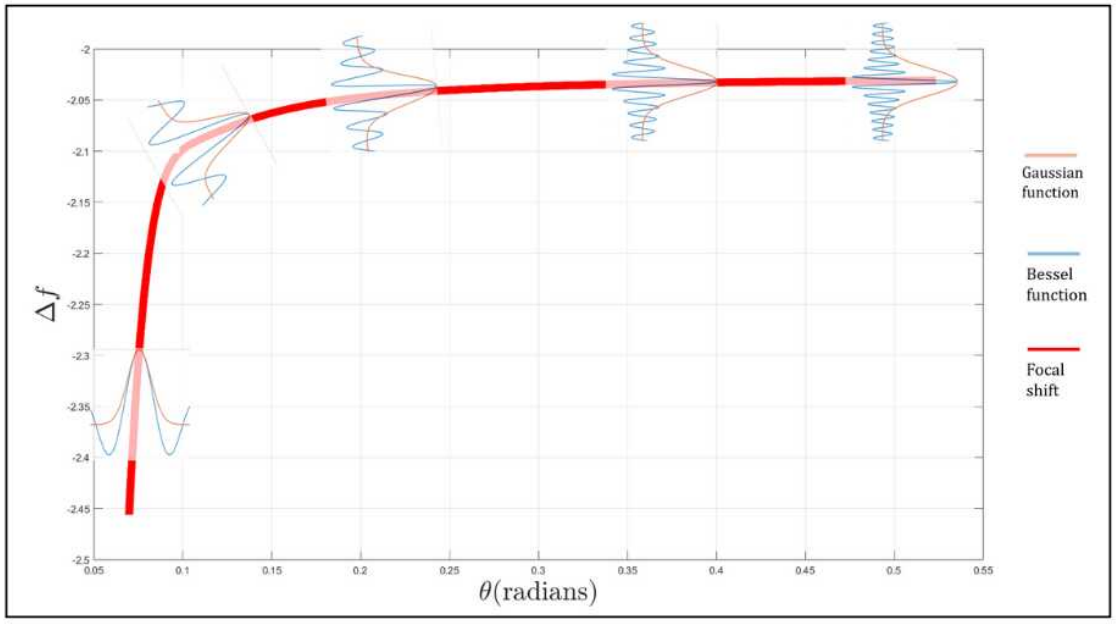

FIGURE 5.12: Notice how for θ smaller than $\frac{1}{5}(=0.2)$ radian the Bessel function resembles a Gaussian function, and for larger values, we have a windowed Bessel function.

where $\beta = k^2 w^2 \sin^2\theta$, and I_n represents the modified Bessel function of the first kind, order n. The diffracted wave field will suffer an off-axis tilt, the one is determined by the angle of the cone of existence of the Bessel beam.

We use Eq.(5.91) and the definition of focal shift Eq. (5.60) for this analysis. We consider angles $\theta > 0$ because for $\theta = 0$ the Bessel function disappears and there will be no cone of interference, and for higher values of θ we ensured these values fell within the paraxial wave approximation. Additionally, we verified the Gaussian beam profile was large enough to

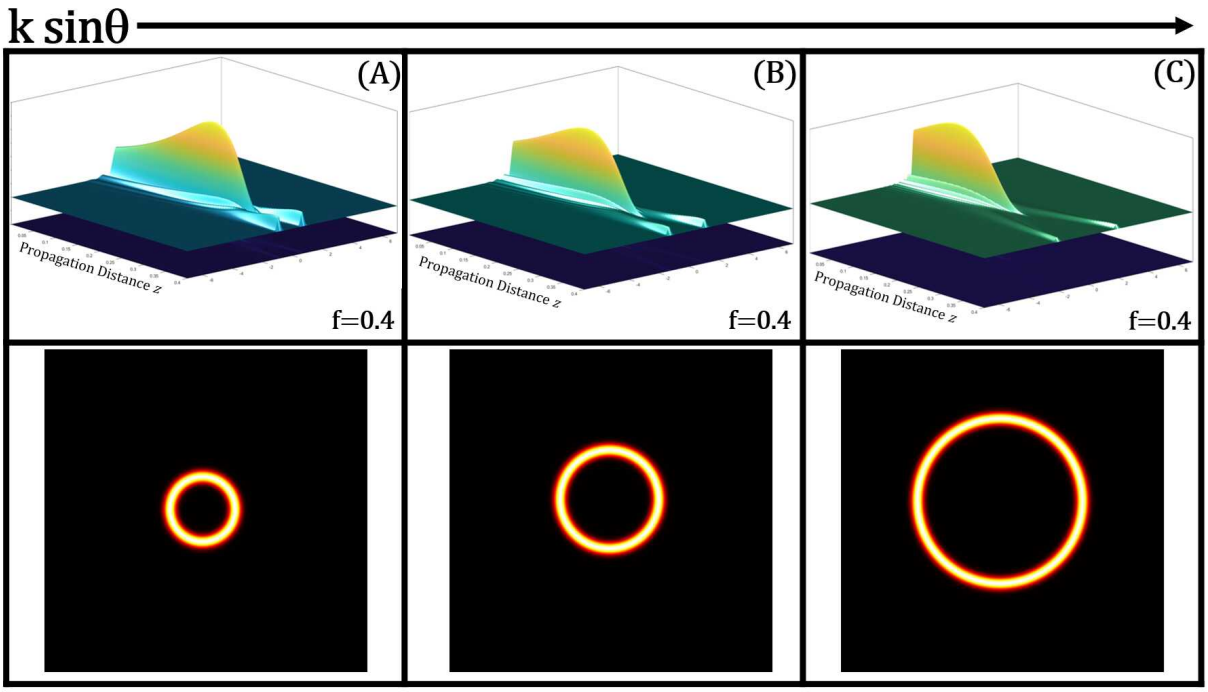

FIGURE 5.13: Representation of the propagation and diffraction pattern of a focused Bessel-Gauss beam for increasing values of $k \sin\theta$.

ensure it contains at least the center lobe of the Bessel function, however the value of w remains constant and we only vary θ. Figure 5.11 depicts our results, the negative value of the relative focal shift signals the displacement is closer to the aperture than to the focus, which was expected.

When θ falls between $(0, \frac{1}{5}$ radian) we notice that for values closer to zero the relative focal shift is large and it increases swiftly as θ grows, and for values of θ larger than $\frac{1}{5}$ radian the focal shift value tends to a constant. This was expected because as mentioned in Section 5.2.2 the focal shift will be the same regardless of the Bessel function amplitude distribution.

For $\theta \to 0$, the BGB's chief axis is closer to the optical axis and its profile is almost identical to the Gaussian beam as illustrated in Figure 5.12 because while w is a constant, k decreases with θ. Moreover, the propagation range z_{MAX} of the Bessel beam tends to infinity, so in summary we have a Gaussian beam propagating almost on-axis which translates into a large focal shift as a consequence of the diffraction of the Gaussian function. This is obvious from Eq.(5.91) when we approximate $\beta \approx 0$ and it reduces to the same Fresnel number we obtained for the Gaussian beam in Eq.(5.10).

For high values of θ, the beam actually resembles an apertured Bessel beam, as seen in Figure 5.12, with a finite range of propagation. Now, in Section 5.2.2 we concluded the light fields that follow an off-axis direction experiment the same focal shift that would experiment on-axis. The Bessel beam can be understood as plane waves whose direction of propagation is dictated by the cone of wavevectors, i.e. tilted plane waves, this means these plane waves will suffer a focal shift which will result in a displacement of the annular ring (Eq.(5.89))with respect to the focal plane. This focal shift of the diffraction pattern with respect to the geometrical focal plane is so minimal that in Figure (5.13) where we show the propagation of BGB for different values of θ the annular ring is always so close to the focal plane $z = 0.4$, that this displacement is imperceptible which is what the curve in Figure 5.12 shows too.

Moreover, from the propagation Figures 5.13, we can appreciate the beam reaches a maximum intensity before the geometrical focal plane and it is the position of this peak in intensity, and the size of the radius of the ring pattern, the most significant variation we can observe as θ increases. The variation in the position is not negligible so if the focal shift was responsible for this peak in intensity the curve in Figure 5.11 for large θ would not represent a Δf small. The next section will explain the reason behind this apparent focal point but for now, it is clear this analysis proves once again the focal shift refers specifically to the relative displacement on-axis or off-axis the diffraction pattern of a field suffers with respect to the geometrical focal plane, and that peak in intensity in Figure 5.13 is not related to it.

5.4.3 Pseudo-focal position.

Consider a Bessel beam generated by an axicon with refractive index n and base angle γ that passes through a lens with focal length f, as a result, the conical waves transform into converging spindle torus waves that interfere beyond the lens in a conical region [30] as shown in Figure 5.14. It is within this conical region, that the Bessel-like beam is created.

It is straightforward to see that the position of the vertex of the cone is located at [29, 30]

$$z_1 = \frac{fR}{R+\rho} \tag{5.92}$$

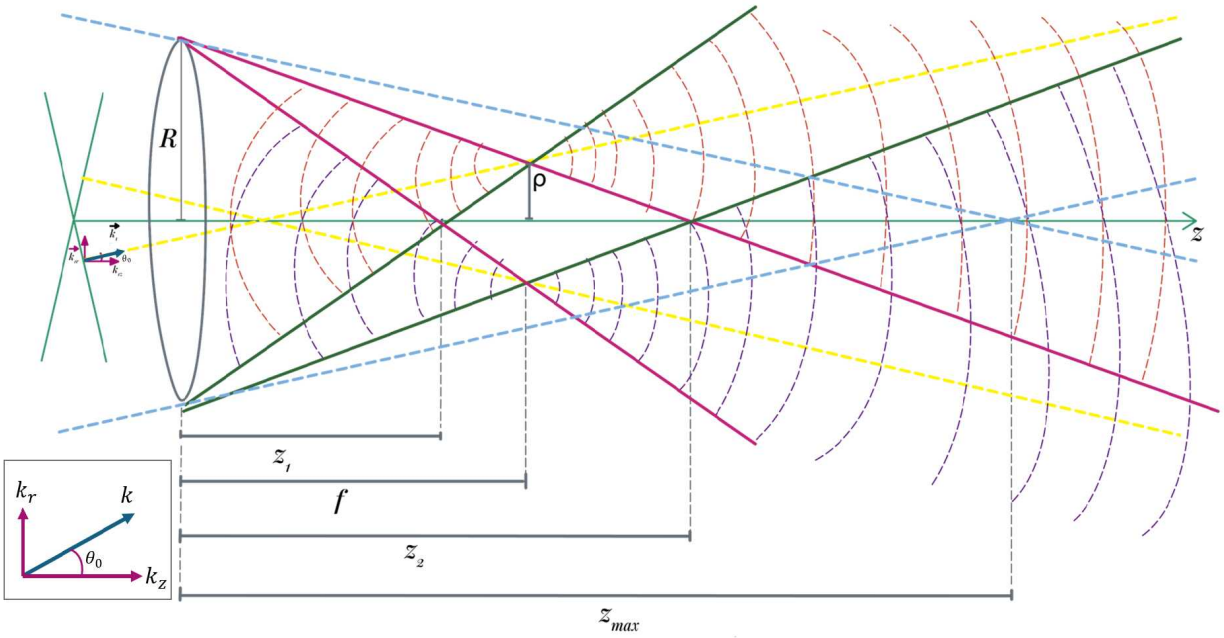

FIGURE 5.14: Geometric evolution of the focusing of a Bessel beam.

where

$$\rho = f \tan \theta_0 \tag{5.93}$$

is the radius of the image ring at the focal plane. Equation (5.92) is the geometrical point on the longitudinal axis where the intensity is maximum, this is the pseudo-focal point that we referred to in the last section.

Figure 5.15 shows the propagation of a Bessel beam with normalized radial wave number $k_r = 4$ after passing through a thin lens of radius $R = 50$, for this simulation, it was used a MatLab program which solves the Helmholtz equation numerically. The focal length used was 4, also in normalized coordinates. On the focal plane, the two peaks represent the ring focus of the conical waves, but in a position behind this point the intensity on-axis reached a maximum, this is the "exact" pseudo-focus, which for this case is reached at 3.32, this is better appreciated in Figure 5.16.

We refer to this point as "exact" because Eq. (5.92) is a geometric approximation, and as such, it provides an approximation to the point of maximum intensity. In Figure 5.16 the red dashed line marks the position of maximum intensity of the Bessel beam, and the green vertical dashed line marks the position z_1 calculated by Eq.(5.92), which gives $z_1 = 3.44$. In

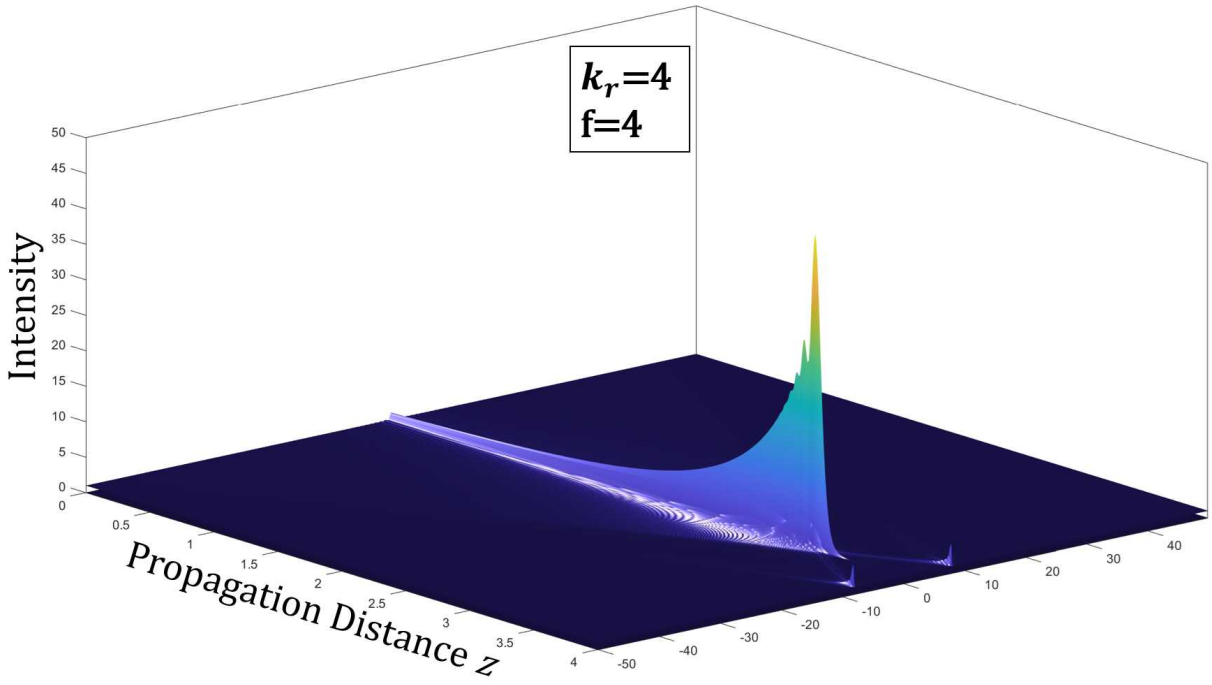

FIGURE 5.15: Propagation of a Bessel beam $J(k_r r)$ after passing through a thin lens.

general, the green dashed curve represents the function that describes the axial intensity of the Bessel beam [28, 29]:

$$I(z) = \frac{f^2}{(z-f)^2} \tag{5.94}$$

At the point where the axial intensity has a value of $0.25I(z_1)$, the position of z_1 is found, similar to what happens with Bessel beam propagating, the position $z_{MAX} = 0.25I_0$ where I_0 is the initial value [28].

If the conical waves theory of the Bessel beams is not taken into account it can lead to misguided interpretations of the focusing evolution of the Bessel beam. One example is found in ref. [23], where the intensity of a focused Bessel beam was studied, and it was reported that the position of maximum intensity along the axis is not at the geometrical focal plane but closer to the aperture, this result is correct as this subsection has shown, the confusion arises when the authors gave an explanation for such behavior, they attributed this displacement to the focal shift effect. However, in Section 5.4.2 we proved the focal shift is strongly associated with the diffraction phenomenon, and as we observed in Figure 5.13 the diffraction pattern of the BG beam, i.e. the annular ring, is always found around the

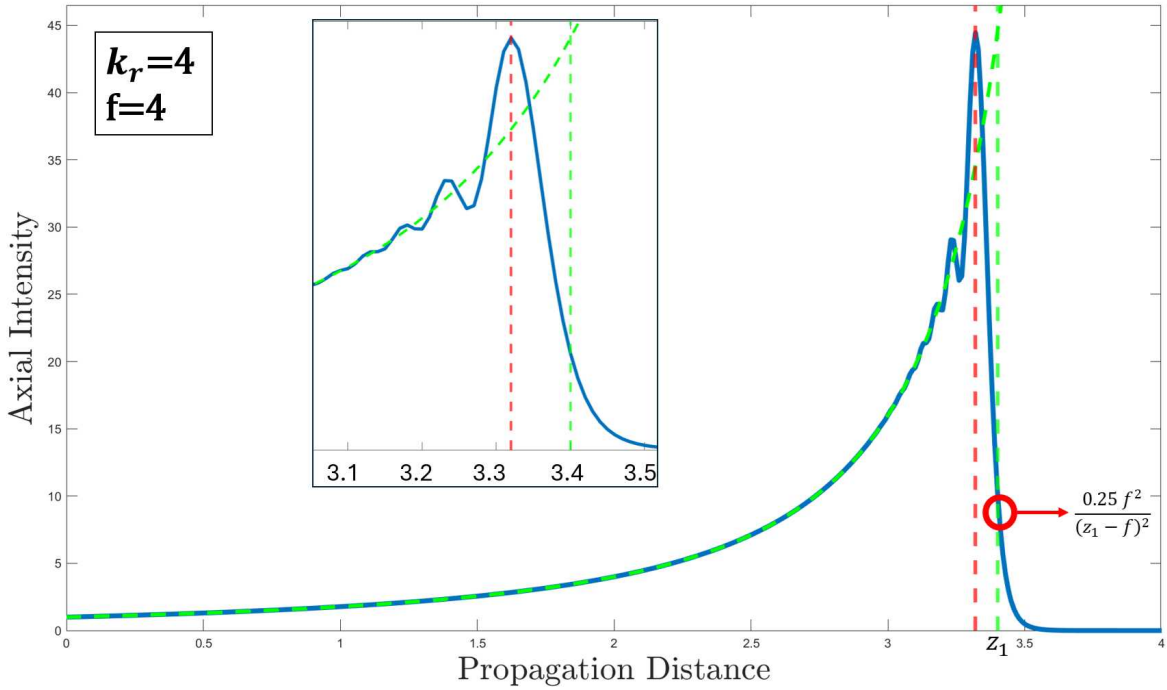

FIGURE 5.16: Axial Intensity of the focused Bessel beam verus z. The red dashed line marks the position of peak axial intensity, at 3.32. The green dashed vertical line marks the position of z_1 (Eq.(5.92)) at 3.44.

geometrical focal plane and the maximum point of intensity is not related to the focal shift effect.

Additionally, if we remember Section 4.2 where we concluded the field generated by a thin converging lens is the far-field pattern then we can understand that for a Gaussian beam, the diffracted pattern spreads but it retains its transversal profile, i.e. for the far-field case the diffracted Gaussian beam remains as a Gaussian beam, and its maximum of intensity is found closer to the lens. However, due to the nature of the Bessel beams we explained in this section this behavior does not happen for them. The far-field diffraction pattern of a Bessel function is an annular ring, not a Bessel beam thus if we wrongly assumed the pseudo-focus is a focal shift effect this would mean the waist of this ring should be found at z_1 [30], which does not occur.

In resume, the separation between the geometrical focus and this pseudo-focus point is not associated with the focal shift, but the existence of this pseudo-focus point proves that the Bessel beams can be focused.

5.4.4 Axial Intensity Behavior

Notice how in Figure 5.14 there is a second interfering region beyond the focal plane that begins at the point z_2. This region can only exists if $\rho < R$ and the point z_2 is given by [29, 28]:

$$z_2 = \frac{f}{1 - \frac{\rho}{R}} \tag{5.95}$$

However, to generate a Bessel beam within this region a second lens must be located in such a way the distance between the lens and the annular ring of radius ρ is the focal length of the former, this way the Bessel beam will be the formed as the imaging of the spherical waves generated by the ring source [28, 22].

Last section we provided the Eq.(5.94) without an explanation, but to arrive at this equation that describes the axial intensity we can use a geometrical approach again. First, we consider the propagation invariant light field, in this case a Bessel beam, is composed of N plane waves and these waves become converging spherical waves after passing through the lens, and the field distribution E inside the conical region is given by the superposition of the N spherical waves [29]

$$E(r) = \exp(ikd) \sum_{n=0}^{N-1} \frac{A_n \exp\left(\pm ik|r - r_n|\right)}{|r - r_n|} \tag{5.96}$$

Where A_n are the complex amplitudes corresponding to the discrete annular spectrum $A(\varphi) = \sum A_n \delta(\varphi - \varphi_n)$. The negative and positive signs inform us about the converging and diverging spherical waves. The factor $|r - r_n|$ is the distance from the nth image point (r_n) to the observation point at r, and $d = \sqrt{\rho^2 + f^2}$ is the distance from those same image points but to the origin $(r = 0)$. To simplify the calculations, it is taken into account only points located along the z-axis which leads to factoring out the distance between the image points and the origin, additionally, the summation can be written as a general complex number in its polar form and find the amplitude when lossless lens is assumed and I_0 as the initial axial intensity so for $z \in [0, z_1]$ and $z \in [z_2, \infty)$ the axial field becomes

$$I(z) = \frac{\rho^2 + f^2}{\rho^2 + (z - f)^2} \tag{5.97}$$

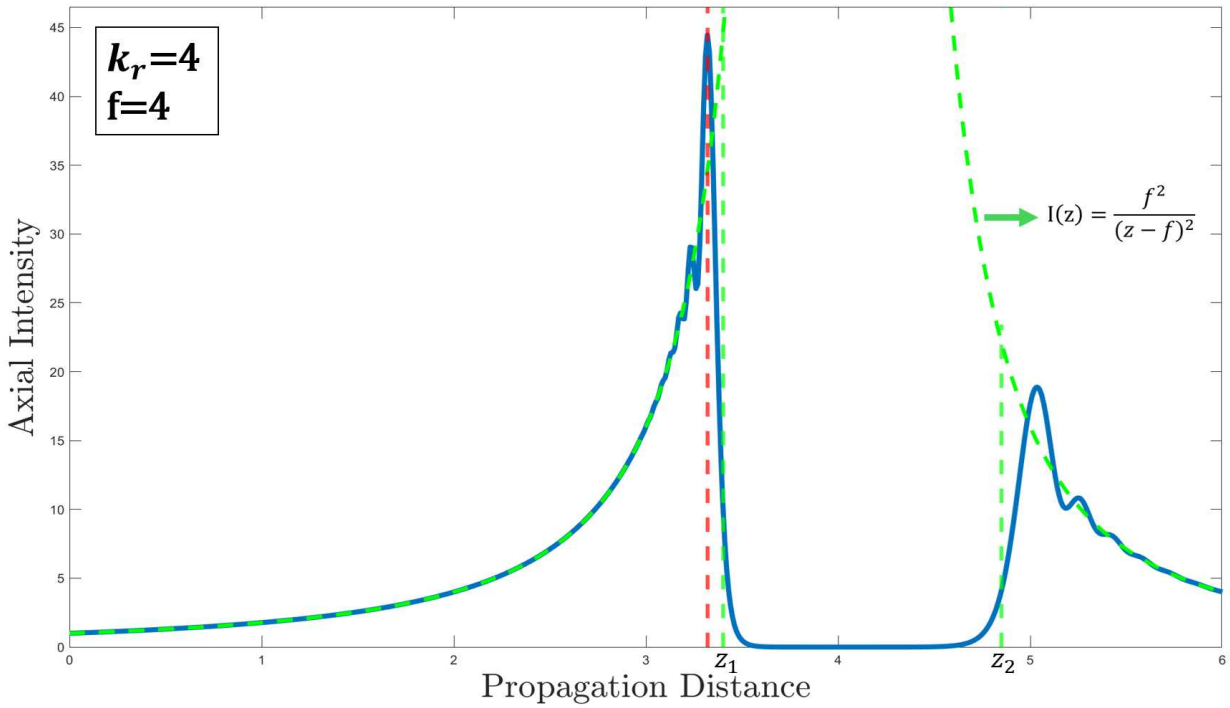

FIGURE 5.17: Evolution of the axial intensity of a focused Bessel beam. The green dashed lines represent the Eq.(5.94).

Notice this expression represents a Lorentzian curve, and it is valid for any propagation invariant optical field, including the Bessel beams.

Although for experimental cases we can consider the inequalities $\rho \ll f$ and $R \ll f$ hold and the Eq.(5.97) can be simplified to Eq.(5.94), which is only valid within the conical region where the Bessel beam exists [29]. This approximation is illustrated in Figure 5.16 and 5.17 where the green dashed line represents the Eq.(5.94), and as we can appreciate describes the behavior of the Bessel beam axial intensity.

5.4.5 Transverse Magnification.

The interest in knowing the transverse magnification of Bessel beams at the pseudo-focal point and along the z-axis relies on the fact it can be used to characterize the coherence of vortex Bessel beams [30], and other applications in optical tweezers and atom guiding. However, it can also be used to build a geometrical approximation of the evolution of the focusing transverse field profile.

The calculations done on the pseudo-focal point start considering the transverse wave vector component of the incident Bessel beam which is related to the incident angle φ, that is $k_{1r} = k_1 \sin\varphi \cong k_1(n-1)\gamma$ where only small angles are considered, and n and γ are the refractive index and base angle of the axicon that creates the Bessel beam, respectively.

We approximate locally the spindle torus waves, created after the conical waves have passed through the lens, as conical waves within the neighborhood of the axis. The conical waves inside the cone region are determined by the tangents to the surfaces at the axis illustrated by pink lines in Figure 5.18.

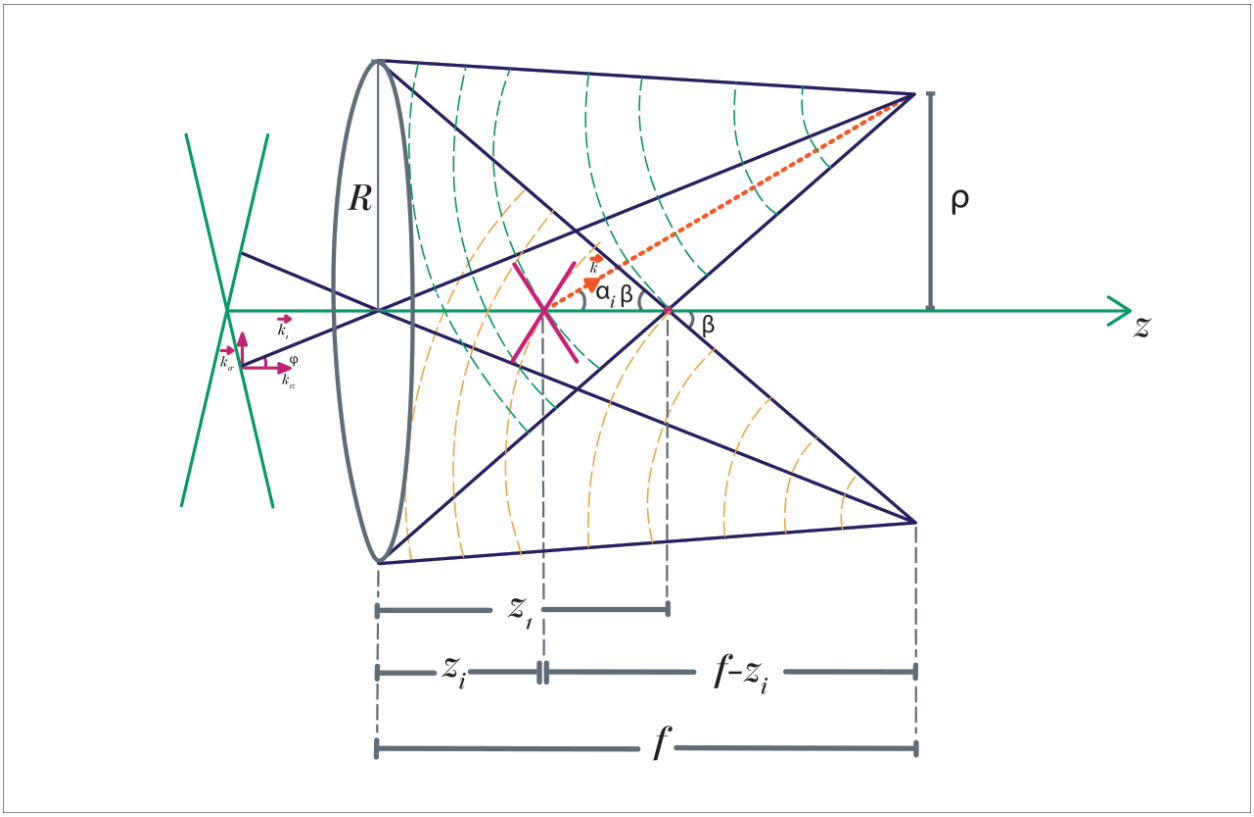

FIGURE 5.18: Schematic evolution of the focusing of a Bessel beam.

Once the Bessel beam has passed through a thin lens the wave vector changes so the conical waves have a new wave vector $\vec{k}_2$ that forms an angle with respect to the z-axis, given by

$$\tan\beta = \frac{\rho}{f - z_1} \tag{5.98}$$

and when it is considered the expression of the pseudo-focus Eq.(5.92), the Eq.(5.98) and the

paraxial approximation, the explicit expression for the transverse wave vector $\vec{k}_2$ is found [30]

$$k_{2r} = k_2 \left[\frac{R}{f} + (n-1)\gamma \right] \tag{5.99}$$

This expression is used to calculate the transverse field at the pseudo-focal place once it is substituted into the Bessel function $J(k_{2r}r)$.

Furthermore, the transverse magnification is easily derived from the definitions of the incident and transmitted wave vectors, that is [30]

$$\frac{k_{2r}}{k_{1r}} = \frac{k_2 \left[\frac{R}{f} + (n-1)\gamma \right]}{k_1 (n-1)\gamma} \tag{5.100}$$

For the case of the same medium behind and ahead of the thin lens, $k_1 = k_2 = \frac{2\pi}{\lambda}$, so the relation is reduced to

$$\frac{k_{2r}}{k_{1r}} = \frac{R}{f(n-1)\gamma} + 1 \tag{5.101}$$

This same mathematical procedure can be performed for the points along the axis within the region between the lens and the pseudo-focus, to do so the tangents of the converging spherical waves are taken and with this, a geometrical approximation of the evolution of the focusing transverse field profile of the Bessel beam is obtained, this will be explained in detail in Section 5.4.7 but first, we analyze the focusing of apertured Bessel beams.

5.4.6 Apertured Bessel Beams: Super-Gaussian beam Vs. Flattened Gaussian beam

Multiple works have studied the propagation of Bessel beams with different apodization functions because reducing the oscillations produced by diffraction is of great interest [74, 75, 76]. These oscillations are created when a field light is limited by an aperture with hard edges, this causes an abrupt discontinuity in the field that requires higher spatial frequencies to represent its spectrum, this translates into fluctuations in the curve that describes its propagation. The apodization of a function reduces these fluctuations by making the edges of the aperture smoother. Here we consider three cases: (1) a Bessel beam focused by a thin

lens with an aperture radius of $R = 50$, the same Bessel beam but apodized by (2) a Super Gaussian profile, and (3) a Flattened Gaussian profile.

We solve numerically the 3D Helmholtz reduced wave equation in cylindrical coordinates using normalized variables to illustrate the main characteristics of each apodization function. We center our attention on the oscillations produced along the axis through the propagation, the peak axial intensity and the position at which it is reached, and the output 2D profile at this position.

Apertured Bessel beam

The following function represents the initial condition

$$E(x, y, z = 0) = \begin{cases} J_0(k_r r) \exp\left(-i\frac{r^2}{f}\right) & \text{if } r \leq R \\ 0 & \text{otherwise} \end{cases} \tag{5.102}$$

where the wavevector was $k_r = 4$, and the focal length f will take two values, $f = 2$ and $f = 4$. From the equation $\rho = k_r f/2$ it follows that the radius of the ring produced at the focal plane is $\rho = 4$ and $\rho = 8$, respectively.

In Figure 5.19 and 5.20 we show the propagation of the apertured Bessel beam and the axial intensity versus the propagating distance z for the two focal length cases. The red line in Figure 5.20 marks the position of peak axial intensity I_p, which we refer to as z_p, and the green line represents the position where the intensity is $0.25I_p$, i.e. the z_1 value calculated by the Eq. (5.92). For the focal length of 2, these positions are $z_p = 1.72$ and $z_1 = 1.85$, and for focal length 4 the values are $z_p = 3.32$ and $z_1 = 3.44$. Both lines are very close in distance from each other, and geometrically we can calculate z_1 which helps us understand the propagation of the Bessel beam in geometrical terms as the diagram in Section 5.4 showed. From the Figures 5.20 the axial oscillations induced by the hard aperture are clearly seen. It is known that apodization is used to reduce this effect. Here, we use two different apodization functions to reduce the oscillations.

The 2D input profile of the apertured Bessel beam at $z = 0$ is shown in Figure 5.21, and the central peak radius r_1 is 0.512. The 2D output profile at the position of maximum axial

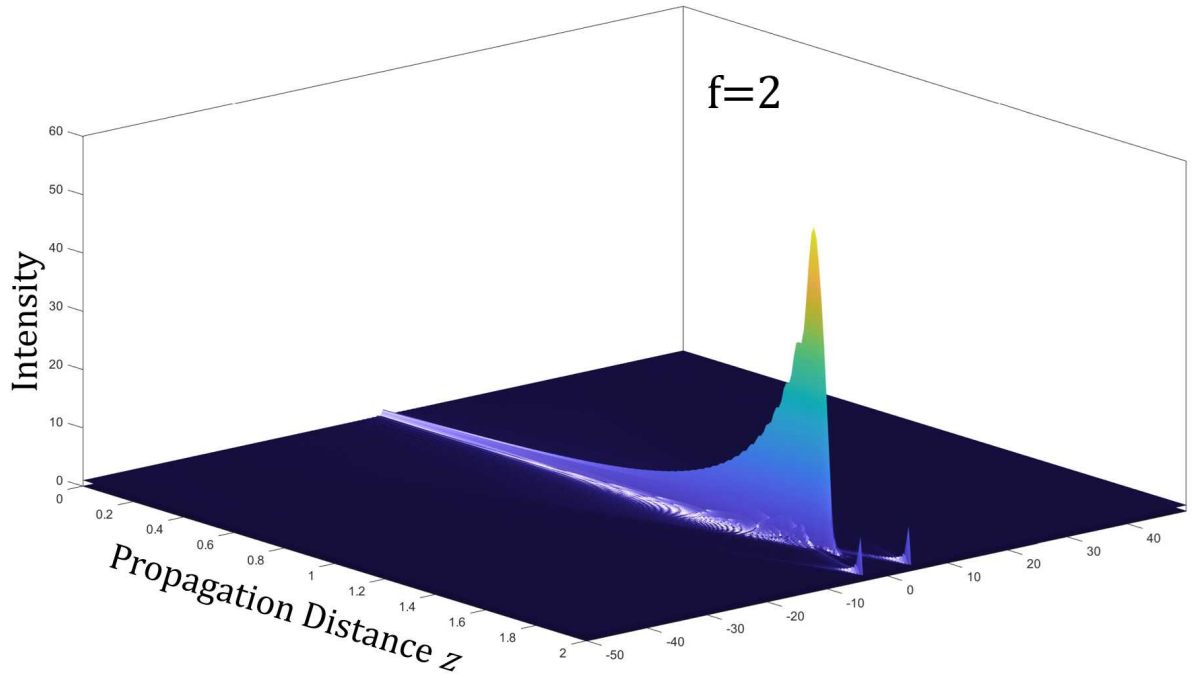

(A)

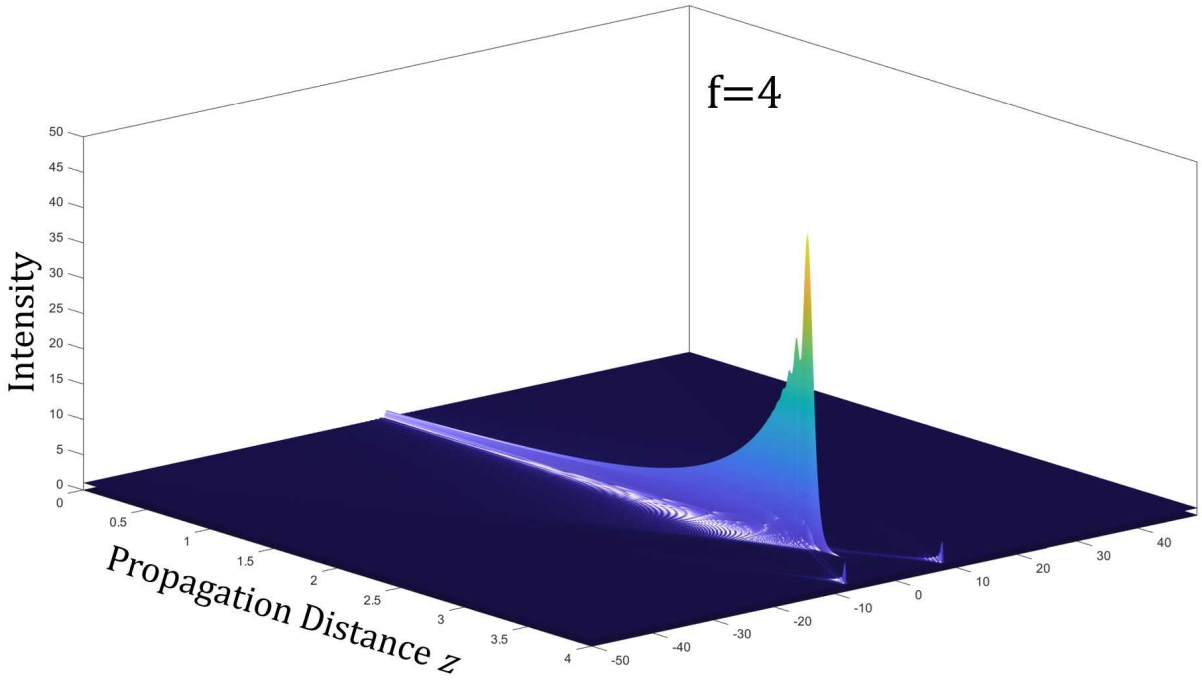

(B)

FIGURE 5.19: Propagation of an apertured Bessel beam through a thin lens of focal length (A) $f = 2$ and (B) $f = 4$.

intensity z_p for the case of a thin lens of focal length 2 is shown in Figure 5.22a and for the focal length of 4 in Figure 5.22b, the center lobe radius is $r_1 = 0.073$ and $r_1 = 0.097$, respectively. As expected, there is a reduction in size at the position z_p where the beam is focused.

It is obvious the increase of energy at the central peak from the colorbar values of Figures 5.22, for the focal length $f = 2$ the peak intensity is $I_p = 54.92$ and for $f = 4$ it is $I_p = 44.46$. The reduction of its radius is more evident too when we look at the ratio of the radius of the input and output profiles, for $f = 2$ the ratio $r_1(\text{output})/r_1(\text{input}) = 0.14$, and for $f = 4$ it is $r_1(\text{output})/r_1(\text{input}) = 0.18$. In Figure 5.23 we show the input and output profiles side to side to better appreciate this. The increase of intensity and reduction of energy at the z_p were expected because at this position the Bessel beam gives the impression of being focused which translates into the beam energy being concentrated in a very small area.

Another evident feature is the downsizing of the side-lobes between Figures 5.22a and 5.22b. This is explained when we consider the dependence the z_1 has on the focal length, which tells us the length of the cone-shaped region of interference of the conical waves, and the radius of the focal ring ρ, grows for larger values of f. This is illustrated in the Figure 5.24.

As we explained in Section 5.3, the Hankel waves are affected by the diffraction effects of the modulation function, in this case, the spreading produced by the circular aperture, so for the case of a larger cone section the diffraction distance increases which means major and faster loss of energy. Additionally, from Figure (5.8) the spreading of the outgoing Hankel wave grows alongside the propagation axis, which means energy is being lost through this action too.

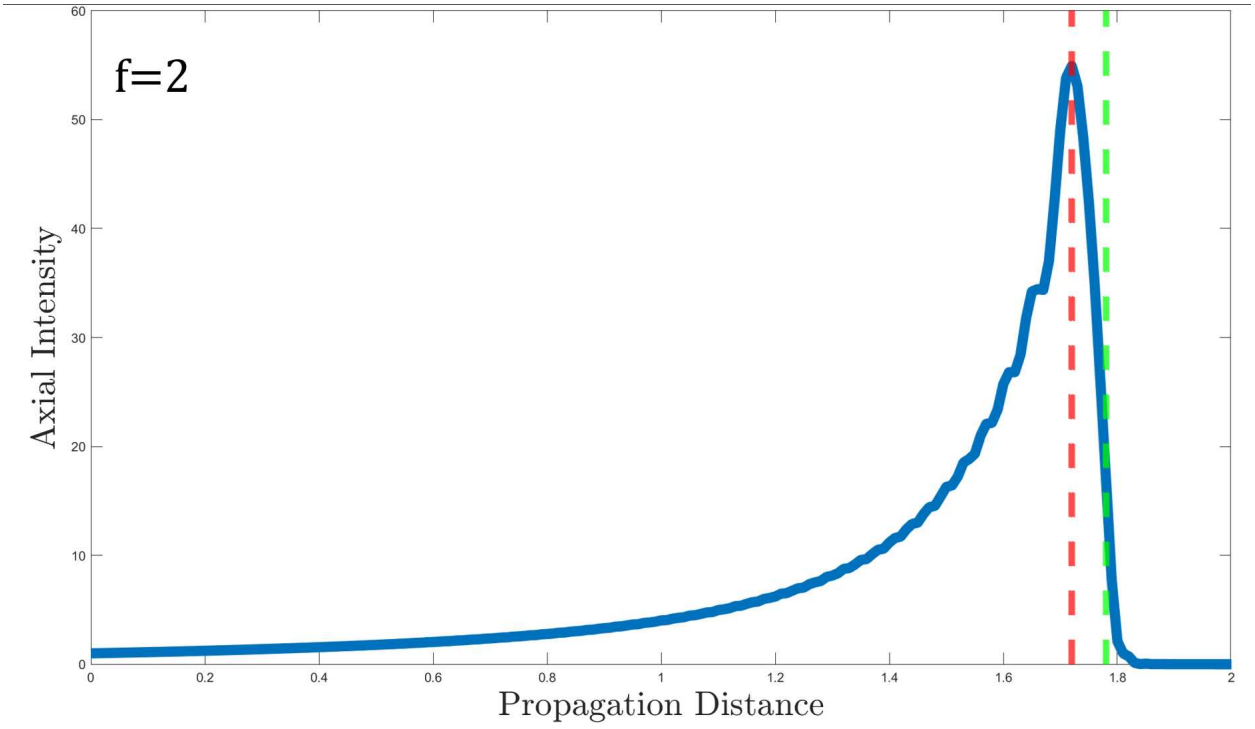

(A)

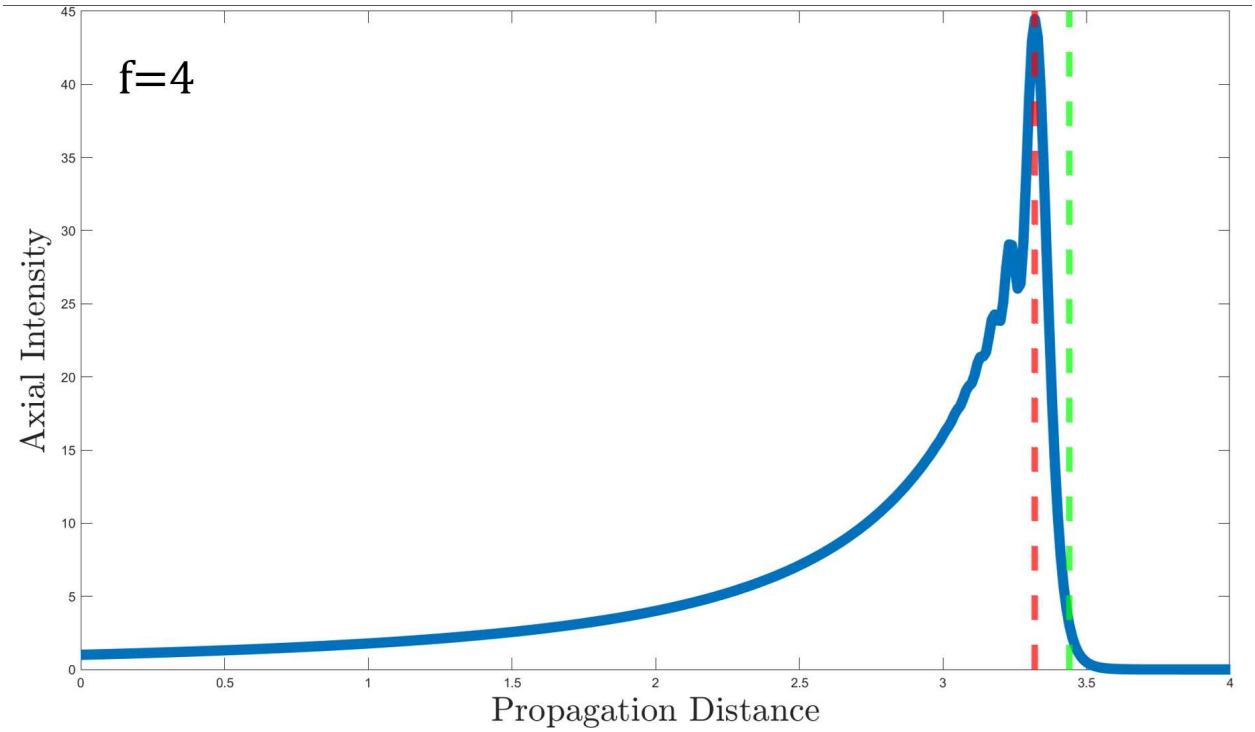

(B)

FIGURE 5.20: Evolution of the axial intensity corresponding to Figure 5.19. The dashed red line represents the position of exact maximum intensity z_p and the dashed green line the position of z_1.

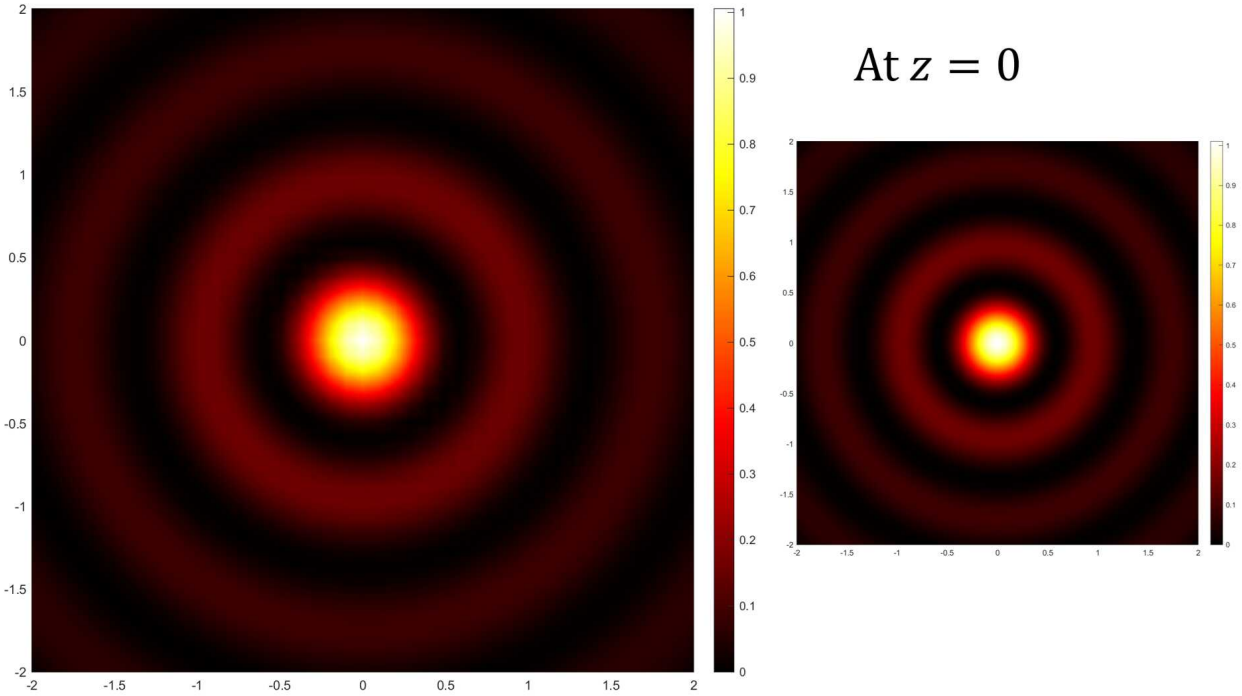

FIGURE 5.21: 2D input profile of the apertured Bessel beam.

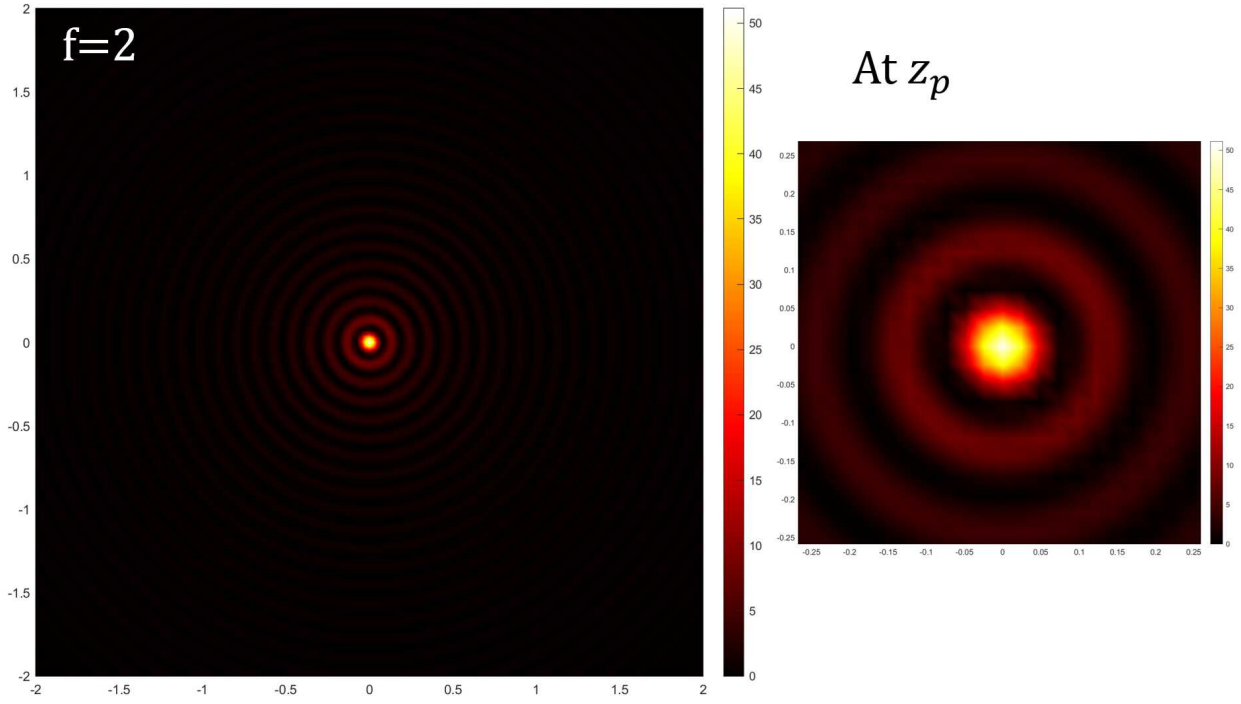

(A)

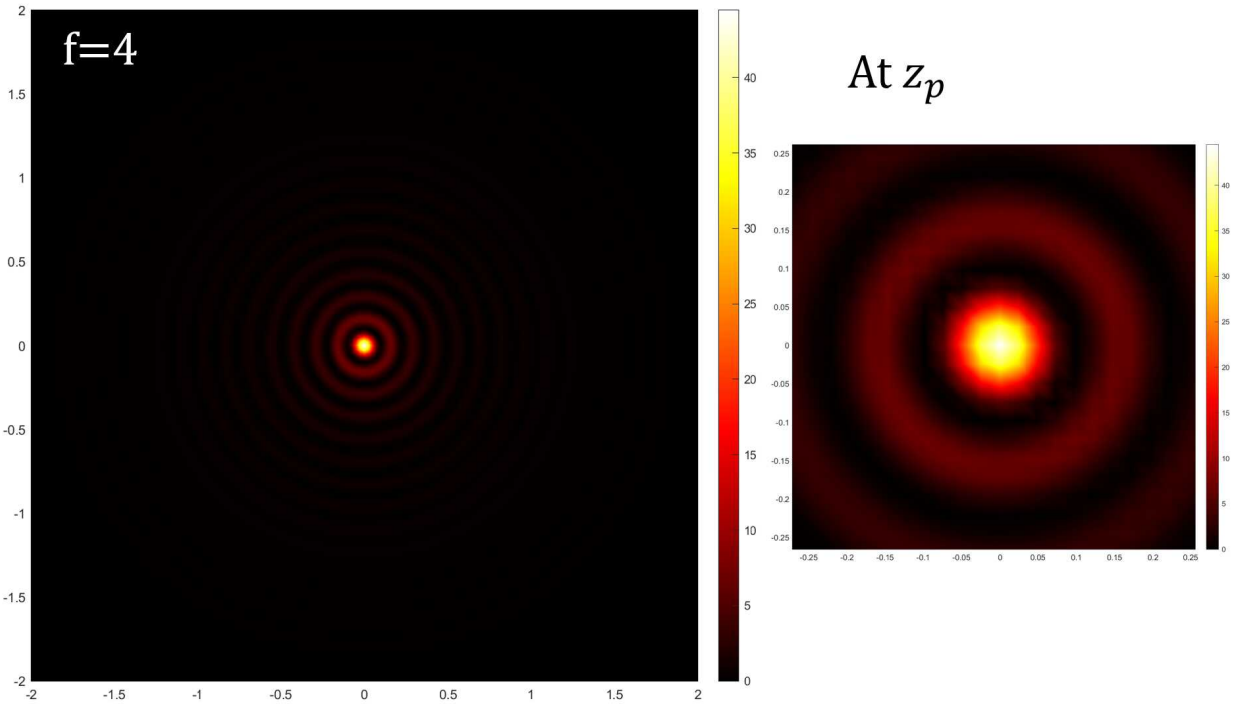

(B)

FIGURE 5.22: 2D output profiles of the focused apertured Bessel beam at the plane where the maximum intensity is reached.

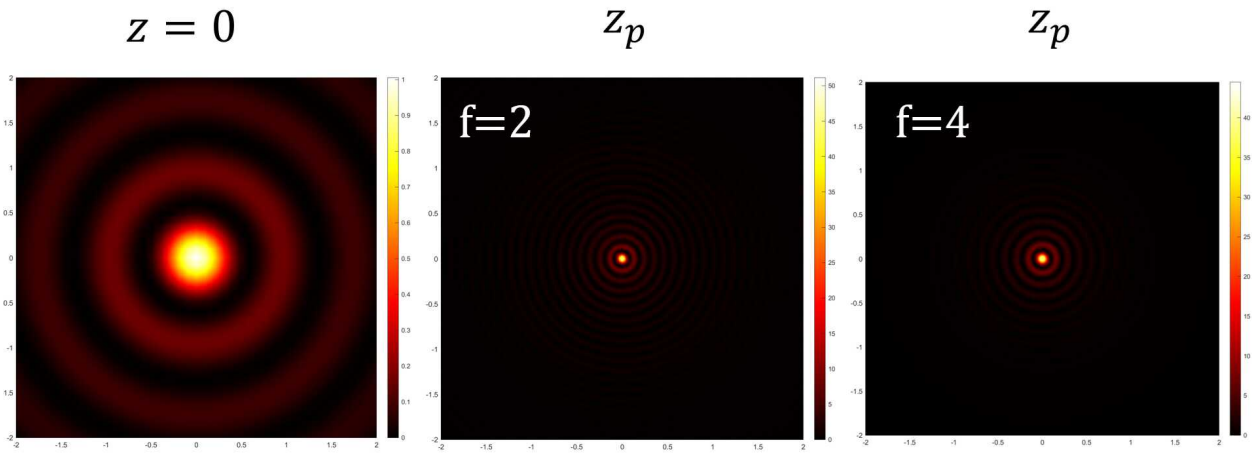

FIGURE 5.23: Comparison of the input and output profiles of the apertured Bessel beam.

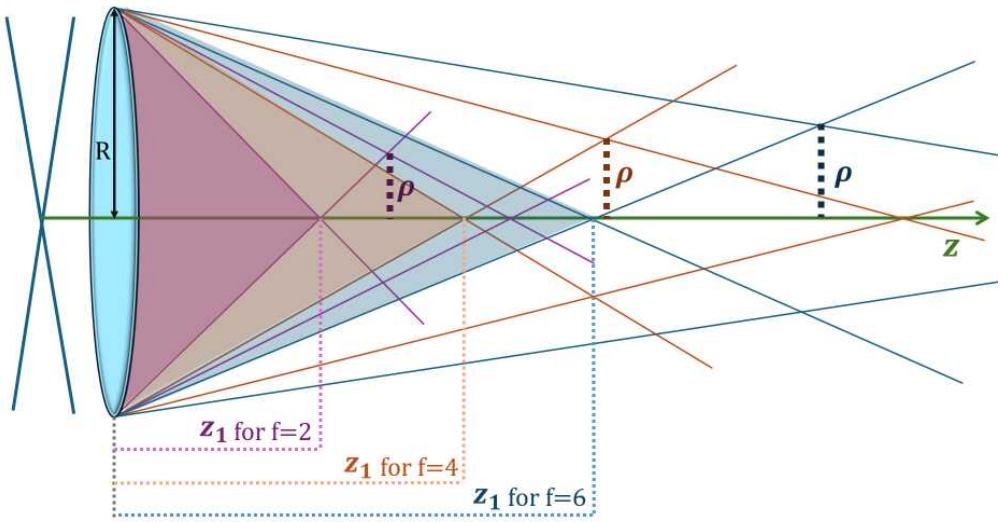

FIGURE 5.24: Comparison of the length of z_1 and ρ for different values of f.

In Table 5.1 we resume the characteristics of the apertured focused Bessel. Note we added the case for a focal length $f = 6$ albeit we did not illustrate their propagation nor profile, this is because it would be repetitive, and with two focal lengths, we could explain the general behavior of the Bessel beam. However, in the next subsections, we make those values.

f=2				**f=4**				**f=6**			
I_p	z_p	z_1	r_1	I_p	z_p	z_1	r_1	I_p	z_p	z_1	r_1
54.92	1.72	1.85	0.073	44.46	3.32	3.44	0.097	23.02	4.58	4.83	0.122

TABLE 5.1: Bessel beam focusing characteristics for the case of a thin lens with focal length $f = 2$, $f = 4$ and $f = 6$.

Before talking about the apodization functions, we briefly describe the preliminary considerations to numerically simulate the propagation.

We consider a system that generates a Bessel beam (an axicon for example) and is illuminated by a light beam (a Gaussian beam for example) with a specific power P_0 as shown in Figure 5.25.

An "unity" quantity is required to serve as a parameter in case this approach could be implemented experimentally. We propose to consider a Gaussian beam described by Eq.

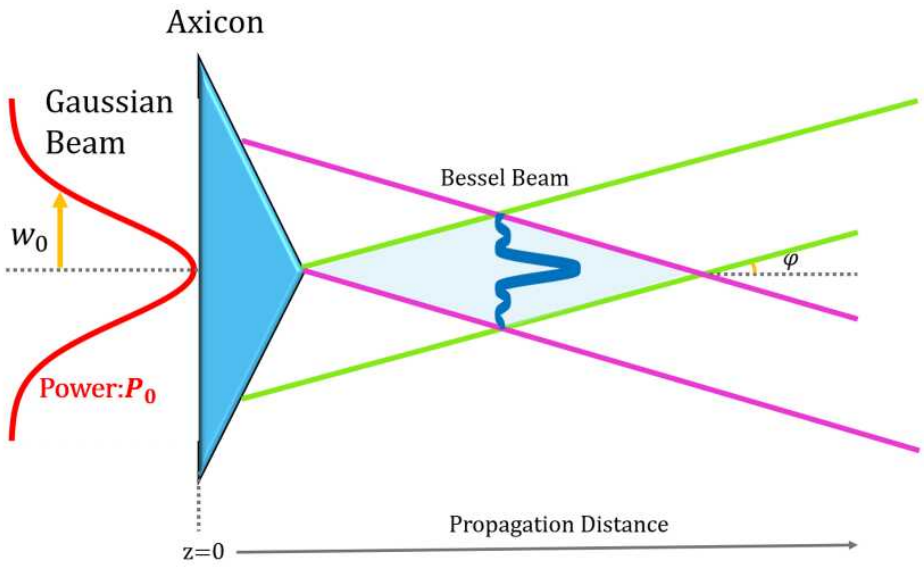

FIGURE 5.25: Example of a generating system of the apertured Bessel beam.

(5.103) as the apodization function.

$$U_G(r) = \exp\left[-\left(\frac{r}{w_G}\right)^2\right] \tag{5.103}$$

To ensure energy conservation, the following integral of the Parsevals's theorem was solved.

$$P_0 = \int_0^\infty \left|\exp\left[-\left(\frac{r}{w_G}\right)^2\right]\right|^2 r dr \tag{5.104}$$

which yields

$$w_G(P_0) = 2\sqrt{P_0} \tag{5.105}$$

With Eq. (5.105) we choose two values of P_0: P_1 and P_2, such that the function Eq.(5.103) takes the values $U_G(r = R) = 0.12$ and $U_G(r = R) = 0.002$ respectively. These quantities obtained make it easier to see $P_1 > P_2$. Their corresponding profiles are shown in Figure 5.26 as a reference, where we have included the Bessel function we are trying to apodize.

Now, this procedure is only meant to serve as a guide, once we introduce the apodization functions the use of $w_G(P)$ to ensure energy conservation will be clearer.

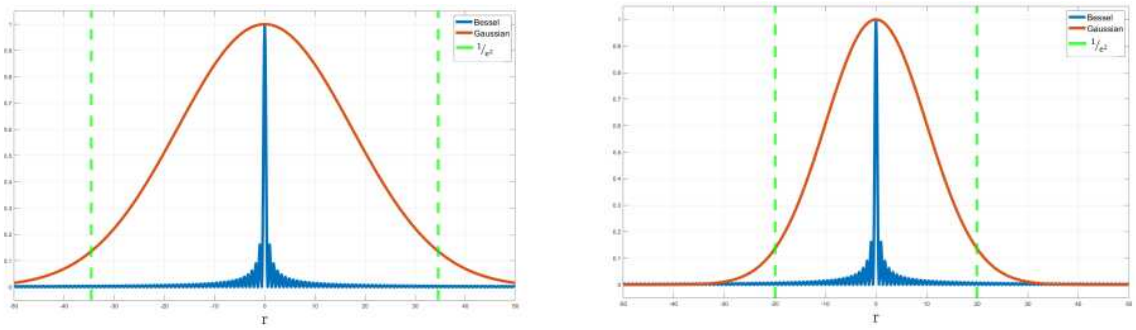

(A) Gaussian beam generated with the power P_1. (B) Gaussian beam generated with the power P_2.

FIGURE 5.26: Gaussian beam used as the basis for the energy conservation procedure.

Super Gaussian beam

In 1988, a Super-Gaussian (SG) function was proposed as the reflectivity profile used to smooth the output beam within an unstable resonator [77]. This profile function can be defined as

$$U_{\mathrm{SG}}(r) = \exp\left[-\left(\frac{r}{w_{SG}}\right)^{2m}\right] \tag{5.106}$$

where r is the radial coordinate, w_{SG} is the beam waist, and m is a positive integer that marks the main difference with an ordinary Gaussian beam when $m > 1$.

Because we want to maximize the energy in our system, we repeat the integration of Eq.(5.104) but replace the Gaussian beam with the Super Gaussian beam, which yields

$$P_0 = \frac{w_{SG}^2}{4}\left[\frac{1}{m}\Gamma\left(\frac{1}{m}\right)\right] \tag{5.107}$$

Rewriting P_0 in terms of the w_G according to Eq.(4.6) we obtain an expression for w_{SG}.

$$w_{SG}(m) = w_G\sqrt{\frac{m}{\Gamma\left(\frac{1}{m}\right)}} \tag{5.108}$$

By doing this we are obtaining a w_{SG} that depends on the initial P_0, however, it is evident Eq.(5.108) depends on the parameter m, for such reason in Table 5.2 we show a list of some values.

And in Figure 5.27 we plot the profiles of the values from Table (5.2) for the case of the

Parameter m	w_{SG}
1	w_G
2	$1.0622w_G$
3	$1.0582w_G$
5	$1.0436w_G$
10	$1.0252w_G$
25	$1.01096w_G$

TABLE 5.2: Numerical calculation of the size of the waist of the Super Gaussian beam for different values of the parameter m.

P_1. If we had used the smaller power P_2 instead, the dashed red line would be shorter, i.e. the "box-shaped" profile would be narrower.

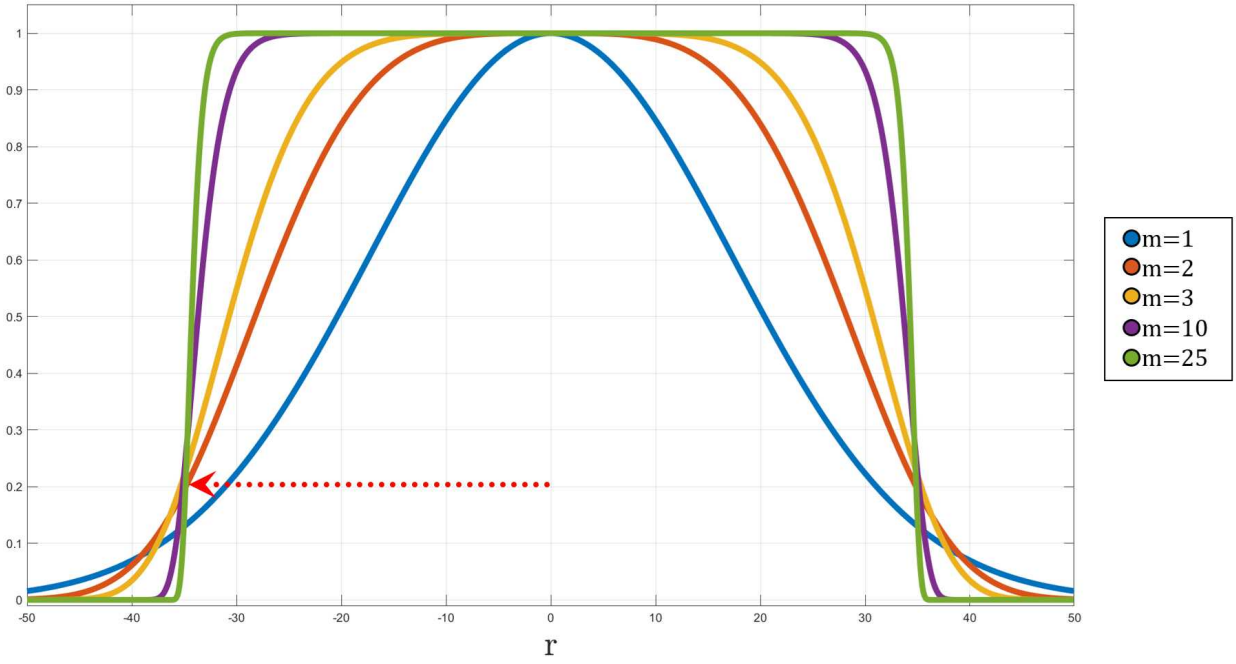

FIGURE 5.27: SG profiles versus r for values of m.

We implemented the Super Gaussian for the two cases of power values, P_1 and P_2, in the program we used to simulate the propagation and focusing of the apertured beam. To analyze the differences that come with using different power values we compare their respective peak axial intensity I_p with respect to the Table (5.1) for the cases $f = 2$ and $f = 4$. The results

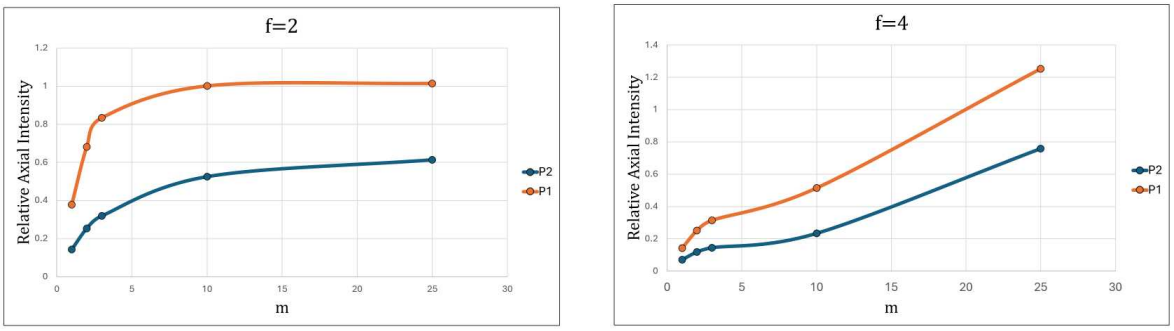

(A) (B)

FIGURE 5.28: Relative peak axial intensity of a Bessel beam with an SG function when focused with a lens with a focal length of (A) 2 and (B) 4.

are shown in Figures 5.28.

We notice that as expected the behavior is the same regardless of the power because the only difference is that if more energy is entering the system, then the peak axial intensity can reach higher values. Moreover, for the case of P_1, the power is enough to reach the exact same value as the apertured Bessel beam for both focal lengths, while for the lower power P_2, this does not happen.

Given that the power is not that relevant for the general behavior, we work from now on with P_1 and analyze the propagation profile because we are concerned with the reduction of the oscillations due to diffraction.

In Figures 5.29 we show the axial intensity versus z for the three cases, $f = 2$, $f = 4$, and $f = 6$, for different values of m. The red dashed line marks the position z_p for the apertured Bessel beam case without apodization, and the green dashed curve represents the Lorentzian curve we explained in Section 5.4.2 that describes the behavior of the axial intensity.

It is necessary to point out that the apodization function for $m = 1$ is a standard Gaussian beam, and as such we have small oscillations mainly caused by diffraction, which was expected [75]. Further, it is straightforward to see in Figure 5.29 that for the cases of $f = 4$ and $f = 6$, the curve is smooth for $m \geq 2$, but this does not happen with $f = 2$, moreover, the oscillations do not decrease. For the three figures, the most notorious changes with the increase of m are the peak axial intensity and the position at which is reached. But to understand why for $f = 2$ the oscillations are not eliminated we used P_2 and propagated the beam again, we noticed the axial intensity curve was smooth for this power, this tells us

the reason behind the "failure" in the apodization function in Figure 5.29a is because as we explained in Figure 5.24, for larger values of f the energy loss is bigger and faster, which is what happens here. The contrast in the oscillations of intensity increases for bigger power. This result is of relevance because it confirms there are cases where the effects of diffraction can be "fixed" at the cost of lower energy [75].

However, when we use the bigger power P_1, we notice for $m \geq 10$ the peak energy reaches the same value I_p as in the apertured Bessel beam, this is because a larger value of m means a bigger "window" which translates into more energy entering the system, but if we look at Figure 5.27 with the profiles for the Super Gaussian beam we note its edges are sharper as m increases, which for its part translates into discontinuities in the field at those points consequently creating oscillations by diffraction.

Moving on, for $f = 4$ the axial intensity reaches the same value as the apertured Bessel beam for $m \geq 25$, and in the case of $f = 6$ at a value of $m = 25$ the peak axial energy will be about the 67% of the I_p of Table (5.1). The explanation for this is the same we provided alongside Figure 5.24, the effects of diffraction of the function that modules the Bessel beam are more evident for larger values of f, and as such energy is lost through the outgoing Hankel wave.

Next, we center our attention on the displacement of the peak axial intensity with respect to the red dashed line, we used the position z_p instead of z_1 because it is easier to see the shift the axial intensity suffers, but this shift happens with respect to the geometrical "pseudo-focal" point z_1 as well. To explain this behavior, we remember the definition Eq.(5.92) which depends on the value of the radius of the focal ring, the focal length, and the radius R of the aperture. For the apertured Bessel beam, the size of the circular function remains constant, but now we need to consider the apodization profile acts as the new aperture, and if we recall from the beginning of the section the w_{SG} depends on the parameter m. Thus, the radius of the aperture is different for every value of m while ρ and f do not change. In Table 5.3 we calculated the values of the z_1 with the Eq.(5.92), for the values of m illustrated in Figure 5.29. We note the value of z_1 is closer to the "real" ones in Table (5.1), especially for the case $f = 2$, but for $f = 4, 6$ the variations are slightly more evident. The fact the positions of maximum intensity do not vary much is due to the condition of conservation of energy we

Parameter m	z_1		
	$f = 2$	$f = 4$	$f = 6$
1	1.79	3.24	4.45
2	1.80	3.28	4.52
3	1.80	3.28	4.52
5	1.80	3.27	4.50
10	1.79	3.26	4.48

TABLE 5.3: Theoretical calculation of z_1 for different values of focal length and m, for the SG case.

established at the beginning because if we considered an arbitrary w_{SG} and used it for every different parameter m then displacement in position will more notorious and similarly with the peak axial intensity, we would not reach values as high as the ones we showed.

Finally, we analyze the 2D output profiles at their respective z_p plane for the case $f = 2$ and $f = 4$, for $m = 2$ and $m = 10$, illustrated in Figures 5.30 and 5.31. For case $f = 2$, the central peak radius is the same as the apertured Bessel beam in Table (5.1), $r_1 = 0.073$, for both values of m. For $f = 4$, the radius is larger, more specifically we obtained a value of 0.146 for $m = 2$ and 0.122 for $m = 10$. But if we look at Figures 5.30 and 5.31 and compare them with Figure 5.22 we notice not only does the colorbar shows smaller values of intensity, as expected, but for both parameters of m we note a downsizing in the visible lobes, whose radii are smaller too. This characteristic is notorious too between them, there is a reduction in side-lobes when using $m = 10$ instead of $m = 2$. The explanation is once again related to the diffraction effects, which not only affect the maximum intensities reached but cause beam divergence, and as a result, we have bigger lobes but with less energy. The reduction of side lobes when using bigger parameters of m is due to the broader shape of the "window" that propagates and suffers diffraction effects.

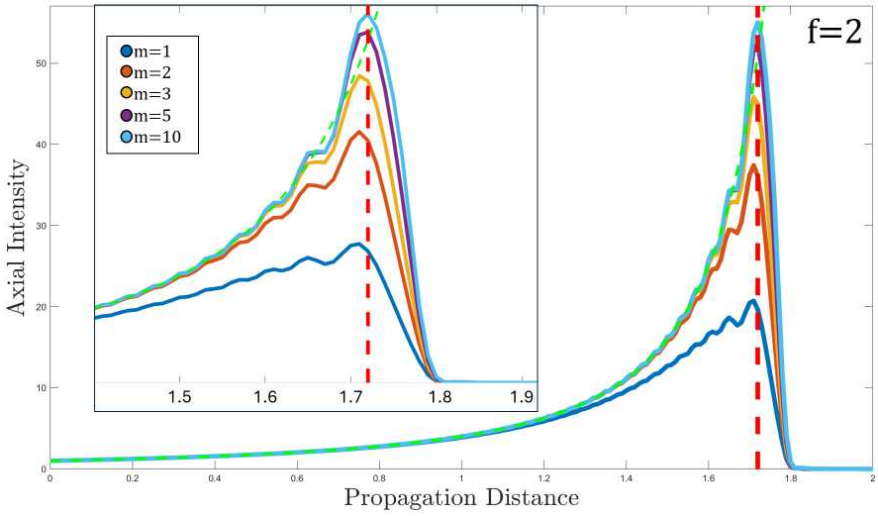

(A)

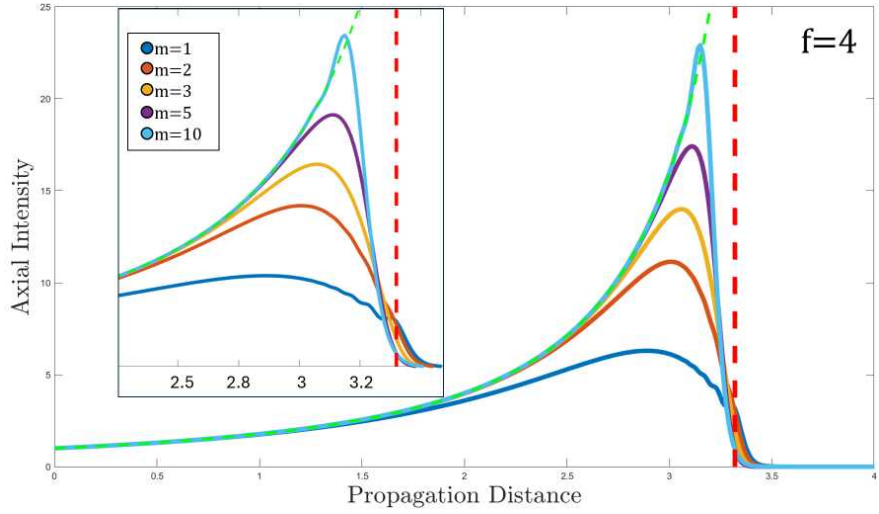

(B)

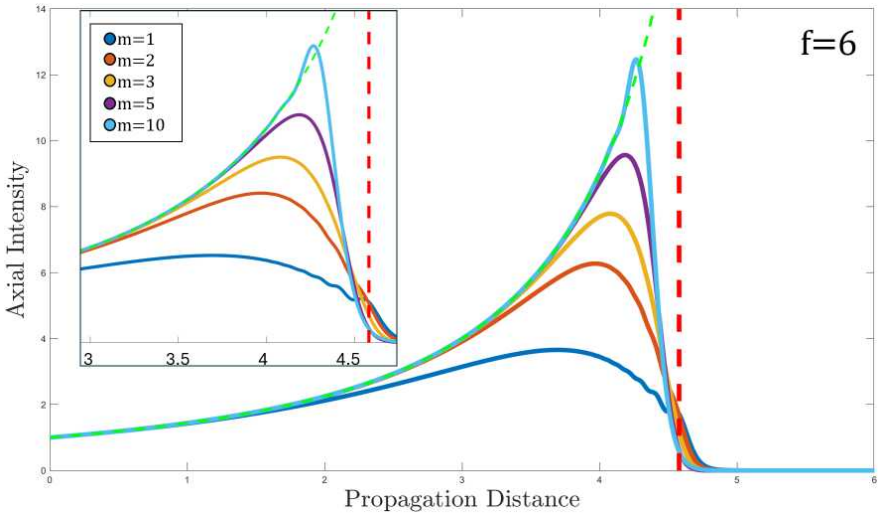

(C)

FIGURE 5.29: Evolution of the axial intensity of the apertured Bessel beam apodized by a Super Gaussian function. The dashed red line represents the position of exact maximum intensity z_p for the beam without apodization.

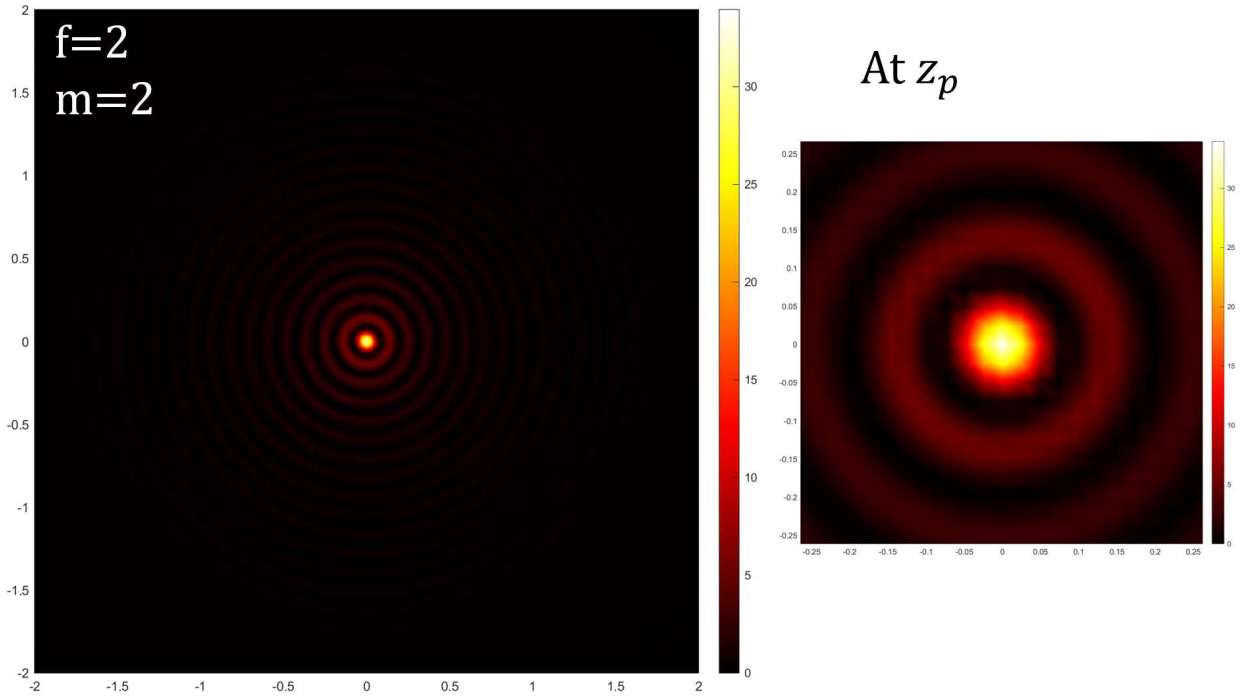

(A)

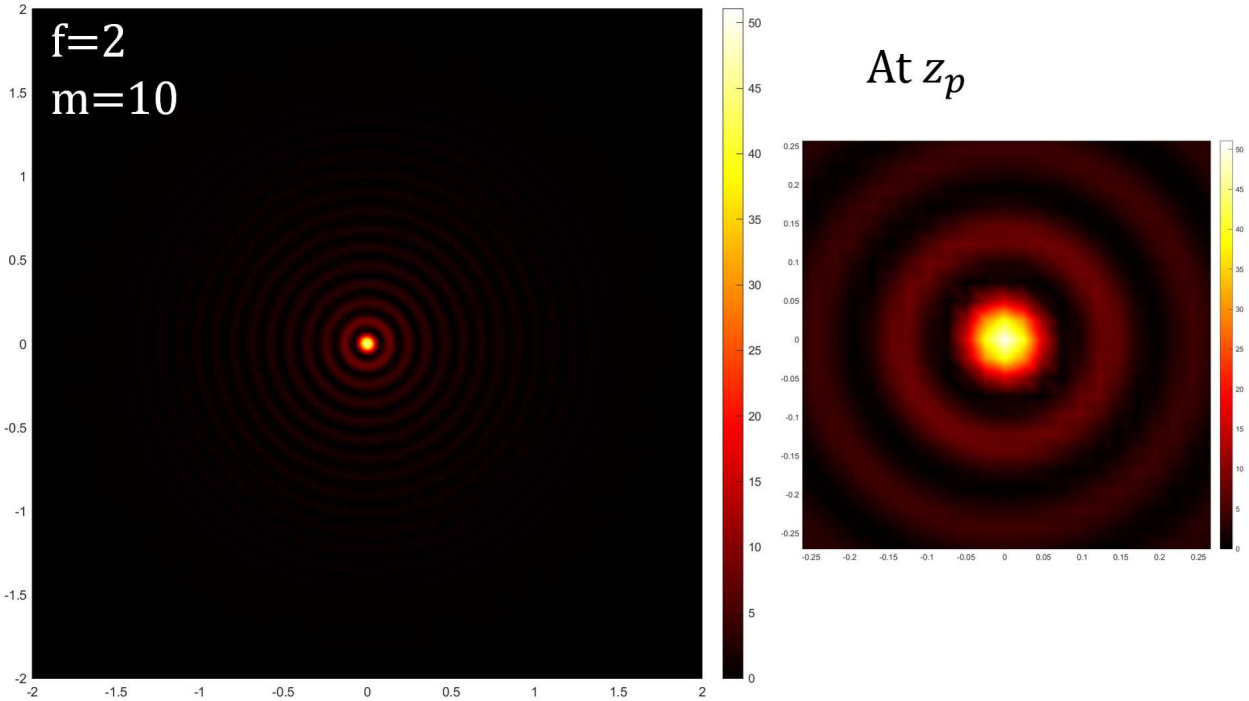

(B)

FIGURE 5.30: 2D output profiles of the focused apertured Bessel beam apodized by the SG function at the plane z_p for a focal length $f = 2$.

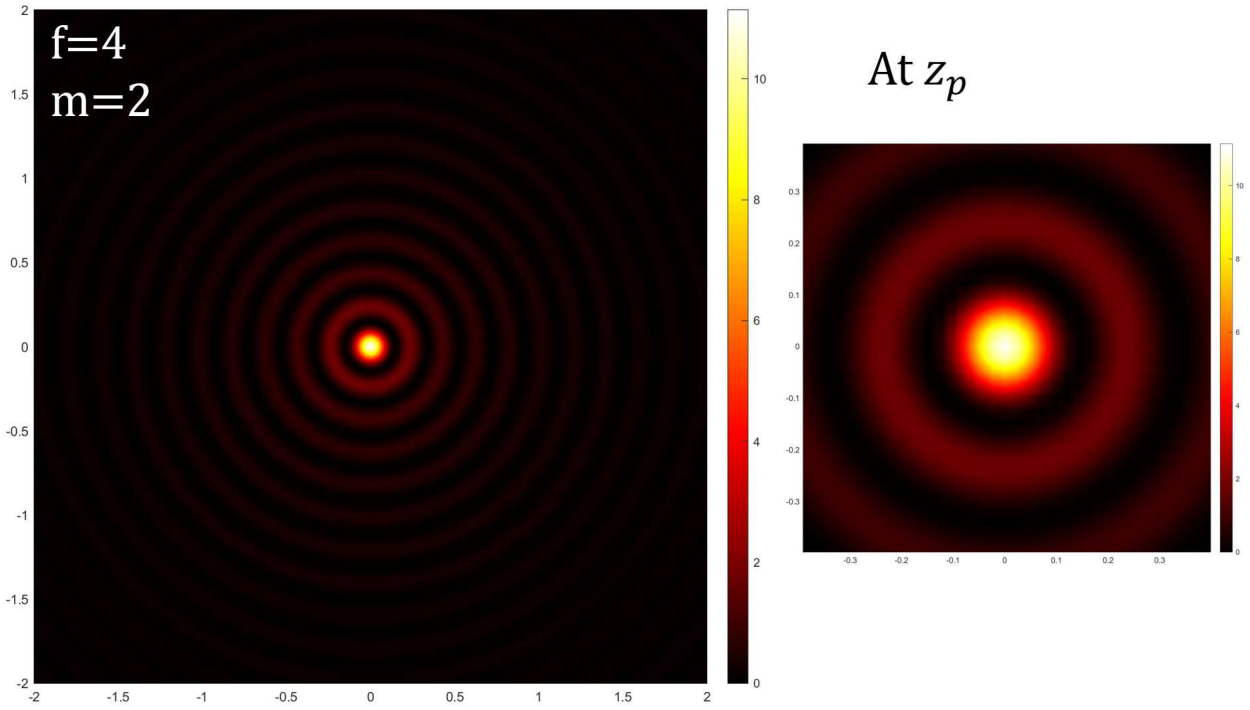

(A)

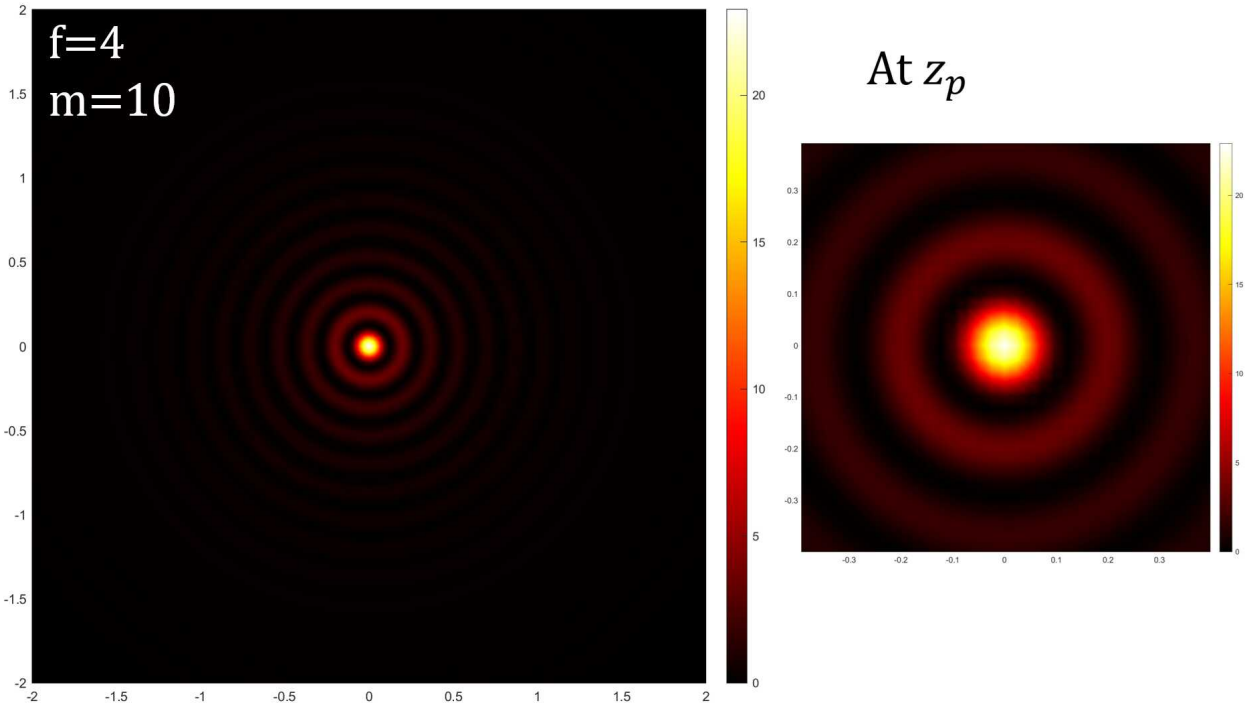

(B)

FIGURE 5.31: 2D output profiles of the focused apertured Bessel beam apodized by the SG function at the plane z_p for a focal length $f = 4$.

Flattened Gaussian beam

F. Gori [78] presented another Gaussian-like function whose steepness is controlled by an integer parameter N, he called them Flattened Gaussian beams (FG beams). Multiple formulas describe this kind of profile, but we will use the one that takes the form

$$U_{\mathrm{FG}}(r) = \exp\left[-\left(\frac{r}{w_{FG}}\right)^2\right] \sum_{j=0}^{j=N} \frac{1}{j!}\left(\frac{r}{w_{FG}}\right)^{2j} \tag{5.109}$$

where r and w_{FG} are again the radial coordinate and beam waist respectively, and N is a positive integer parameter.

The analysis follows the same order we employed for the SG function, first, we solved the Eq. (5.104) which yields

$$P_0 = \frac{w_{FG}}{2} C_F(N) \tag{5.110}$$

where the

$$C_F(N) = \int_0^{\infty} \exp(-2u)\left(\sum_{j=0}^{N} \frac{u^j}{j!}\right) du \tag{5.111}$$

Thus, when we write the P_0 in terms of w_G we obtain

$$w_{FG} = \frac{w_G}{\sqrt{2C_F(N)}} \tag{5.112}$$

Eq. (5.112) was solved numerically for different values of N, the values are shown in Table 5.4.

In Figure 5.32 we illustrate the profile of this function for different values of N according to the values of Table 5.4 and the same w_G we used for the SG function. It is evident that the center is flat and the shape around the waist resembles an ordinary Gaussian function. Additionally, the FG takes the form of an ordinary Gaussian when $N = 0$.

As expected the behavior with respect to the two powers, P_1 and P_2, is analogous to the SG case, more energy means the peak axial intensity is larger. However, the main difference lies in the fact that the FG case seems to not reach the same peak axial intensity described in Table 5.1 for the apertured Bessel beam regardless of the focal length or power used, this is illustrated in Figure 5.33.

Parameter N	w_{SG}
0	w_G
1	$0.6324w_G$
2	$0.4923w_G$
10	$0.2337w_G$
25	$0.1470w_G$
50	$0.1031w_G$

TABLE 5.4: Numerical calculation of the size of the waist of the Flattened Gaussian beam for different values of the parameter N.

The reason for the lower peak axial intensities reached with this apodization function is found in its profile (see Figure 5.32). The red dashed line is shorter for the FG function than it was for the SG beam, which means the "window" is narrower and as such it has a lower transmittance. However, we work with power P_1 to analyze the same characteristics we analyzed for the other apodization profile.

In Figure 5.34 we show the axial intensity versus z for different values of N and the same three cases of focal length: $f = 2$,$f = 4$, and $f = 6$. Once again, the red dashed lines mark the position z_p at which the axial intensity of the apertured Bessel beam without anodization is maximum, and the green dashed curve represents the Lorentzian that describes the axial intensity.

Analogously to the SG case, the energy reaches higher values when N increases. As we mentioned, $N = 0$ corresponds to the standard Gaussian profile, which is the reason the curve is the same as in Figure 5.29 for $m = 1$. However, the maximum peak intensities reached for each case were 68%, 28.3%, and 31.5% of the peak intensity of 5.1 for $f = 2, 5, 6$ respectively when using $N = 25$. But we note the curve for the $f = 2$ case is smothered for $N \geq 25$, which if we recall, the SG function could not smooth no matter how large the parameter m was. The reason for this once again can be placed on the profile of the apodization function. The lower transmittance of this function results in the decrease of the contrast of the axial oscillations. Now, if we considered the energy had to be conserved and found the "appropriate" size of w_FG to ensure this when using Parseval's theorem, then

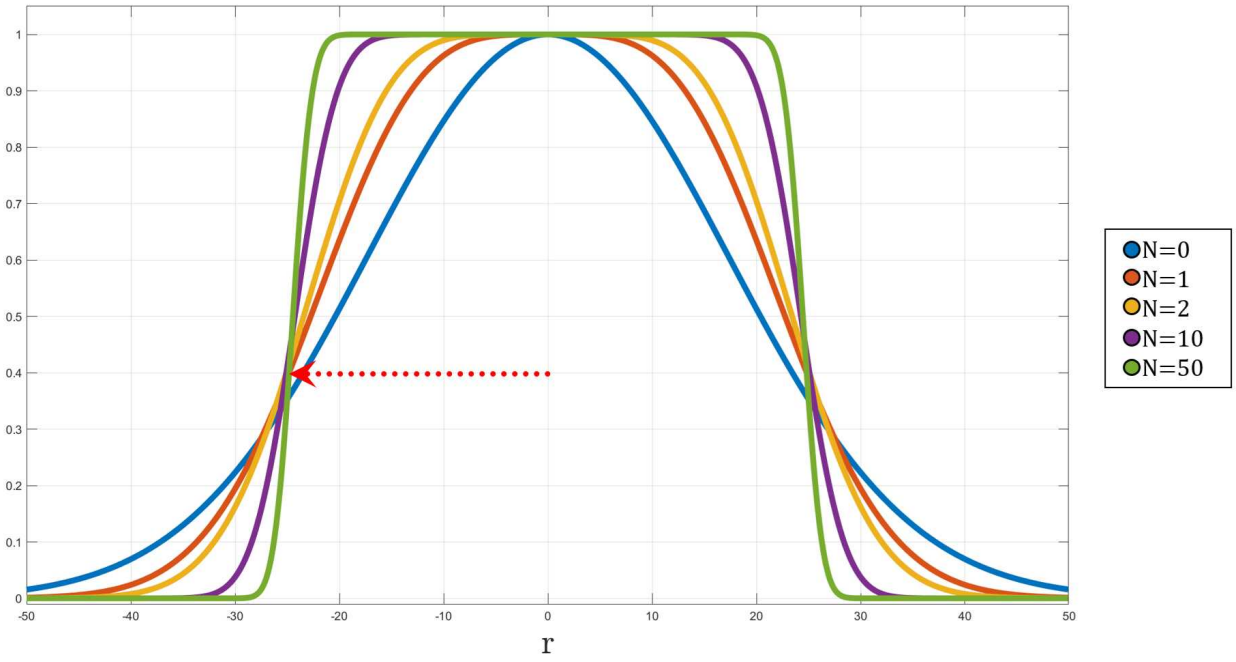

FIGURE 5.32: FG profiles versus r for values of N.

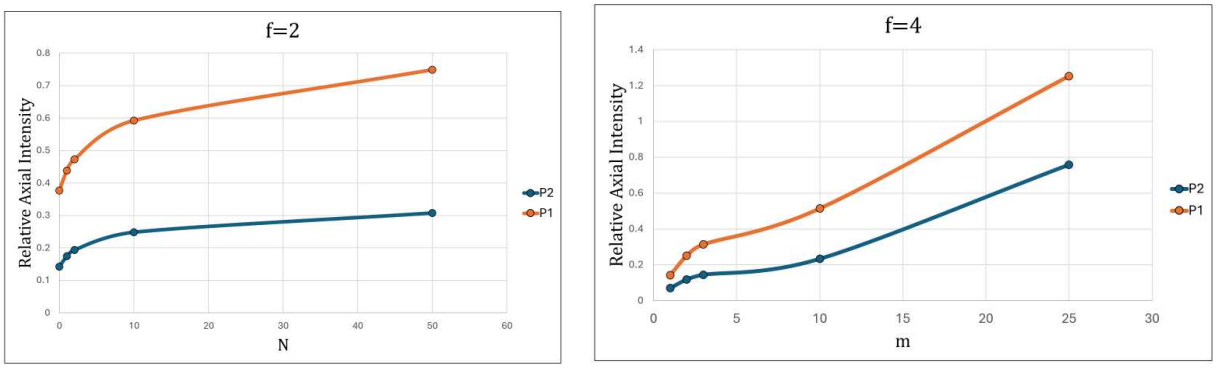

(A) (B)

FIGURE 5.33: Relative peak axial intensity of a Bessel beam with an SG function when focused with a lens with a focal length of (A) 2 and (B) 4.

why do we say the transmittance is lower? This is because if we pay attention both SG and FG functions have a similar shape, i.e. similarly to the SG function the center of the FG function is flat but the shape around the waist of the latter resembles an ordinary Gaussian function, while the borders of the SG function are more vertical. Thus, this "Gaussian-like tail" is responsible for the low "real" transmittance, because as it has been proved [75] a Gaussian profile with low transmission creates an axial intensity with small oscillations at the expense of a fast loss of energy. This is notorious in the three plots of Figure 5.34, and

Parameter N	z_1		
	$f = 2$	$f = 4$	$f = 6$
0	1.79	3.24	4.45
1	1.69	2.92	3.87
2	1.62	2.72	3.52
4	1.51	2.44	3.07
10	1.33	2.01	2.41
25	1.12	1.55	1.78
50	0.94	1.23	1.37

TABLE 5.5: Theoretical calculation of z_1 for different values of focal length and N, for the FG case.

not only that. Nevertheless, putting the energy matter aside as an apodization function this profile proves to produce a slighter smoother curve than the SG profile, and it does not require large values of N, for the cases $f = 4$ and $f = 6$ with $N > 0$ is enough.

Continuing with the displacement with respect to the red dashed line, we note this is much larger than the one we observed in Figures 5.29. But before providing an explanation, in Table 5.4 we calculated the values of z_1 with the use of Eq. (5.92) for some values of N.

From Table 5.5 we see the value of z_1 becomes smaller while N grows. This is explained when we remember z_1 depends on the aperture radius which in this case is equivalent to w_{FG}, and these values vary for every parameter N, and as we described when we analyzed the axial intensity, the transmittance of the FG function is lower because its waist is narrower, consequently, this impacts on the value of the "pseudo-focal" point, making it shorter.

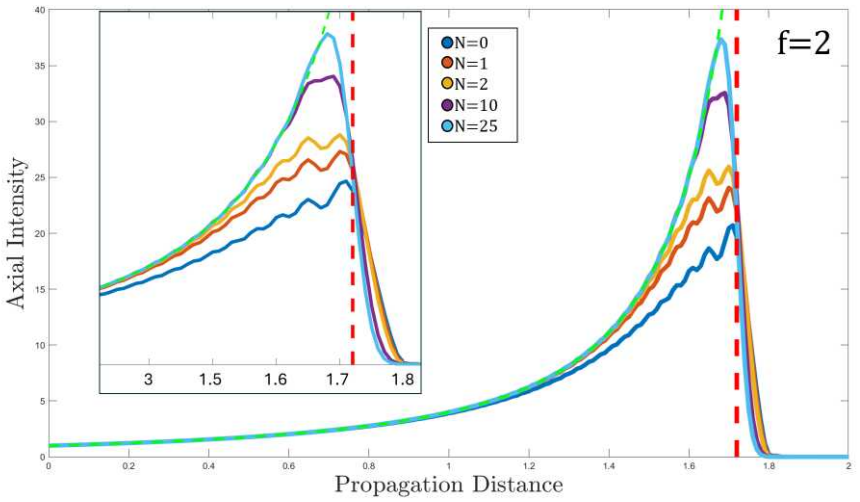

(A)

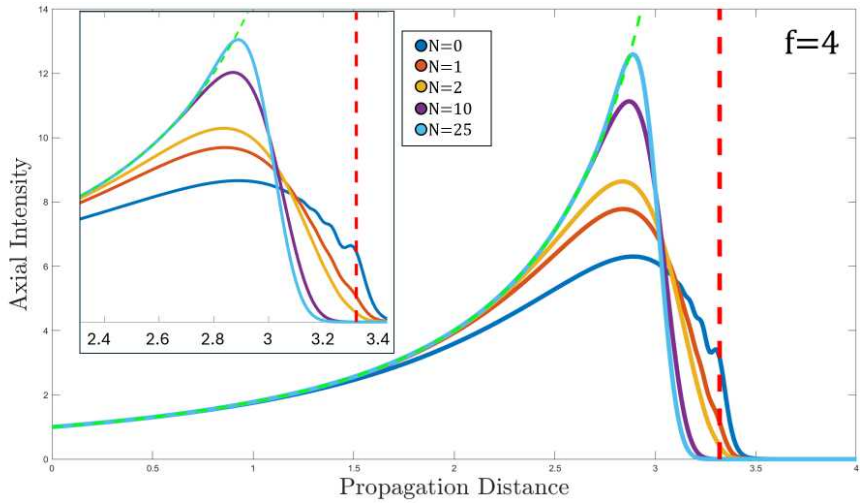

(B)

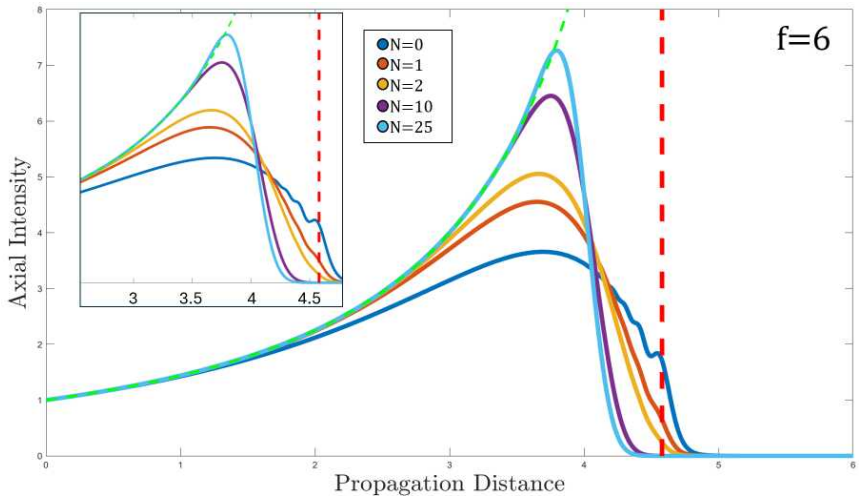

(C)

FIGURE 5.34: Evolution of the axial intensity of the apertured Bessel beam apodized by a Flattened Gaussian function. The dashed red line represents the position of exact maximum intensity z_p for the beam without apodization.

Lastly, we center our attention on the 2D output profiles for the two cases, $f = 2$ and $f = 4$, at their respective z_p plane, illustrated in Figures 5.35 and 5.36. For the case $f = 2$, the central peak radius r_1 has a value of 0.097 for $N = 1$ and 0.073 for $N = 10$. For its part, when $f = 4$, the radius takes the values 0.170 for $N = 1$ and 0.146 for $N = 10$.

We analyze the case $f = 2$ and notice the value of 0.073 from Table 5.1 is reached for $N = 10$, but with a reduction of intensity amplitude and a downsizing of the visible size-lobes with respect to the apertured case. However, for $f = 4$ this is not the case. The behavior is the same, an increase in intensity amplitude at the center lobe with respect for a larger N but a downsizing of the visible side-lobes. The explanation for this result is the same as we gave for the SG beam about the loss of energy by diffraction effects.

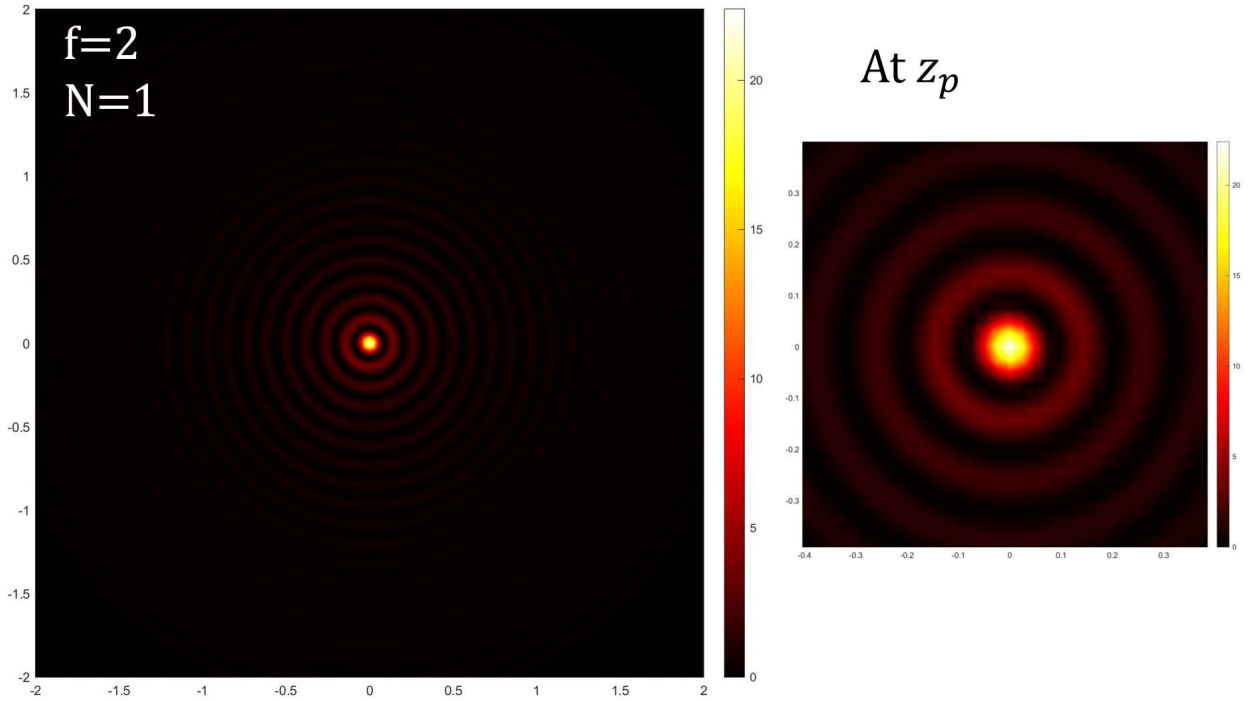

(A)

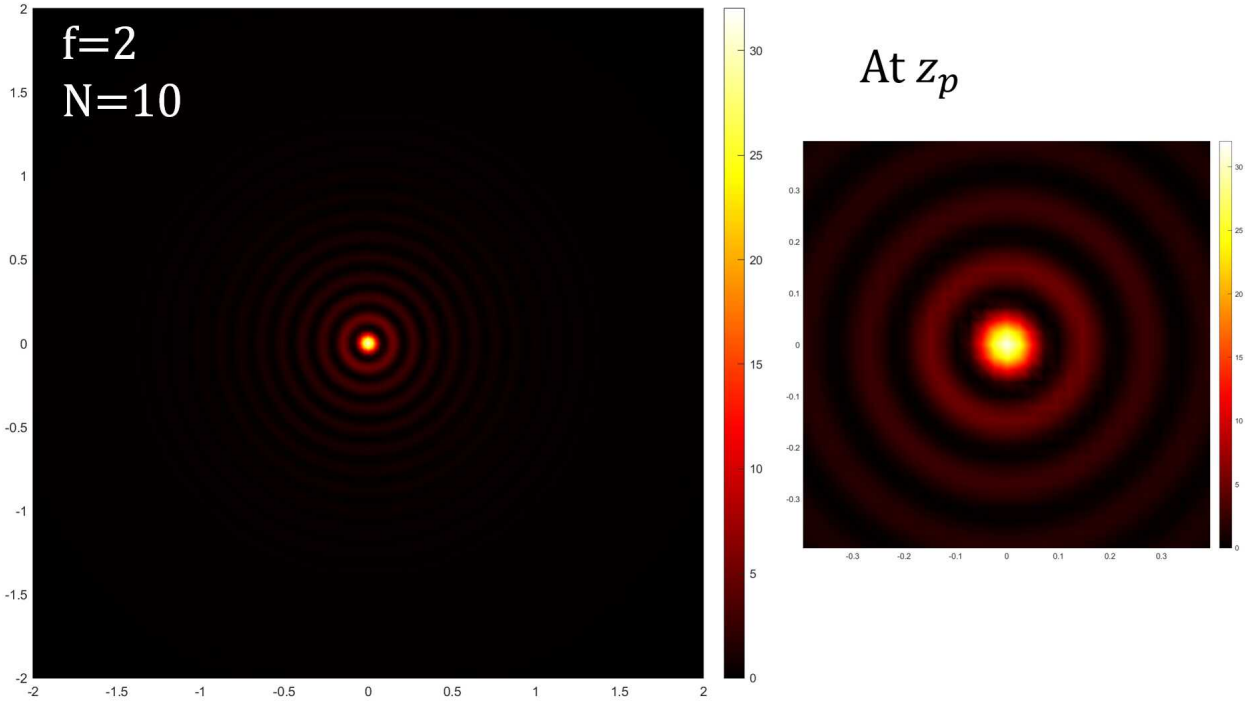

(B)

FIGURE 5.35: 2D output profiles of the focused apertured Bessel beam apodized by the FG function at the plane z_p for a focal length $f = 2$.

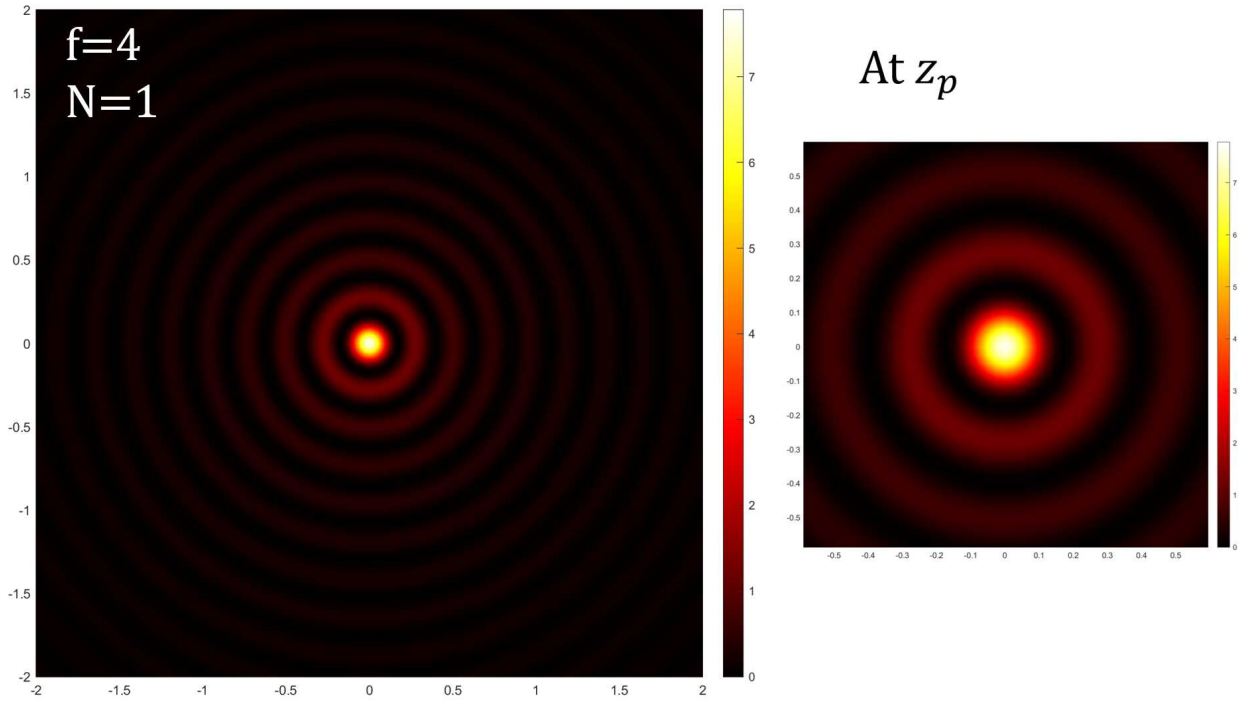

(A)

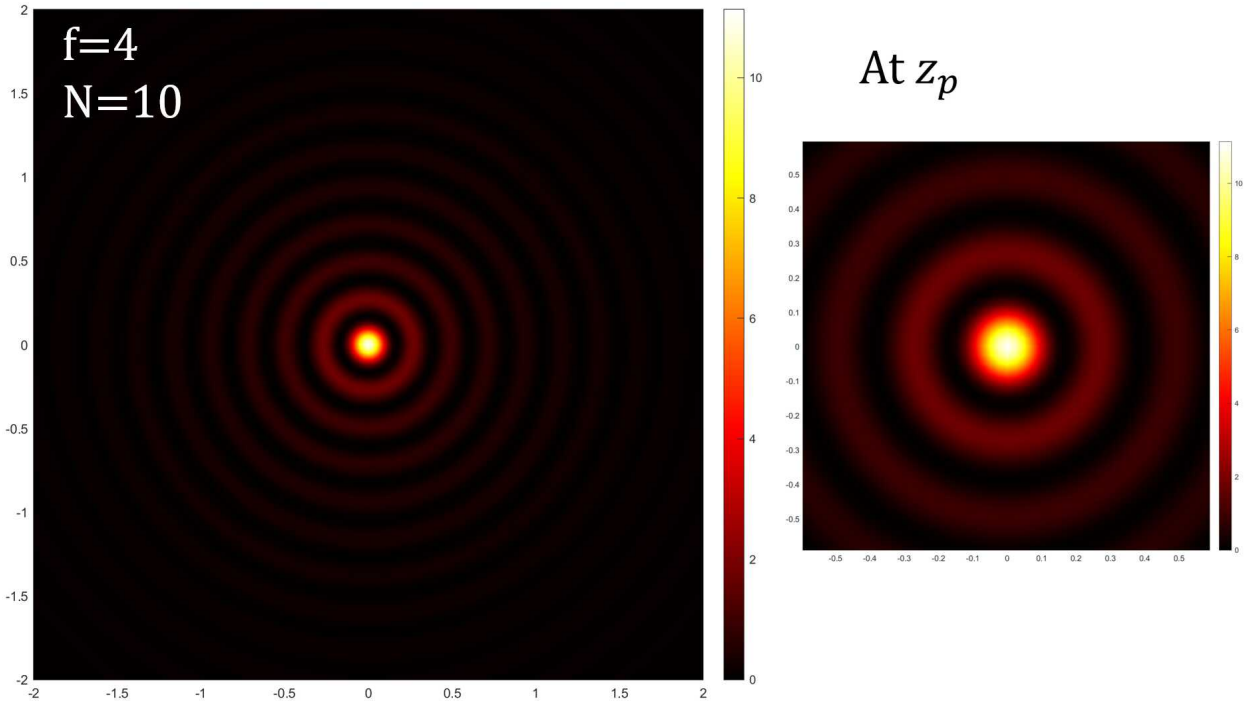

(B)

FIGURE 5.36: 2D output profiles of the focused apertured Bessel beam apodized by the FG function at the plane z_p for a focal length $f = 4$.

SG vs FG

To close this section, we present a short direct comparison between both apodization functions. In Figures 5.37 we contrast their relative peak axial intensities, both show oscillations for their first order after the standard Gaussian beam, the main difference at the intensity amplitude which is higher for the SG beam. But the disparity is evident in Figures 5.38 where we increased both parameters to 10. Some small oscillations are still found in Figure 5.38a while the curve in the case of an FG beam shows little to no oscillations. However, as we concluded before this reduction in oscillations is at the expense of energy loss which is due to the shape of the FG beam.

Figure 5.39 shows the profiles of SG beam, the FG beam, the standard Gaussian beam, and the Bessel beam to help visualize the differences between the apodization functions, which impact in their transmission and consequently the oscillations, peak intensity, and positions z_p as we have observed through all this section. Notice how the edges of the SG are sharper which causes major diffraction effects, but the waist w_{FG} is narrowed which means the energy entering the system is lower.

Lastly, the comparison of the 2D output is presented in Figure 5.40 at the point of maximum intensity for each beam for specific values of m and N. We calculated the ratio $r_1(\text{apodized})/r_1(\text{input}) = \alpha_1$ between the radius of the focused beam with an apodization function at z_p and the radius of the Table 5.1, and we observed that for $f = 2$ the SG and FG beams have an $\alpha_1 = 1$ for $m = 10$ and $N = 10$. For $f = 4$, the value $\alpha_1 = 1.5$ for both beams is obtained for $m = 2$ and $N = 10$, which is why we illustrate these four cases in Figure 5.40. Thus, it is possible to use any of the apodization functions and maintain the size of the center lobe or increase it, but as we have emphasized throughout this section, these results are at the expense of energy.

In summary, when using Parseval's theorem to ensure energy conservation we can obtain the values of the waist w_{SG} and w_{FG} for the apodization functions. The function SG showed to be able to focus the Bessel beam while reaching a peak in intensity of the same magnitude as the case without apodization and for $f > 2$ the oscillations caused are greatly reduced for $m > 1$, and the spot size of the center lobe is maintained for $m = 10$ in the case of $f = 2$. For

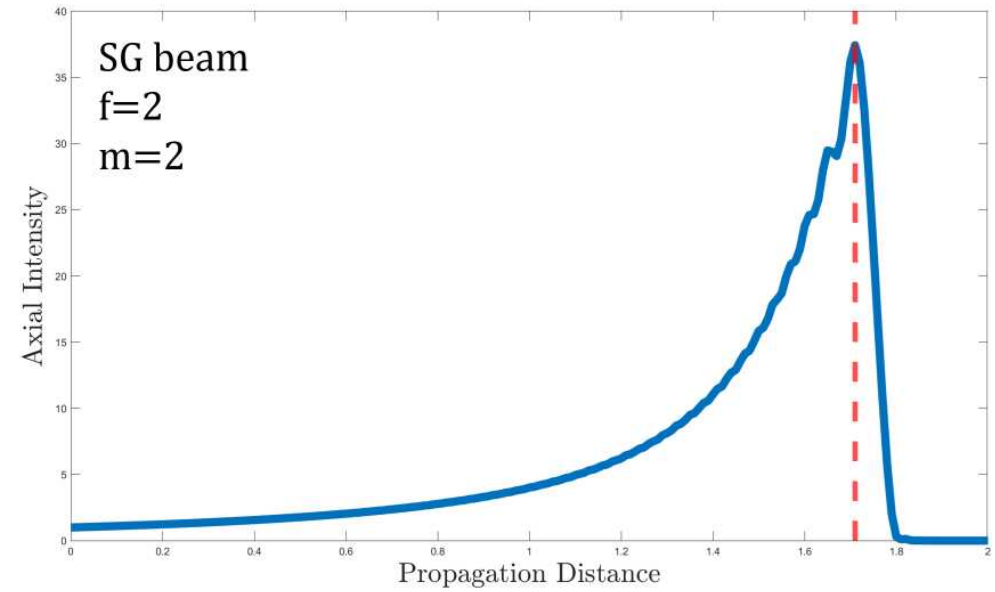

(A)

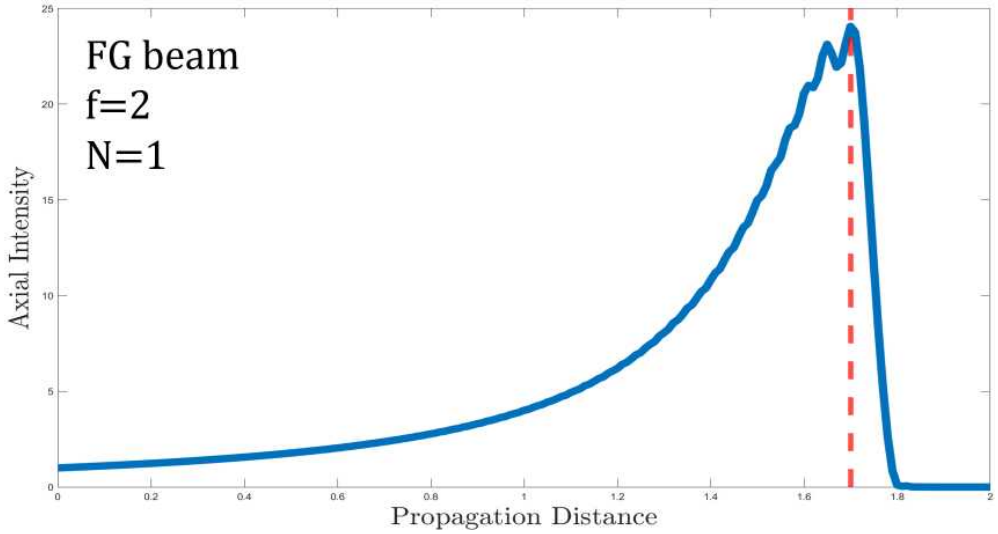

(B)

FIGURE 5.37: Comparison of the evolution of the axial intensity of the apertured Bessel beam apodized by (A) a Super Gaussian function and (B) a Flattened Gaussian function, for the first order after the standard Gaussian beam.

its part, the FG beam reduces the oscillations far better than the SG, for the focal length of 2 it can do it for $N \geq 25$, and for the other focal lengths when $N > 0$. However, the peak intensities reached are never higher than 32% for $f \geq 4$. Similarly to the SG beam, it is possible to keep the size of the center lobe for $f = 2$ when $N = 10$.

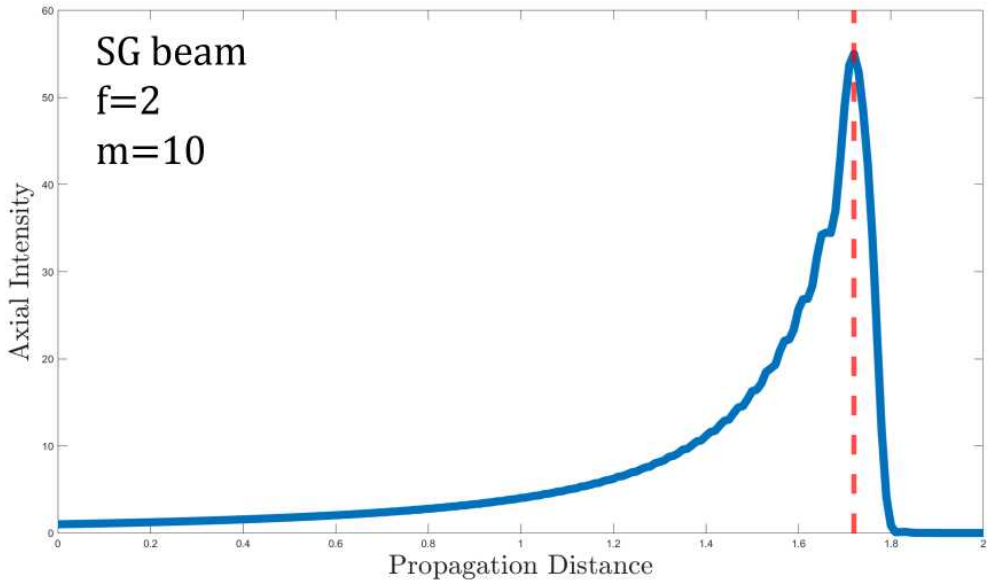

(A)

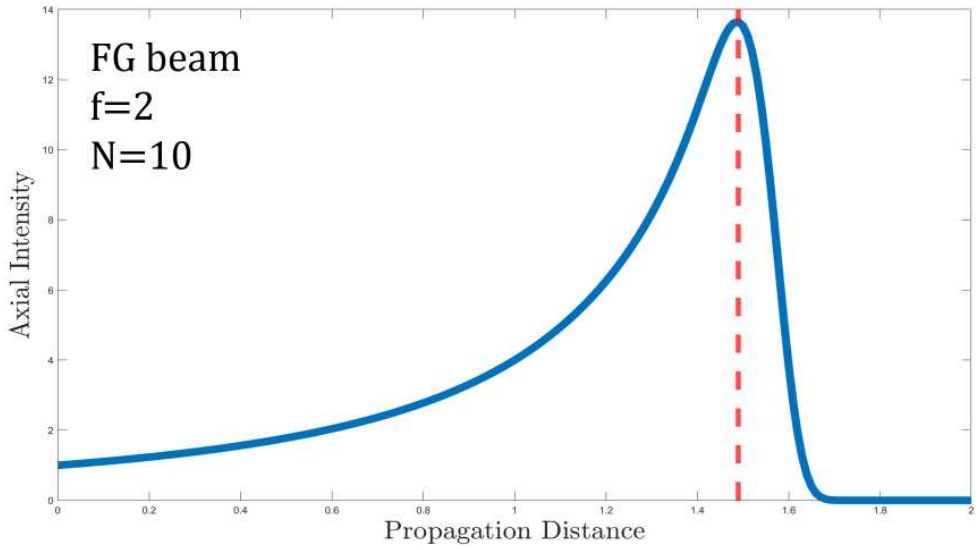

(B)

FIGURE 5.38: Comparison of the evolution of the axial intensity of the apertured Bessel beam apodized by (A) a Super Gaussian function and (B) a Flattened Gaussian function, for the tenth order.

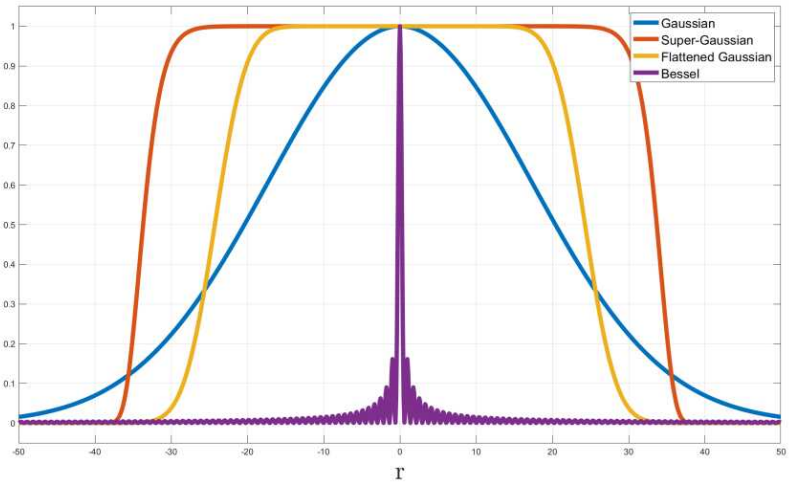

FIGURE 5.39: Transverse profiles of the Bessel beam, the standard Gaussian beam, and the two apodization functions: SG beam and FG beam.

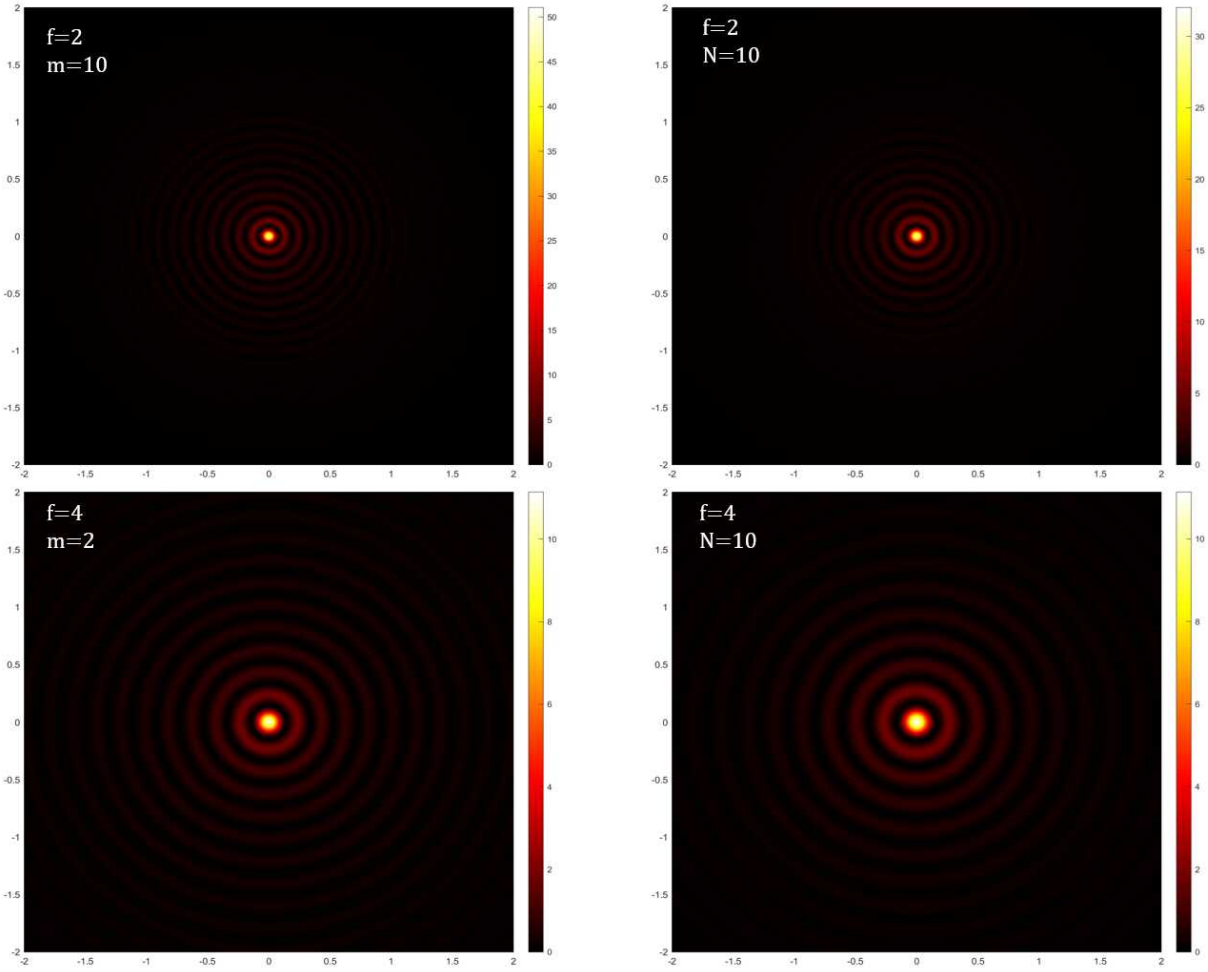

FIGURE 5.40: Comparison of the 2D output profiles of the focused Bessel beam apodized where the center lobe is of the same size.

5.4.7 Geometrical Approximation

For the final section, we revisit the method employed in Section 5.4.5 to calculate the transverse magnification at the "pseudo-focal" plane of the focused Bessel beam.

In the section where we calculated the transverse wave vector of the Bessel beam transmitted through a lens and found it is described by:

$$k_{2r} = k_2 \sin\beta = k \sin\beta \tag{5.113}$$

when the medium behind and ahead of the lens is the same, this value is obtained at the "pseudo-focal" point, and as we mentioned we can find the value of k_{2r} for each point along the axis.

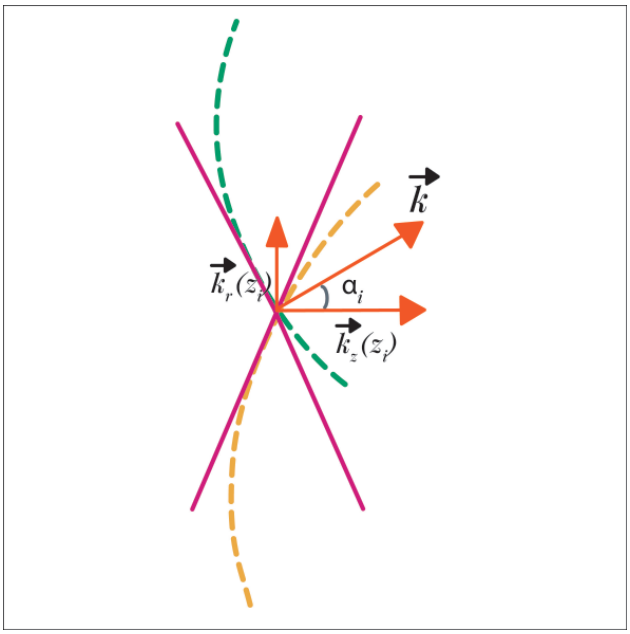

FIGURE 5.41: Zoom in on the Figure 5.14, we show the tangents of the converging waves at one arbitrary point along the axis as pink lines.

The paraxial approximation $\tan\varphi = \sin\varphi$ is required here because we only examine points close to the z-axis. From Figures 5.14 and 5.41 we note that for each point on the axis, the exact value of the angle formed between the tangent of each point and the z-axis is described by

$$\sin\alpha_i = \frac{\rho}{\sqrt{\rho^2 + (f - z_i)^2}} \tag{5.114}$$

and according to Eq.(5.113), but also from Figure 5.41, we have that the value of the transverse wave vector for each point on the axis $k_r(z_i)$ is given by

$$k_r(z_i) = k \sin \alpha_i \tag{5.115}$$

So substituting Eq.(5.114) into Eq.(5.115) we obtain

$$k_r(z_i) = \frac{k\rho}{\sqrt{\rho^2 + (f - z_i)^2}} \tag{5.116}$$

To write the last equation in terms of the incident Bessel beam, whose intensity is proportional to $|J_0(k_{1r}r)|^2$ we notice from Figure 5.18 that under the paraxial approximation, the radius of the focal ring can be written as:

$$\rho = f \sin \varphi = f \frac{k_{1r}}{k} \tag{5.117}$$

Substituting Eq.(5.117) into Eq.(5.116) yields the geometrical approximation of the transverse wave vector we were looking for

$$k_r(z_i) = \frac{f k_{1r}}{\sqrt{\rho^2 + (f - z_i)^2}} \tag{5.118}$$

Eq.(5.118) is used to simulate numerically the evolution of a focused Bessel beam when substituted in the argument of the Bessel function $J_0(k_r(z_i r))$.

We also need a function that modulates the axial intensity and for that, we use the Eq. (5.94) that we know describes the propagation on-axis of the Bessel beam, that is:

$$I(z_i) = \frac{f^2}{(z_i - f)^2} \tag{5.119}$$

Still, additionally, we require a windowing function written in geometrical parameters as $k_r(z_i)$ to simulate the light funnel, i.e. to transversally limit the beam. But first, we need a geometrical approximation for the waist $W(z_i)$ of the windowing function for each point on the axis in terms of the radius of the lens R.

First, we calculate $\tan\beta$ in terms of z_i

$$\tan\beta = \frac{W(z_i)}{z - z_i} \tag{5.120}$$

and from Figure 5.18, we notice under the paraxial approximations $\tan\beta = R/z_1$, thus the radius of the windowing function is

$$W_i(z_i) = (z_1 - z_i)\frac{R}{z_1} \tag{5.121}$$

Eq.(5.121) is necessary because it acts as the waist of the windowing function that is going to avoid the Bessel beam extents in all the transversal space, we use here the super-Gaussian function or Flattened Gaussian profiles to modulate the propagation of the Bessel beam.

For the SG function, we have

$$U_{SG}(r, z_i) = \exp\left[-\left(\frac{r}{W(z_i)}\right)^{2m}\right] \tag{5.122}$$

and for the Flattened Gaussian function the expression takes the form

$$U_{FG}(r, z_i) = \exp\left[-\left(\frac{r}{W(z_i)}\right)^{2}\right]\sum_{j=0}^{j=N}\frac{1}{j!}\left(\frac{r}{W(z_i)}\right)^{2j} \tag{5.123}$$

Finally, the expression for the evolution of a focused Bessel beam as a geometrical approximation is formed by the Eqs. (5.118) , 5.119 , and the (5.121) along one of the windowing functions. If we use the SG function we obtain

$$E_{\text{AproxGeo1}}(r, z_i) = \frac{f^2}{(z_i - f)^2}J_0\left(k_r(z_i)r\right)\exp\left[-\left(\frac{r}{W(z_i)}\right)^{2m}\right] \tag{5.124}$$

and for the FG function, the equation is

$$E_{\text{AproxGeo2}}(r, z_i) = \frac{f^2}{(z_i - f)^2}J_0\left(k_r(z_i)r\right)\exp\left[-\left(\frac{r}{W(z_i)}\right)^{2}\right]\sum_{j=0}^{j=N}\frac{1}{j!}\left(\frac{r}{W(z_i)}\right)^{2j} \tag{5.125}$$

Both of these geometrical approximations are valid only within the region between the

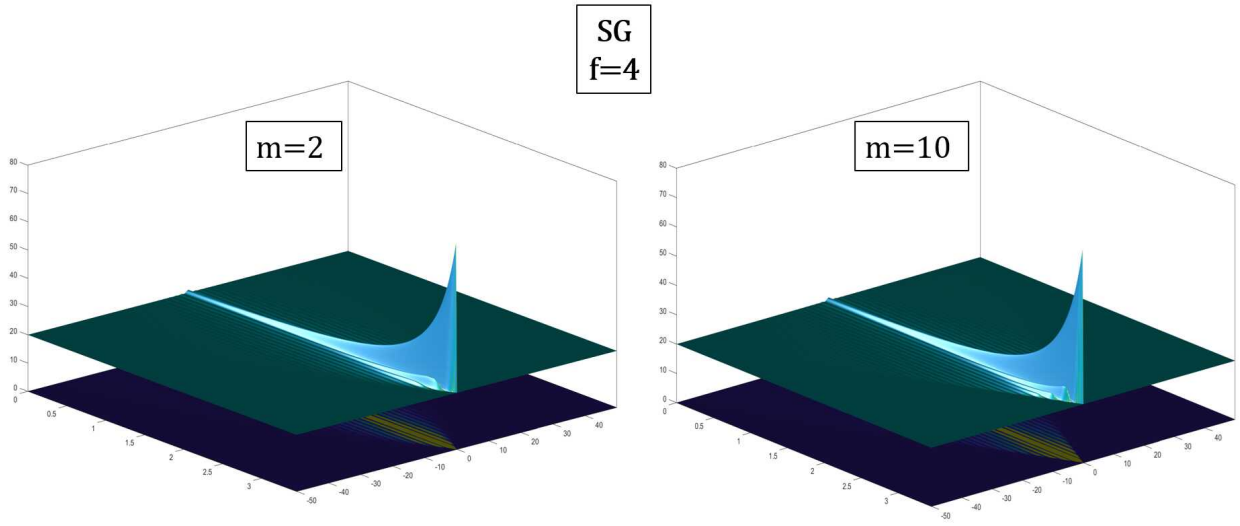

FIGURE 5.42: Evolution of the propagation of a Bessel beam with the SG function passing through a thin lens using the geometric approximation.

lens and pseudo-focus point, i.e. for $z \in [0, z_1]$. In Figure 5.42 we show an example of a tridimensional profile of a focused Bessel beam obtained using Eq.(5.124) for two values of m. The case with the Eq.(5.125) is illustrated in Figure 5.43 for two values of N. In both cases, we assumed a focal length of 4, a lens of radius $\boldsymbol{R} = 50$, and the radial wave vector of the Bessel beam is $k_r = 4$, all of them in normalized coordinates.

The program calculates the value of the pseudo-focal point z_1 using Eq.(5.92) and for the particular case of the examples shown, the value is $z_1 = 3.44$. Meanwhile, the peak intensity the program reports from the geometrical approximation is $z_{ag1} = 3.45$ for both cases of windowing functions. This approximation predicts correctly that in the z_1 point, geometrically we find a peak in the axial intensity of the beam.

Additionally, an interesting feature we noticed while working with this program was that for both, the SG and FG function, we obtained the same value of the pseudo-focal point and peak axial intensity regardless of the value of k_r. Further, from Figures 5.42 and5.43 we notice the parameters m and N only increase the number of side-lobes of the Bessel profile, this is due to the profile of each windowing function, the FG function is wider than the SG function as the Figure 5.44 shows, which means the window boundary coincides with a bigger zero of the Bessel function, that is more energy is transmitted. Notice the profiles of SG and FG functions are different from the ones shown in Figure 5.39, this is because last

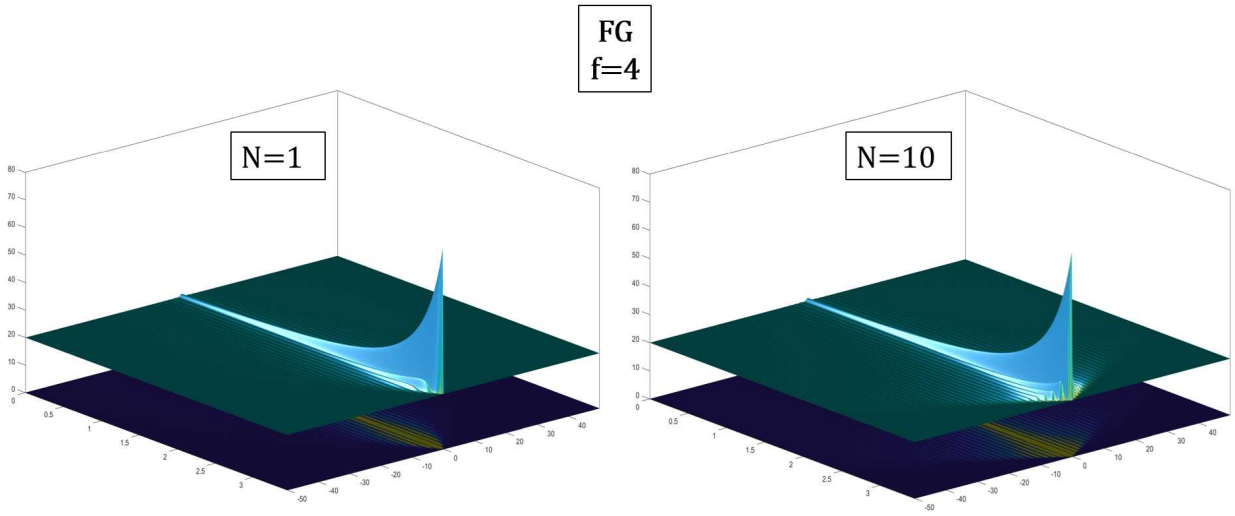

FIGURE 5.43: Evolution of the propagation of a Bessel beam with the FG function passing through a thin lens using the geometric approximation.

section we considered energy conservation for the values of the waists of both functions, and here not.

From Figure 5.42 and 5.43 we notice the shape of the axial intensity, the peak intensity, and the value of z_1 remain the same, this is expected because the axial intensity is modulated by Eq.(5.119), that does not depend on the windowing parameters. However, the peak intensity does vary for different values of f, the larger f is, the lower the intensity reached, the explanation for this is the same as we provided last section with Fig. 5.24, the propagation of distance increases with f, which translates into less energy due to diffraction effects.

Now, we also examine the output intensity profiles for both Eqs. (5.124) and (5.125) at the point z_{ag1}, the results are shown in Figure 5.45 where we noticed something interesting. For $f \geq 4$ the shape and the approximate radius r_1 of the center lobe do not change for any of the windowing functions, and no change is observed for different values of m or N either. But for $f \simeq 2$, the size of the spot varies. For the FG case, as we increase N, the radius of the center lobes does it too, and as Figure 5.45 illustrates, its shape is rounder too. For its part, the shape of the peak lobe is only slightly rounder for the SG case, and the radius r_1 also varies with m.

In general, from our observations and numerous tests, we conclude the radius r_1 and shape of the center peak depend on the propagation distance z, that is, the maximum value

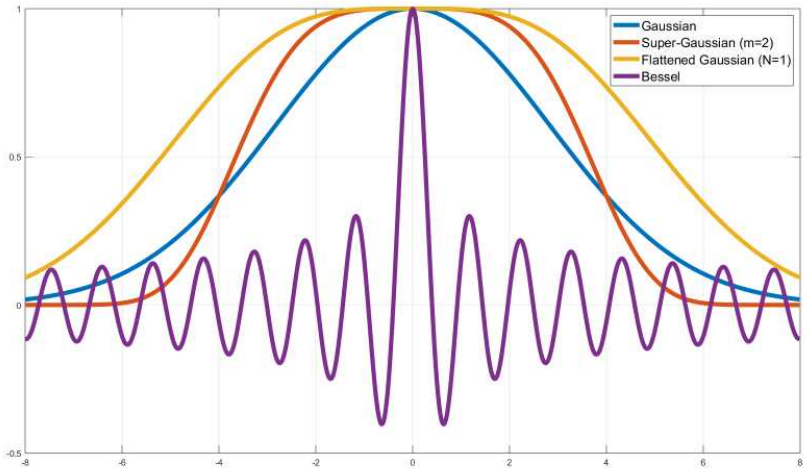

FIGURE 5.44: Transverse profiles comparison of the SG, FG, and Bessel functions.

z_i takes within the program, which is why for $f \simeq 2$ ("small" focal length) the propagation distance is short which means less energy is lost and as a consequence the variations in shape and size of the lobe are more notorious, this is similar to what happened with the oscillations caused by diffraction when their contrast was higher when more energy was in the system. And for "large" focal lengths much more energy is lost (see upper right corner of each profile in Figure 5.45) which translates into no noticeable changes.

Our geometrical approximation is flawed because so far we do not have control of the energy of the system which means we cannot analyze the relative axial intensity as we did last section, but the energy is increased as we expected due to the implementation of the Loretzian approximation (Eq.(5.119)). Moreover, we are also limited by the size of the matrix we use to run our geometrical approximation in MatLab, which as we can observe from Figure 5.45 leads to output profiles with a poor quality. Further improvements could be made to the code to fix these limitations.

Finally, this approximation could be useful when working with Bessel beams experimentally because the expression that describes the propagation of the Bessel beam is written in measurable and controlled parameters, which could provide an insight into its behavior for specific parameters and a preliminary prediction of the energy loss the beam will suffer.

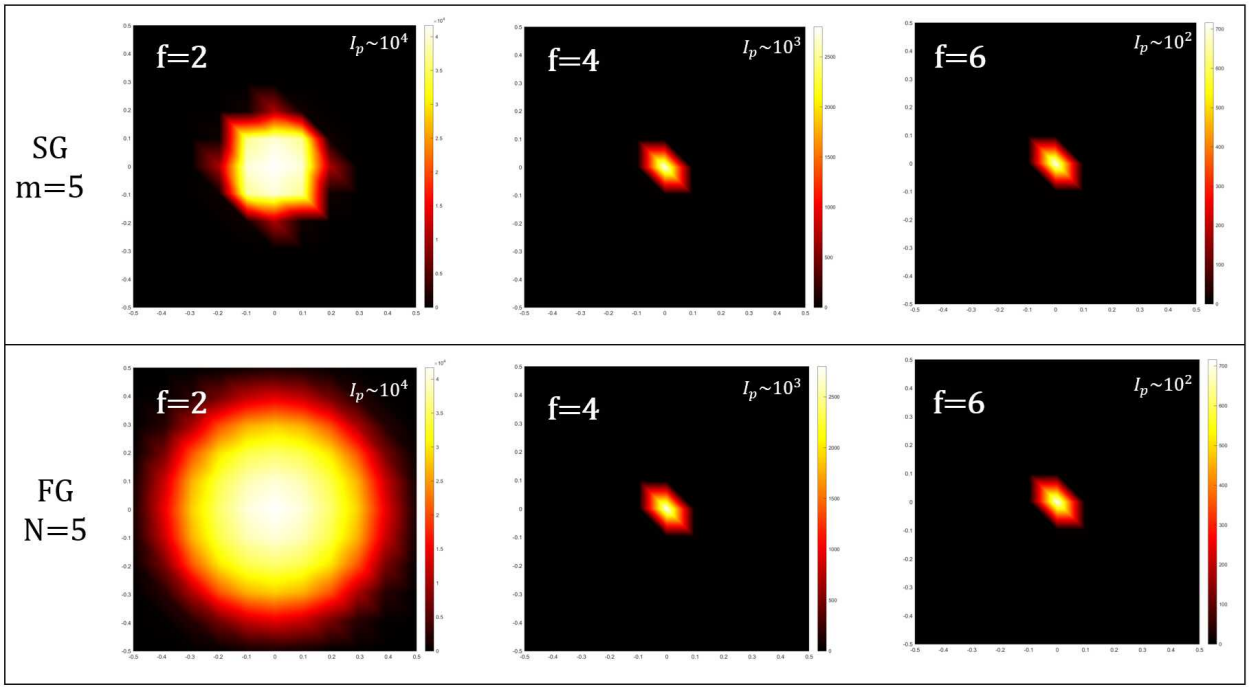

FIGURE 5.45: Center lobe of the output intensity distribution using the SG and FG function for different focal lengths.

Chapter 6

Conclusions

This work was fundamentally an expansion of the formalism based on the traveling conical waves that explain the nature of Bessel beams, we presented an ordered and comprehensive explanation of the concepts necessary to understand this theory. Furthermore, we presented a detailed analysis of the focusing properties of a Bessel beam.

We revisited the theory of diffraction and presented a detailed description of the diffraction integrals which ultimately helped us to give a conscience and clear definition of the diffraction phenomenon, which states that this phenomenon is the result of an element, be this an aperture, an obstacle, a film, a crystal, a spatial light modulator, etc., that modifies the amplitude and/or the phase of a propagating wave.

We analyzed two apodization functions for the Bessel beam, the Super Gaussian beam, and the Flattened Gaussian beam to reduce the oscillations caused by diffraction and provided numerical demonstrations. In our analysis, we made use of energy conservation theorems which allowed us to obtain relations between the parameters that modulate the apodization functions and the radius of their waist which proved to be very effective in the case of the Super Gaussian profile because it showed to be able to reduce the contrast of the oscillations, especially for $f > 2$, and also capable of reaching results similar to the ones obtained without the apodization function in terms of peak intensity and its position z_1. However, the Flattened Gaussian beam demonstrated to be in general more effective in smoothing the axial intensity curve than the SG profile, and it does not require large values of N, especially for the cases $f = 4$ and $f = 6$, this was achieved at the expense of a bigger loss of energy in

comparison. Finally, both apodization functions can keep the size of the center lobe when they are of the order of 10th when $f = 2$.

We also explained the behavior of both apodization functions when modulating the propagation of the Bessel beam after it has passed a thin lens in terms of the description of the Bessel beams as a decomposition into its constituent conical wave components.

Further, we have given a geometrical approximation of the transverse wave vector of the Bessel beam for each point on the propagating axis, which we used to give two functions that represent geometrical approximations, that reproduce the evolution of the focusing of a Bessel beam within the cone-shaped region delimited by the "pseudo-focal" position, and analyzed their transverse output profiles which showed that for $f > 2$ the size of the center lobe does not change regardless of the function used and the focal length, this is due to the loss of energy caused by diffraction of the aperture functions used to form the geometrical approximation.

Future work that remains to be done involves the study of the propagating and focusing features of the Bessel beam within a GRIN medium. The challenge that presents going forward is how the traveling Hankel wave formalism explains the behavior of this beam when they are propagating in a non-homogeneous medium, so far, we have run numerical simulations that showed the traveling waves that compose the beam follow the trajectories determined by the ray equation. Our early results show that the quadratic GRIN medium behaves as a Fourier lens, and we plan to continue our investigations.

List of Figures

List of Tables

Bibliography

[1] Halina Rubinsztein-Dunlop et al. "Roadmap on structured light". In: *Journal of Optics* 19.1 (Nov. 2016), p. 013001. DOI: 10.1088/2040-8978/19/1/013001. URL: https://dx.doi.org/10.1088/2040-8978/19/1/013001.

[2] J.W. Goodman. *Introduction to Fourier Optics*. 2nd ed. McGraw-Hill physical and quantum electronics series. McGraw-Hill Companies, 1996. Chap. 3. ISBN: 0070242542.

[3] Colin J. R. Sheppard. "The Fresnel Approximation and Diffraction of Focused Waves". In: *Photonics* 11.4 (2024). ISSN: 2304-6732. DOI: 10.3390/photonics11040346. URL: https://www.mdpi.com/2304-6732/11/4/346.

[4] M. Born, E. Wolf, and A.B. Bhatia. *Principles of Optics: Electromagnetic Theory of Propagation, Interference and Diffraction of Light*. Cambridge University Press, 1999. Chap. 8, pp. 370–382. ISBN: 0080264824.

[5] C.F. Meyer. *The Diffraction of Light, X-rays, and Material Particles: An Introductory Treatment*. University of Chicago, 1939. Chap. 1.

[6] A. Sommerfeld. *Lectures on Theoretical Physics: Optics*. Lectures on Theoretical Physics. Academic Press, 1964, pp. 1–5.

[7] Olivier Emile and Janine Emile. "The Arago–Poisson Spot: New Applications for an Old Concept". In: *Photonics* 11.1 (2024). ISSN: 2304-6732. DOI: 10.3390/photonics11010055. URL: https://www.mdpi.com/2304-6732/11/1/55.

[8] American Philosophical Society. *Transactions of the American Philosophical Society*. Transactions of the American Philosophical Society v. 2. American Philosophical Society, 1786. URL: https://books.google.com.mx/books?id=OLgAAAAAYAAJ.

[9] M. Born, E. Wolf, and A.B. Bhatia. *Principles of Optics: Electromagnetic Theory of Propagation, Interference and Diffraction of Light*. Cambridge University Press, 1999. Chap. 11, pp. 580–581. ISBN: 0080264824.

[10] A. Sommerfeld. *Lectures on Theoretical Physics: Optics*. Lectures on Theoretical Physics. Academic Press, 1964. Chap. 6, pp. 273–274.

[11] A. Sommerfeld. *Lectures on Theoretical Physics: Optics*. Lectures on Theoretical Physics. Academic Press, 1964. Chap. 5, pp. 179–201.

[12] A. G. Fox and Tingye Li. "Resonant modes in a maser interferometer". In: *The Bell System Technical Journal* 40.2 (1961), pp. 453–488. DOI: 10.1002/j.1538-7305.1961.tb01625.x.

[13] G. D. Boyd and J. P. Gordon. "Confocal multimode resonator for millimeter through optical wavelength masers". In: *The Bell System Technical Journal* 40.2 (1961), pp. 489–508. DOI: 10.1002/j.1538-7305.1961.tb01626.x.

[14] G. Goubau and F. Schwering. "On the guided propagation of electromagnetic wave beams". In: *IRE Transactions on Antennas and Propagation* 9.3 (1961), pp. 248–256. DOI: 10.1109/TAP.1961.1144999.

[15] G. D. Boyd and H. Kogelnik. "Generalized confocal resonator theory". In: *The Bell System Technical Journal* 41.4 (1962), pp. 1347–1369. DOI: 10.1002/j.1538-7305.1962.tb03281.x.

[16] H. Kogelnik and T. Li. "Laser Beams and Resonators". In: *Appl. Opt.* 5.10 (Oct. 1966), pp. 1550–1567. DOI: 10.1364/AO.5.001550. URL: https://opg.optica.org/ao/abstract.cfm?URI=ao-5-10-1550.

[17] Georg Goubau. "Optical relations for coherent wave beams". In: *Electromagnetic Theory and Antennas* Part 2 (1963), pp. 907–918.

[18] Herwig Kogelnik. "Imaging of optical modes-resonators with internal lenses". In: *Bell Sys. Tech. J.* 44 (Mar. 1965), pp. 455–494.

[19] J. Durnin. "Exact solutions for nondiffracting beams. I. The scalar theory". In: *J. Opt. Soc. Am. A* 4.4 (Apr. 1987), pp. 651–654. DOI: 10.1364/JOSAA.4.000651. URL: https://opg.optica.org/josaa/abstract.cfm?URI=josaa-4-4-651.

[20] J.A. Stratton. *Electromagnetic Theory*. International series in physics. McGraw-Hill book Company, Incorporated, 1941. ISBN: 9780070621503. URL: https://books.google.com.mx/books?id=LiZRAAAAMAAJ.

[21] J. Durnin, J. J. Miceli, and J. H. Eberly. "Diffraction-free beams". In: *Phys. Rev. Lett.* 58 (15 Apr. 1987), pp. 1499–1501. DOI: 10.1103/PhysRevLett.58.1499. URL: https://link.aps.org/doi/10.1103/PhysRevLett.58.1499.

[22] Zdenek Bouchal, Jaroslav Wagner, and Marek Olivik. "Bessel beams in the focal region". In: *Optical Engineering* 34.6 (1995), pp. 1680–1688. DOI: 10.1117/12.201641. URL: https://doi.org/10.1117/12.201641.

[23] Baida Lü et al. "Focusing properties of Bessel beams". In: *Optics Communications* 131.4 (1996), pp. 223–228. ISSN: 0030-4018. DOI: https://doi.org/10.1016/0030-4018(96)00274-X. URL: https://www.sciencedirect.com/science/article/pii/003040189600274X.

[24] Z Bouchal, J Wagner, and M Chlup. "Self-reconstruction of a distorted nondiffracting beam". In: *Optics Communications* 151.4 (1998), pp. 207–211. ISSN: 0030-4018. DOI: https://doi.org/10.1016/S0030-4018(98)00085-6. URL: https://www.sciencedirect.com/science/article/pii/S0030401898000856.

[25] S. Chávez-cerda. "A new approach to bessel beams". In: *Journal of Modern Optics* 46.6 (1999), pp. 923–930. DOI: 10.1080/09500349908231313.

[26] Marcelino Anguiano-Morales et al. "Conical dynamics of Bessel beams". In: *Optical Engineering* 46.7 (2007), p. 078001. DOI: 10.1117/1.2752167. URL: https://doi.org/10.1117/1.2752167.

[27] S. Chávez-Cerda, G.S. McDonald, and G.H.C. New. "Nondiffracting beams: travelling, standing, rotating and spiral waves". In: *Optics Communications* 123.1 (1996), pp. 225–

233. ISSN: 0030-4018. DOI: https://doi.org/10.1016/0030-4018(95)00538-2. URL: https://www.sciencedirect.com/science/article/pii/0030401895005382.

[28] S Chávez-Cerda and G.H.C New. "Evolution of focused Hankel waves and Bessel beams". In: *Optics Communications* 181.4 (2000), pp. 369–377. ISSN: 0030-4018. DOI: https://doi.org/10.1016/S0030-4018(00)00779-3. URL: https://www.sciencedirect.com/science/article/pii/S0030401800007793.

[29] J C Gutiérrez-Vega, R Rodríguez-Masegosa, and S Chávez-Cerda. "Focusing evolution of generalized propagation invariant optical fields". In: *Journal of Optics A: Pure and Applied Optics* 5.3 (Apr. 2003), p. 276. DOI: 10.1088/1464-4258/5/3/322. URL: https://dx.doi.org/10.1088/1464-4258/5/3/322.

[30] Xi He et al. "Transverse characterization of focused Bessel beams with angular momentum applied to study degree of coherence". In: *Journal of Optics* 18.5 (Mar. 2016), p. 055605. DOI: 10.1088/2040-8978/18/5/055605. URL: https://dx.doi.org/10.1088/2040-8978/18/5/055605.

[31] Fuping Wu, Yi Luo, and Zhiwei Cui. "A Systematic Summary and Comparison of Scalar Diffraction Theories for Structured Light Beams". In: *Photonics* 10.9 (2023). ISSN: 2304-6732. DOI: 10.3390/photonics10091041. URL: https://www.mdpi.com/2304-6732/10/9/1041.

[32] David J. Griffiths. *Introduction to Electrodynamics*. 4th ed. Pearson, 2013. Chap. 7, pp. 340–342. ISBN: 0321856562.

[33] B.E.A. Saleh and M.C. Teich. *Fundamentals of Photonics*. Wiley Series in Pure and Applied Optics. John Wiley Sons, Ltd, 2007. Chap. 5, pp. 152–170. ISBN: 9780471358329.

[34] G.R. Fowles. *Introduction to Modern Optics*. Dover Books on Physics Series. Dover Publications, 1989. Chap. 6, pp. 152–155. ISBN: 0486659577.

[35] M. Born, E. Wolf, and A.B. Bhatia. *Principles of Optics: Electromagnetic Theory of Propagation, Interference and Diffraction of Light*. Cambridge University Press, 1999. Chap. 1, pp. 14–15. ISBN: 0080264824.

[36] Jean le Rond d'Alembert. "Récherches sur la courbe que forme une corde tenduë mise en vibration". In: *Memoires de l'Academie royale des sciences et belles lettres. Classe de mathematique.* 3 (1747), pp. 214–219. URL: https://www.exhibit.xavier.edu/oresme_2017Sept/4/.

[37] G.B. Arfken et al. *Mathematical Methods for Physicists: A Comprehensive Guide*. Elsevier Science, 2013. Chap. 14, pp. 688–690. ISBN: 9780123846549.

[38] B.E.A. Saleh and M.C. Teich. *Wave Optics*. John Wiley Sons, Ltd, 1991. Chap. 2, pp. 40–46. ISBN: 9780471358329.

[39] C.S. Adams and I.G. Hughes. *Optics F2f: From Fourier to Fresnel*. Oxford University Press, 2018. Chap. 1, pp. 3–4. ISBN: 9780198786788.

[40] C.S. Adams and I.G. Hughes. *Optics F2f: From Fourier to Fresnel*. Oxford University Press, 2018. Chap. 2, pp. 15–16. ISBN: 9780198786788.

[41] P.M.C. Morse and H. Feshbach. *Methods of Theoretical Physics: Types of fields*. International series in pure and applied physics. McGraw-Hill, 1953. Chap. 1, pp. 21–23.

[42] G.B. Arfken et al. *Mathematical Methods for Physicists: A Comprehensive Guide*. Elsevier Science, 2013. Chap. 3, pp. 190–192. ISBN: 9780123846549.

[43] G.B. Arfken et al. *Mathematical Methods for Physicists: A Comprehensive Guide*. Elsevier Science, 2013. Chap. 3, pp. 187–189. ISBN: 9780123846549.

[44] E. Hecht and A. Zając. *Optics*. Addison-Wesley series in physics. Addison-Wesley Publishing Company, 2002. Chap. 2, p. 31. ISBN: 0321188780.

[45] R. Paschotta. *Optical Apertures*. RP Photonics Encyclopedia. Available online at https://www.rp-photonics.com/optical_apertures.html, url = https://www.rp-photonics.com/optical$_a$*pertures.html*. DOI: 10.61835/2nf. (Visited on 06/15/2024).

[46] J.W. Goodman. *Introduction to Fourier Optics*. 2nd ed. McGraw-Hill physical and quantum electronics series. McGraw-Hill Companies, 1996. Chap. 3, pp. 39–42. ISBN: 0070242542.

[47] J.W. Goodman. *Introduction to Fourier Optics*. 2nd ed. McGraw-Hill physical and quantum electronics series. McGraw-Hill Companies, 1996. Chap. 3, pp. 43–46. ISBN: 0070242542.

[48] J.W. Goodman. *Introduction to Fourier Optics*. 2nd ed. McGraw-Hill physical and quantum electronics series. McGraw-Hill Companies, 1996. Chap. 3, pp. 46–49. ISBN: 0070242542.

[49] J.W. Goodman. *Introduction to Fourier Optics*. 2nd ed. McGraw-Hill physical and quantum electronics series. McGraw-Hill Companies, 1996. Chap. 3, pp. 49–50. ISBN: 0070242542.

[50] Alfredo Dubra and José A Ferrari. "Diffracted field by an arbitrary aperture". In: *American Journal of Physics* 67.1 (1999), pp. 87–92.

[51] C.S. Adams and I.G. Hughes. *Optics F2f: From Fourier to Fresnel*. Oxford University Press, 2018. Chap. 6, pp. 104–105. ISBN: 9780198786788.

[52] Robert L Lucke. "Rayleigh–Sommerfeld diffraction and Poisson's spot". In: *European Journal of Physics* 27.2 (Jan. 2006), p. 193. DOI: 10.1088/0143-0807/27/2/002. URL: https://dx.doi.org/10.1088/0143-0807/27/2/002.

[53] B.E.A. Saleh and M.C. Teich. *Wave Optics*. John Wiley Sons, Ltd, 1991. Chap. 4, p. 115. ISBN: 9780471358329.

[54] J.W. Goodman. *Introduction to Fourier Optics*. 2nd ed. McGraw-Hill physical and quantum electronics series. McGraw-Hill Companies, 1996. Chap. 4, pp. 66–67. ISBN: 0070242542.

[55] C.S. Adams and I.G. Hughes. *Optics F2f: From Fourier to Fresnel*. Oxford University Press, 2018. Chap. 5, pp. 77–79. ISBN: 9780198786788.

[56] B.E.A. Saleh and M.C. Teich. *Wave Optics*. John Wiley Sons, Ltd, 1991. Chap. 2, pp. 47–48. ISBN: 9780471358329.

[57] J.T. Verdeyen. *Laser Electronics*. Laser electronics. Prentice Hall, 1995. Chap. 3, pp. 66–69. ISBN: 9780137066667.

[58] G.J. Gbur. *Mathematical Methods for Optical Physics and Engineering*. Cambridge University Press, 2011. Chap. 18, pp. 647–649. ISBN: 9781139492690.

[59] A.E. Siegman. *Lasers*. G - Reference,Information and Interdisciplinary Subjects Series. University Science Books, 1986. Chap. 16, pp. 628–630. ISBN: 9780935702118.

[60] W.A. Granville. *Cálculo diferencial e integral*. Area Matemáticas y estadıstica. Limusa, 1984. Chap. 10, pp. 180–181. ISBN: 9789681811785. URL: https://books.google.com.mx/books?id=1paUbwAACAAJ.

[61] B.E.A. Saleh and M.C. Teich. *Wave Optics*. John Wiley Sons, Ltd, 1991. Chap. 3, pp. 80–82. ISBN: 9780471358329.

[62] David J. Griffiths. *Introduction to Electrodynamics*. 4th ed. Pearson, 2013. Chap. 9, pp. 398–399. ISBN: 0321856562.

[63] M. Born, E. Wolf, and A.B. Bhatia. *Principles of Optics: Electromagnetic Theory of Propagation, Interference and Diffraction of Light*. Cambridge University Press, 1999. Chap. 8, pp. 435–442. ISBN: 0080264824.

[64] A.G. van Nie. "Rigorous calculation of the electromagnetic field for wave beams". In: 19 (1965), pp. 455–594.

[65] Emil Wolf and Yajun Li. "Conditions for the validity of the Debye integral representation of focused fields". In: *Optics Communications* 39.4 (1981), pp. 205–210. DOI: 10.1016/0030-4018(81)90107-3.

[66] Yajun Li and Emil Wolf. "Focal shifts in diffracted converging spherical waves". In: *Optics Communications* 39.4 (1981), pp. 211–215. ISSN: 0030-4018. DOI: https://doi.org/10.1016/0030-4018(81)90108-5. URL: https://www.sciencedirect.com/science/article/pii/0030401881901085.

[67] Ting-Chung Poon. "Focal shift in focused annular beams". In: *Optics Communications* 65.6 (1988), pp. 401–406. ISSN: 0030-4018. DOI: https://doi.org/10.1016/0030-4018(88)90112-5. URL: https://www.sciencedirect.com/science/article/pii/0030401888901125.

[68] Yajun Li and Emil Wolf. "Focal shift in focused truncated gaussian beams". In: *Optics Communications* 42.3 (1982), pp. 151–156. ISSN: 0030-4018. DOI: https://doi.org/10.1016/0030-4018(82)90128-6. URL: https://www.sciencedirect.com/science/article/pii/0030401882901286.

[69] Carlos J. Zapata-Rodrıguez, Genaro Saavedra, and Manuel Martınez-Corral. "Focal shift in optical waves with off-axis focus". In: *Optics Communications* 216.1 (2003), pp. 11–17. ISSN: 0030-4018. DOI: https://doi.org/10.1016/S0030-4018(02)02280-0. URL: https://www.sciencedirect.com/science/article/pii/S0030401802022800.

[70] J. Durnin, J. J. Miceli, and J. H. Eberly. "Comparison of Bessel and Gaussian beams". In: *Opt. Lett.* 13.2 (Feb. 1988), pp. 79–80. DOI: 10.1364/OL.13.000079. URL: https://opg.optica.org/ol/abstract.cfm?URI=ol-13-2-79.

[71] E.T. Whittaker. "On the partial differential equations of mathematical physics." In: *Mathematische Annalen* 57 (1903), pp. 333–355. URL: http://eudml.org/doc/158101.

[72] I. S. Gradshteyn and I. M. Ryzhik. *Table of integrals, series, and products*. Seventh. Translated from the Russian, Translation edited and with a preface by Alan Jeffrey and Daniel Zwillinger, With one CD-ROM (Windows, Macintosh and UNIX). Elsevier/Academic Press, Amsterdam, 2007. Chap. 6, p. 665. ISBN: 978-0-12-373637-6; 0-12-373637-4.

[73] F. Gori, G. Guattari, and C. Padovani. "Bessel-Gauss beams". In: *Optics Communications* 64.6 (1987), pp. 491–495. ISSN: 0030-4018. DOI: https://doi.org/10.1016/0030-4018(87)90276-8. URL: https://www.sciencedirect.com/science/article/pii/0030401887902768.

[74] H. Wang et al. "Fighting against diffraction: apodization and near field diffraction structures". In: *Laser & Photonics Reviews* 6.3 (2012), pp. 354–392. DOI: https://doi.org/10.1002/lpor.201100009. eprint: https://onlinelibrary.wiley.com/doi/pdf/10.1002/lpor.201100009. URL: https://onlinelibrary.wiley.com/doi/abs/10.1002/lpor.201100009.

[75] A. J. Cox and Joseph D'Anna. "Constant-axial-intensity nondiffracting beam". In: *Opt. Lett.* 17.4 (Feb. 1992), pp. 232–234. DOI: 10.1364/OL.17.000232. URL: https://opg.optica.org/ol/abstract.cfm?URI=ol-17-4-232.

[76] R. Borghi, M. Santarsiero, and F. Gori. "Axial intensity of apertured Bessel beams". In: *J. Opt. Soc. Am. A* 14.1 (Jan. 1997), pp. 23–26. DOI: 10.1364/JOSAA.14.000023. URL: https://opg.optica.org/josaa/abstract.cfm?URI=josaa-14-1-23.

[77] S. De Silvestri et al. "Solid-state laser unstable resonators with tapered reflectivity mirrors: the super-Gaussian approach". In: *IEEE Journal of Quantum Electronics* 24.6 (1988), pp. 1172–1177. DOI: 10.1109/3.240.

[78] F. Gori. "Flattened gaussian beams". In: *Optics Communications* 107.5 (1994), pp. 335–341. ISSN: 0030-4018. DOI: https://doi.org/10.1016/0030-4018(94)90342-5. URL: https://www.sciencedirect.com/science/article/pii/0030401894903425.